Nearshore wind-wave modelling in semi-enclosed seas: cross calibration and application

Dissertation
zur Erlangung des Doktorgrades
der Mathematisch-Naturwissenschaftlichen Fakultät
der Christian-Albrechts-Universität zu Kiel

Vorgelegt von
Natacha Fery
Kiel, 2017

Betreuer: Prof. Dr. Roberto Mayerle
Zweitgutachter: Ass. Prof. Dr. Gerd Bruss

Tag der mündlichen Prüfung: 21. Juli 2017
Zum Druck genehmigt: 21. Juli 2017

gez., Dekanin Prof. Dr. Natascha Oppelt

Zusammenfassung

Die numerische Modellierung von windgenerierten Wellen findet vielfältige Anwendungen bei Offshore- und küstennahen Aktivitäten innerhalb von teilweise abgeschlossenen Meeresgebieten. Genaue Vorhersagen von Wellen sind unverzichtbar für das Design von Offshore Strukturen, die maritime Sicherheit und den Schiffsverkehr in tiefem Wasser, wohingegen sie bedeutend sind für Planungen im Küstenschutz, für die Aquakultur und Fischerei in Küstenregionen. Die Vorhersage von Windseen in Randmeeren ist allerdings nicht so gut dokumentiert wie auf dem offenen Meer. Außerdem ist die numerische Modellierung ein weithin genutztes Werkzeug, um den Mangel an beobachteten räumlichen und zeitlichen Wellendaten zu überwinden.

Eine zentrale Frage in dieser Arbeit ist die Beurteilung und die Verbesserung der Genauigkeit von Vorhersagen für Windseen in halb geschlossenen Meeresgebieten. Es wurde untersucht wie die Parametrisierung des Wellenmodels modifiziert werden kann, um genaue Vorhersagen für die untersuchten Gebiete bereitzustellen. Außerdem umreißt diese Arbeit, wie die physikalischen Eingangsgrößen des Wellenmodells, der Windantrieb und die Bathymetrie die Vorhersage von Wellen beeinflussen können. Ein weiteres Ziel dieser Arbeit besteht darin, die Genauigkeit der In-Situ- und Fernerkundungsdaten einzuschätzen, die im Kalibrierungs- und Validierungsprozess des numerischen Modells benutzt wurden.

Um diese Fragen zu untersuchen, wurden Windseen mit dem spektralen Wellenmodel Simulating WAves Nearshore (SWAN) simuliert, dass in der Modellierungssoftware Delft3D (Deltares, Holland) enthalten ist. Die Windfelder aus dem Reanalyse-Zyklus des globalen meteorologischen Models des Deutschen Wetterdienstes (DWD) wurden herangezogen, um das Wellenmodell anzutreiben. Eine umfassende Kalibrierung und Validierung des Wellenmodells und seines Antriebs durch Wind wurde mit Hilfe großer Datensätze aus In-Situ- und Fernerkundungs-Meßtechniken erreicht. Örtliche In-Situ Messungen der Wellen wurden mit akustischen Doppler-Strömungs-Profilern (ADCP), mit Meßbojen, wie einer Wave-Rider Boje und einer ozeanographisch-meteorologischen Boje, sowie mit Tidepegeln ausgeführt. Wellenmessungen mittels Fernerkundung wurden mithilfe des Satelliten-Altimeters ENVISAT und JASON-2 und mit einem Hochfrequenz-Radar durchgeführt. Statistische Analysen wurden ausgeführt, um die Genauigkeit der Wellenmessungen und die Leistungsfähigkeit des numerischen Wellenmodells zu ermitteln.

Numerische Vorhersagen von windgenerierten Wellen in zwei halb geschlossenen Meeresgebieten, dem Roten Meer und der Bohai See, wurden mit Hilfe von Modifikationen des Quellterms verbessert, der für die Erzeugung von Wellenenergie durch Wind in der Gleichung der spektrale Wirkungsdichte des Wellenmodels verantwortlich ist. Das Wellenmodell zeigte eine hohe Sensitivität gegenüber der Formulierung für das Wellenwachstum durch Wind und den Koeffizienten des White-Capping-Disspations-Terms. Die Standard-Parametrierung von SWAN, die die Formulierung für das Wellenwachstum durch Wind nach Komen et al. [1984] anwendet, erwies sich als angemessen, um niedrige und kurze Wellen in küstennahen Bereichen solcher spezifischen Meeresgebiete zu simulieren. Hingegen versagte diese Formulierung, um hohe Wellen in den tieferen und küstenfernen Teilen der betrachteten Gebiete zu erfassen. Verbesserungen dieser Wellen-Vorhersagen wurden durch die

Implementierung der Formulierung des Wellenwachstums nach Janssen [1991] und mit einer Modifikation des White-Capping-Terms erreicht.

Die realisierten Wellen-Vorhersagen über kurze und lange Zeiträume verbesserten unsere Kenntnisse über die Seegangsbedingungen im Roten Meer und in der Bohai See. Im Roten Meer wurde der deutliche Einfluss des Windes auf die Wellenentstehung herausgearbeitet. Wellen sind generell höher und länger im Frühjahr und Sommer mit einer maximalen Wellenhöhe im Frühjahr um den Mai herum und niedrigeren Wellen im November. In der Bohai See werden die Wellen durch die zwei gegenläufigen Systeme des ostasiatischen Monsuns beeinflusst. Südliche niedrige Wellen breiten sich im Sommer aus und höhere westliche bis nördliche Wellen pflanzen sich im Winter fort.

Die Befunde liefern Unterstützung für die Wissenschaftler auf dem Gebiet der operativen Ozeanographie. Die Ergebnisse aus dem Wellenmodell für das Rote Meer und die Küstengewässer von Jeddah wurden in ein Küsten-Monitoring-System integriert. Das Wellenmodell, dass für die Bohai See aufgestellt wurde, ist ein Bestandteil eines Entscheidungshilfesystems (DSS) für die Shandong Halbinsel. Die beiden Informationssysteme stellen Hindcasts und Vorhersagen hydrodynamischer Parameter bereit. Zukünftige Arbeiten, die die operationale Anwendung von SWAN betreffen, einschließlich der Assimilation örtlicher und räumlicher Wellenbeobachtungen, könnten bedeutsam werden für die Planung küstennaher und küstenferner Aktivitäten in den teilweise geschlossenen Meeresgebieten.

Abstract

Numerical modelling of wind-generated waves finds several applications in offshore and coastal activities within semi-enclosed seas. Accurate predictions of waves are essential for the design of offshore structures, marine safety and ship traffic in deep waters, whereas they are relevant for shore protection planning, aquaculture and fisheries in coastal areas. The prediction of wind-waves in semi-enclosed seas is however not as well referenced as in the open seas. In addition, numerical modelling is a widely used tool to overcome the lack of observational wave data in space and in time.

A central question in this study is the evaluation and the improvement of the accuracy of wind-wave predictions in semi-enclosed seas. It was investigated how the parametrization of the wave models can be modified to provide accurate predictions in these specific areas. Furthermore, this work outlines how the physical inputs of the wave model such as the wind forcing and the bathymetry can affect wave predictions. An additional objective of this work is to assess the accuracy of the in-situ and remote field observations used in the calibration and validation processes of the numerical wave model.

To examine these questions, wind-waves were simulated with the spectral wave model Simulating WAves Nearshore (SWAN) included in the Delft3D modelling package (Deltares, the Netherlands). Wind fields from the reanalysis cycle of the global meteorological model of the German Weather Service (DWD) were used to drive the wave model. Extensive calibration and validation of the wave model and its wind forcing were achieved by means of large datasets of in-situ and remote measurement technologies. Local in-situ wave measurements were carried out with Acoustic Doppler Current Profilers (ADCPs), buoys such as a waverider and a met-ocean buoy, and tidal gauges. Remote wave measurements were carried out by the satellite altimeters ENVISAT and JASON-2, and a High Frequency (HF) radar. Statistical analyses to determine the accuracy of the wave measurements and the performance of the numerical wave model were realised.

Numerical predictions of wind-generated waves in two semi-enclosed seas, the Red Sea and the Bohai Sea were improved by means of modifications of the source term responsible of the generation of wave energy by wind in the action balance equation of the wave model. The wave model showed high sensitivity to the formulation of the wave growth by wind and to the coefficients of the white-capping dissipation term. The default parametrization of SWAN that implements the formulation of the wave growth by wind after Komen et al. [1984] was found to be appropriate to simulate small and short waves in the nearshore areas of such specific seas. However, this formulation failed in capturing high waves in the deeper and offshore parts of the considered areas. Improvements of these wave predictions were achieved with the implementation of the wave growth formulation after Janssen [1991] and with the modification of the white-capping term.

The realised wave predictions over the short and the long term enhanced our knowledge of wave conditions in the Red Sea and in the Bohai Sea. In the Red Sea, clear influence of the wind on the wave generation was highlighted. Waves are generally higher and longer in spring and summer with a maximum wave height in spring around May and lower waves in November. In the Bohai Sea, the waves are influenced by the two reversal systems of the

East Asian Monsoon. Southern small waves propagate in summer and higher western to northern waves propagate in winter.

The findings provide support to the scientific community in the field of the operational oceanography. The outputs of the wave model for the Red Sea and the coastal waters of Jeddah were integrated into a coastal monitoring system. The wave model set up for the Bohai Sea is part of a Decision Support System (DSS) for the Shandong peninsula. The two information systems provide hindcasts and forecasts of hydrodynamic parameters. Future work considering the operational use of SWAN including the assimilation of local and spatial wave observations to provide synoptic wave information might be relevant in the planning of coastal and offshore activities in semi-enclosed seas.

Contents

Chapter 1

General Introduction

General Scope

The knowledge of the wind-wave parameters is crucial in the field of coastal engineering for the development of coastal protection solutions. Other nearshore activities such as ship traffic, harbour activities, oil and gas extraction, fishing and tourism are as well affected by wind-waves. In the field of water transport, wind-waves can generate accidents in which ships are confronted with strong oscillations and less commonly with freak waves. Along the coastlines, wind-generated waves can dynamically contribute to coastal changes in terms of erosion or deposition. Erosion occurs for strong incoming waves. Large waves as those from storm surges break and induce a large backwash of the sediments. On the contrary, deposition occurs when the sediment transport nourishes the beach. Wind-generated waves develop over all water surfaces such as lakes, reservoirs, seas and oceans. The knowledge of wind-generated waves is as well of interest for studies on interactions between air and sea interface.

Wind-generated waves are short waves that are generated by the action of the wind. The energy of the moving air is transferred to the water surface. This energy triggers surface currents or waves. First explanations to describe the generation of waves by wind were given by Jeffreys [1925, 1926]. The sheltering theory by Jeffreys [1925] states that in the presence of an airflow, a low pressure eddy forms on the leeward slope of the waves while a high pressure eddy forms on the windward slope. It contributes to increase the wave energy. However, this theory was valid only for non flat sea surfaces. Later, Phillips [1957] developed a theory to explain the initial growth of the waves by means of the wind action through pressure fluctuations caused by the turbulences. He gave an explanation on the formation of ripples (also called capillary waves) at the water surface, but not on the formation of higher waves. The work of Miles [1957, 1960] explains the second stage of the wave growth by wind. The energy of the wind is passed on the wave at a given critical height. This critical height corresponds to the height where the wind speed is equal to the wave speed. Above this height, the wind speed is higher than the wave speed, and the air flow is moving in the same direction as the wave. Below this limit, the wind speed is lower than the wave speed and the air flow is reversed relatively to the moving wave direction. The presence of the two flow directions causes pressure fluctuations that increase the energy of waves. The wave is exponentially growing with the wind duration and the fetch. Nowadays, the generation of wind-waves is explained by a combination of the two theories, the Phillips'-Miles' model [Miles, 1965]. Ripples develop first and with increasing wind speeds, wave height begins to increase through pressure fluctuations. The wind-generated waves can develop into a fully developed sea state when the wind transfers its maximal energy to the waves. Wave height can reach a maximum height and break.

Wind-generated waves have a characteristic period of 3s contrary to the swell waves that

have a characteristic period of 15s. However, for strong velocity, large duration and large fetch of the wind, large wind-waves can develop. The duration corresponds to the time during which the wind is blowing in a constant direction whereas the fetch is the distance over which the wind blows in this same constant direction. High wind-waves will only form if a strong wind blows in the same direction for a long time and over a large distance. If the fetch is unlimited and the duration is short, no large wave will be generated. The same happens if a strong wind blows for a short time. Other type of wave formation are storm surge waves that form over the ocean during a low atmospheric pressure system and waves caused by earthquakes, the tsunamis.

The prediction of wind-generated waves is based on numerical modelling. Nowadays, numerical wave models are a useful tool to obtain synoptic wave information at places around the world that are poor in wave measurements.

Spectral wave models

The model Simulating WAves Nearshore (SWAN) is used in this study to simulate waves in coastal waters. Both wave models, the open source wave model SWAN [The SWAN Team, 2006] and the the model SWAN included in the modelling package of Delft3D [Deltares The Netherlands, 2014] were implemented. Simulating WAves Nearshore (SWAN) is a spectral model widely used to compute wave-current interactions [Ris et al., 1999, Booij et al., 1999]. Spectral wave models are used to reproduce the evolution of random wind waves. The more recent spectral models are called third generation spectral wave models. The main difference with the first and second generation spectral wave model is the consideration of non-linear wave wave interactions. These models are phase-averaged models. It means that they deal with the conservation of the wave action in cases where waves interact with currents (or with the wave energy without wave-current interactions). The wave action (or wave energy) equation describes the evolution of the wave spectrum in time, space, direction and frequency in which the wave spectrum is a statistical representation of the sea surface (Equation (1.1)).

$$\frac{\partial N}{\partial t} + \frac{\partial C_x N}{\partial x} + \frac{\partial C_y N}{\partial y} + \frac{\partial C_\sigma N}{\partial \sigma} + \frac{\partial C_\theta N}{\partial \theta} = \frac{S}{\sigma} \tag{1.1}$$

Where N is the wave action spectrum and S the source term that contains the generation, dissipation and non-linear wave-wave interactions terms. The equation above is given in Cartesian coordinates.

Propagation terms of the wave action are found on the left side of the action balance equation. On the right side of the equation, we find the source terms that account for the generation and the dissipation of the wave energy. These are the wind input, the white-capping, the bottom friction and the surf breaking [Holthuijsen, 2007]. In addition to the above-mentioned physical processes available in SWAN, the numerical settings of a wave simulation can as well be defined. Propagation scheme, computation mode and step sizes (i.e. in time, space, direction and frequency) can be modified for own modelling purposes.

Differences between phase-resolving models (also known as deterministic models) and phase-averaged models lie in the size of the computation domain. The commonly used Bousinesq-type equation that integrates the 3D wave equation over the depth can only be applied to small water depths (Peregrine [1967]; Madsen and Fuhrman [2010]; Nwogu [1993]). It is used to simulate coastal wave processes such as diffraction, refraction, shoaling and related non-linear effects in shallow water.

The more common spectral wave models used nowadays are WAM Cycle 4 [WAMDI, 1988] which is one of the first third generation spectral wave models, WAVEWATCH-III

(WW3) developed at the National Oceanic and Atmospheric Administration (NOAA) [Tolman, 1997, 1999a, 2009] and SWAN [Ris et al., 1999, Booij et al., 1999]. The use of one or another model is dependent on the area where the waves are to be simulated. WAve Model (WAM) and WW3 are recommended for the simulation of waves in deep water while SWAN is more often used in coastal areas. SWAN is actually designed for coastal application. The model accounts for coastal processes such as shoaling and refraction, i.e. depth-induced breaking and triad wave-wave interaction. The other processes, i.e. the generation by wind, the quadruplet wave-wave interaction, the white-capping and the bottom friction are found in all spectral models but their formulation differs from one model to another. Furthermore, contrary to WW3 and WAM, propagation and source terms are integrated simultaneously in time in SWAN. Indeed, the propagation scheme of SWAN is based on an implicit scheme whereas the WAM is based on an explicit scheme. In terms of time computation, WW3 is generally slower than SWAN [Roland, 2008].

The wave model SWAN can be implemented in the open oceans, in coastal areas and in enclosed or semi-enclosed seas. It was used to simulate waves in several seas, coastal areas or lakes around the world. The driving forces are usually analysed surface winds from meteorological models. Among these atmospheric models, we can cite the worldwide used models from European Centre for Medium range Weather Forecasts (ECMWF) and from the German Weather Service (DWD) [1]. The spatial and time resolution of the wind fields vary with the studied area. The parametrization of the wave model depends as well on the modelling purpose in the considered study.

Wave predictions in the coastal area using the model SWAN are the matter of several studies. Rogers et al. [2003] studied the wave growth in two coastal areas, at SandyDuck and in the Mississippi Bight. This study was realised to overcome the poor agreement observed between the model results and the measurements. Modifying the white-capping formulation and disabling the swell breaking allowed the authors to improve the prediction oh the wave parameters. Zubier et al. [2003] found out a good agreement between model results and gauges measurements using the model SWAN in the north Carolina. Gorrell et al. [2011] simulated waves in the coastal waters of San Diego in California. Emphasis was given to the wave modelling over strong bathymetric variations. In the latter, waves were generally accurately predicted and higher errors of the predicted wave parameters were reported at decreasing water depths. Saket et al. [2013] ran the model SWAN in the coastal waters of Chabahar in the Arabian Sea. The model was tuned using a combination of the white-capping rate and the bottom friction coefficients. So as in coastal areas, wave modelling studies based on SWAN have been realised in semi-enclosed seas or closed seas and lakes. Kang-Ren and Zhen-Gang [2001b] found a good agreement between model results and observations for a one week comparison using SWAN in the Lake Okeechobee in Florida. Most studies in such regions reported an underestimation and/or an overestimation of the modelled wave parameters. In Rogers et al. [2003], wave simulations within the Lake Michigan were done and a poor agreement between model results and measurements was found. Similar results were found in the Adriatic Sea [Signell et al., 2005], in the northwestern Mediterranean Sea [Bolaños et al., 2007, Alomar et al., 2014], in Lake Erie in Pennsylvania in the United States [Moeni and Etemad-Shadidi, 2009] and in the Iranian Sea [Mazaheri et al., 2013].

Tools for validation of numerical wave models

The results delivered by numerical wave models need to be validated. Two steps are usually necessary to validate a wave model. The first step is the calibration. The calibration consists

[1] Deutscher Wetter Dienst in German

in comparing part of the measured data set with the model outputs and tune the model settings in case of high discrepancies between the model outputs and the measurements. The validation work consists in comparing the model outputs with the remaining data set that was not used in the calibration.

Wave parameters can be measured directly at the water surface or within the water column, i.e. in-situ measurements or indirectly using the properties of electromagnetic waves in the atmosphere. Usual techniques of in-situ wave measurements are directional and non-directional buoys, wave gauges and Acoustic Doppler Current Profiler (ADCP). Among the indirect measurement techniques, we can find the Synthetic Aperture Radars (SAR), satellite altimeters and High Frequency (HF) radars.

In-situ measurement techniques

Instruments used in this study to calibrate and validate the numerical wave models are presented here. To measure the wave parameters directly at the water surface or below it, wave buoys and Acoustic Doppler Current Profiler (ADCP)s were deployed. Wave measurements by means of a wave buoy consist in following the water particles at its vicinity. An accelerometer built inside measures the vertical displacement of the buoy that moves up and down according the waves' motion. The buoys deployed in the area of study are of two types: a waverider and a metocean buoy. The waverider manufactured by Datawell (The Netherlands) is a displacement buoy, and more precisely a directional buoy of small diameter (0.9m) that was equipped with a Global Positioning System (GPS) wave motion sensor [Datawell Oceanographic Instruments, 2009]. It measures the wave height and the wave direction. The metocean buoy that was deployed was manufactured by OSIL Environmental Instruments and Solutions (United Kingdom). The Fulmar metocean buoy was equipped with sensors that measured meteorological and oceanic parameters. Among the meteorological parameters, the wind magnitude, the wind direction, the air pressure, the air temperature and the air humidity were measured. Regarding the oceanic parameters, current velocities and direction, wave parameters, sea temperature, salinity, turbidity, dissolved oxygen and chlorophyll data were collected. The measured data was radio transmitted via SMS (Short Message Service) or GPRS (General Packet Radio Service) to a station located onshore.

The ADCPs deployed during the measurement campaigns were manufactured by RD Instruments. ADCPs are usually used to measure currents and waves characteristics. To measure waves, the devices are deployed in a upward-looking position at the sea bottom. The measurement principle is based on the Doppler shift of sound pulses (or pings) emitted by the device and reflected back from particles in motion within the water column. The velocity of the particles can be calculated with the difference of frequency between the emitted ping and the backscattered ping. Wave measurements with an ADCP are based on the wave-induced orbital velocities. These are obtained by averaging several bins along the full water column. The wave height can as well be obtained using the surface track and the pressure sensor [Terray et al., 1999, RD Instruments Acoustic Doppler Solutions, 2001]. The measured data is obtained once the instrument is recovered from the water.

Remote-sensing measurement techniques

Most remote-sensing techniques allow indirect wave measurements from the shore, ships, air-planes or satellites using the RAdio Detecting And Ranging (RADAR) principle. Electromagnetic waves sent by an emitting device are reflected (or backscattered) to the device by the ocean surface. Some radar techniques produce images of the ocean surface. This technique, known as Synthetic Aperture Radar (SAR) imagery is found on satellites and is based on the calculation of the amplitude of energy that is backscattered to the satellite.

Remote-sensing techniques have the advantage of measuring synoptic data over large areas. Main drawbacks are the costs and the lower measurement accuracy namely in coastal areas [Cipollini and Co-Authors, 2010]. In this study, non-imaging remote-sensing techniques such as satellite altimeters and High Frequency (HF) radar were used to obtain wave data.

Satellite radar altimeters measure the sea surface height sending microwave pulses to the sea surface. Properties of the backscattered signal such as time, distance, location and amplitude yield to the sea surface height. Distortions in the radar signal are used to calculate the roughness of the sea surface. The latter yields then to a measure of the significant wave height. The selected operation frequency of an altimeter is mainly 13.5GHz (Ku-band), but some altimeters also operate with other frequencies such as 3.2GHz (S-band), 15.3GHz (C-band) or Ka-band (35GHz). The operating frequency affects the pulse length and thus the footprint, that is to say the surface covered by the radar beam. The higher the frequency, the smaller the footprint. Altimeter data used in this work is retrieved from the Radar Altimeter Database System (TU Delft, The Netherlands) that contains altimeter information since 1985 [Scharroo et al., 2013]. Table 1.1 lists the satellites equipped with an altimeter and their properties.

Table 1.1: Deployed satellite altimeters since 1985 and measured parameters. SSH = Sea Surface Height; SWH = Significant Wave Height.

Name	**Time**	**Properties**
Geosat	1985-1989	SSH
		Wind
		Ku-band (13.5GHz)
ERS-1	1991-1996	Ku-band (13.8GHz)
TOPEX	1992-2002	accuracy on SSH $\pm 3.2cm$
		Ku-band (13.8GHz) and C-band (5.3GHz)
POSEIDON	1992-2002	accuracy on SSH $\pm 3.2cm$
		Ku-band (13.8GHz) and C-band (5.3GHz)
ERS-2	1995-2011	Ku-band (13.8GHz)
GFO-1	2000-2008	accuracy on SSH $\pm 3.5cm$
JASON-1	2002-2013	accuracy on SSH 2cm
		Ku-band (13.6GHz) and C Band (5.3GHz)
ENVISAT1	2002-2012	Ku-band (13.8GHz) and S-band (3.2GHz)
JASON-2	2008-2016	accuracy on SSH $\pm 4.2cm$
		SSH
		SWH
		Wind Speed
CRYOSAT2	2010-2016	SSH
		SWH
		Wind Speed
		Ice Thickness
SARAL	2013-2016	SSH
		SWH
		Wind Speed
		Ice Thickness

High Frequency radar is a recent technique that enables measurements of oceanographic parameters at shorter ranges than the satellite altimeters. The first deployed HF radar was the Coastal Ocean Dynamics Applications Radar (CODAR) by Barrick et al. [1977]. Later, the Ocean Surface Current Radar (OSCR) was developed to measure surface currents [King et al., 1984]. The most recent HF radar is the WEllen RAdar (WERA) HF radar developed at the technical University of Hamburg in Germany [Gurgel et al., 1999a, 2001]. Additional HF radars were developed independently for specific purposes such as Shearmann and Moorhead [1988] who developed a HF radar being able to map wave characteristics. At the James Cook University in Australia, Heron et al. [1985] focused on the measure of HF radar parameters other than surface currents. As well, the OSMAR2000 [Huang et al., 2002] for measuring waves and wind over the Eastern China Sea was developed by the University of Wuhan and its maximal measurement range reached 200km.

HF radar is used to measure surface waves, currents and wind parameters. The device is ground-based and is looking at the horizon over the water surface. Similarly to the altimeter, the HF radar transmits electromagnetic waves that are reflected back from the

water surface. Emitted frequency vary between 1MHz and 30MHz, which corresponds to wavelengths of 10m to 300m. However, the transmission is done horizontally over the sea surface and not vertically for the altimeters. The range of transmission is increased with increasing sea water conductivity. The Bragg scatter, that is the resonance between the radar waves and the features at the water surface is the main mechanism exploited by HF radars [Crombie, 1955]. The electromagnetic waves having twice the wavelength as the ocean surface waves are backscattered and amplified. The backscattered signal is processed as a Doppler power spectrum where several peaks are identified. The peaks are Doppler shifted in frequency and symmetrical around the centre frequency. While the peaks of highest intensity corresponding to the echo from the Bragg resonant waves (also called first-order peaks) are used to compute surface currents, surface wave parameters are obtained using the second-order characteristics of the Doppler spectrum. Methods for obtaining directional wave spectrum from HF radars are described in Wyatt [1986, 1990, 1991], Heron and Heron [1998]. They implement inverse techniques algorithms [Wyatt, 1997]. Such algorithms are based on the inversion of the radar echo equation as a function of the wave spectrum described by Barrick et al. [1977]. The accuracy of HF radar measurements and their application has been demonstrated in numerous studies. Surface currents measured by HF radar were validated in Paduan and Rosenfeld [1996], Chapman et al. [1997], Kohut and Glenn [1999], Teague et al. [2001], Kohut and Glenn [2003], Paduan et al. [2006], Archer et al. [2015], whereas HF radar wave measurements validation studies can be found in Graber and Heron [1997], Wyatt et al. [1999, 2005], Wyatt and Green [2009], Wyatt et al. [2011].

In this work, two WERA HF radar systems were deployed along the coast of Yantai, a city located in the Shandong Peninsula in China. Each system is equipped with 4 transmitting and an array of 12 receiving antennas aligned along the shore. Nine kilometres separate the two systems. Each system transmits a continuous frequency of 26.27MHz. The WERA HF radar transmits a Frequency Modulated Continuous Wave (FMCW) [Helzel et al., 2010]. The spatial and temporal resolution are 1.5km and 20min. The WERA processing software is used to combine and interpolate radial components of the two sites of currents and waves over a 500mx500m regular grid. Significant wave height and wave direction are obtained by regression of an empirical fit, i.e. wave measurements from a buoy, with the second-order Doppler spectrum [Essen et al., 1999, Gurgel et al., 2006].

Case studies

The aim of this work is to improve the predictions of the spectral wave model SWAN in two semi-enclosed seas where waves are mainly wind-generated. A focus is given to the analysis of wave parameters over the short and the long-term in the semi-enclosed seas and in a coastal city in each of the seas, Jeddah in the Kingdom of Saudi Arabia and Yantai on the Shandong Peninsula in China. These cities were selected as a result of two projects with on the one hand, a cooperation with the King Abdulaziz University of Jeddah and on the second hand, a cooperation with the Yantai Institute of Coastal Zone Research. The fist project, the Jeddah-Transect aimed at the development of a coastal monitoring system for Jeddah. The second project, SPLASH (Sustainable PLAnning of SHandong Peninsula) aimed at the development of a Decision Support System based on a coupled system to evaluate vulnerable zones to hydrodynamics and to erosion along the peninsula of Shandong. The Red Sea and the Bohai Sea are characterized by different geographic, climatic and hydrodynamic conditions but are similar in the way that both are semi-enclosed seas. Indeed, semi-enclosed seas are characterized by limited communication with the open oceans (Nihoul [1982]; Oguz and Su [2004]).

The methodology used in this work is based on the implementation of the spectral third

generation wave model SWAN. Improvements of the predictions of the wave parameters are realized calibrating and validating the numerical models by means of in-situ and remote-sensing techniques. Recent remote-sensing technique such as the High Frequency radar is deployed to help the validation of the wave model in China. By means of hindcasts simulated with SWAN, the wind and wave climates are evaluated for both seas, the Red Sea and the Bohai Sea. Additionally, an overview of the characteristics of the wave seasonality on a more regional scale is given, i.e. in the coastal waters of Jeddah for the Red Sea and in the coastal waters of Yantai for the Bohai Sea. In parallel, the accuracy and the limits of the in-situ and remote measurements used in this work are evaluated.

Contributions of this work to the scientific community are shown throughout several publications. Emphasis was given to the adaptation of wind-generated wave modelling in semi enclosed areas. Numerical wave modelling in the Red Sea and in the coastal waters off Jeddah are presented in Chapter 2. A parametrization of the SWAN model for the wave modelling in the Red Sea is described in the first publication of Chapter 2. The second publication of Chapter 2 describes the parametrization of the wave model for the coastal area of complex bathymetry near Jeddah. It highlights the importance of the bathymetric and the wind driving inputs for wave modelling purposes in coastal areas. Additional research consisted in evaluating the wave climate on the short- and long-term ranges in the Red Sea and near Jeddah, respectively. Chapter 3 focuses on the wave modelling in the second considered semi-enclosed sea, the Bohai Sea, and the coastal waters of Yantai. The first publication of Chapter 3 presents a modelling study of wind-generated waves in the coastal waters off Yantai. Emphasis is given to the validation of the model SWAN and to the validity of wave and wind measurements realized by the HF radar. Here, the covered research topic is the assessment of the accuracy of wave and wind measurements in the frame of wave modelling purposes. Lastly, a hindcast over 6 years between 2008 and 2014 in the north of the Shandong peninsula is realised and the wave seasonality near Yantai is assessed. In the second publication of Chapter 3, the settings of a coupled flow-wave model for its implementation into a Decision Support System (DSS) are described. The calibrated and validated hydrodynamic models are used to identify areas vulnerable to flow and wave conditions along the Shandong Peninsula. The coupled system is as well implemented into a nowcasting system for the prediction of hydrodynamics properties in real- and near-time in the Bohai Sea. The application of these wave models to different aspects of the operational oceanography highlights the importance of implementing accurate wave models. The assessment of the accuracy of these numerical models is part of the research presented in this work.

The Red Sea and the city of Jeddah

Geographic and hydrodynamic features

The Red Sea is a sea bounded by Egypt, Sudan, Ethiopia and Saudi Arabia (Figure 1.1). The Red Sea has an average length of 2300km and an average width of 350km. It has a connection to the Gulf of Aden through the strait of Bab-el-Mandeb. Due to this limited connection, only small exchange of water masses can be carried out with the open ocean, i.e. the Gulf of Aden and farther the Arabian Sea and the Indian Ocean. The Red Sea is part of the Red Sea rift system. It has an average depth of 791m and a maximal depth of 1500m in the central deep trough. The coastal areas of the Red Sea are characterized by shallow coral reefs. Then, the depth decreases sharply to 600m until it reaches the deepest trough at about 1000m. The average depth near the entrance strait of Bab-el-Mandeb is about 160m which is relatively shallow for the Red Sea [Medio et al., 2000].

Owing to the mountains surrounding the Red Sea, dominant winds blow along the length of the Red Sea. The Arabian monsoons that are the North East Monsoon and the South

West Monsoon trigger two wind regimes in the northern and in the southern part of the Red Sea. In summer, the wind blows from the north west in the entire Red Sea. In winter, northerly winds blow in the northern part of the Red Sea while southerly winds blow in its southern part [Morcos, 1970, Patzert, 1974, Quadfasel and Baudner, 1993]. Additionally to these seasonal winds, localized winds are generated offshore and near the shore because of the differences of temperature between the land surface and the sea surface [Medio et al., 2000]. The wind is the most important factor that controls the direction of the currents and the waves in the Red Sea.

Surface currents are weak and vary with the wind fluctuations, in other words with the seasonal fluctuations of the monsoons. Water masses are pushed to the south of the Red Sea in summer. In winter, water masses from the Gulf of Aden enter in the Red Sea. The tidal regime of the Red Sea is semi-diurnal with a period of 12,4h. Tidal ranges are of small amplitude and reach 0.6m in the north and 0.9m in the south. A recent modelling study of the tides characteristics within the Red Sea is shown in Madah et al. [2015].

Jeddah is the second largest city of the Kingdom of Saudi Arabia and is located on the central eastern coast of the Red Sea at 21.54° N, 39.17° E (Figure 1.1). The city experienced a rapid demographic and economic growth. It is now an important stopping point in the shipping route between the Arabian Sea and the Mediterranean Sea [Al-Hathoul and Mughal, 1991]. The coastal waters of the city of Jeddah are characterized by a shallow nearshore area with coral reef structures. The depth increases rapidly to the main trench at around 600m.

Wave modelling in the Red Sea

We report several wave modelling studies with the model SWAN in the Red Sea [Zubier et al., 2008, Gharbi, 2012, Ralston et al., 2013]. Validation was carried out using the data of satellite altimeters and buoys. Wave conditions were simulated for some months [Zubier et al., 2008, Gharbi, 2012] to some years [Ralston et al., 2013]. In the latter, waves were simulated with a coupled flow-wave model.

Here, the wave model set for the Red Sea and the coastal waters of Jeddah is based on a unique curvilinear grid. The resolution of this grid increases from 43km in the north and the south of the Red Sea to 50m in front of Jeddah. No boundary was imposed at the south of the domain. Indeed, swell from the Arabian Sea is dissipated before reaching the coastal waters of Jeddah. The wave model is driven with the reanalysed wind fields of the global model of the German Weather Service (DWD). To reproduce the bathymetry of the Red Sea, data from GEneral Bathymetric Charts of the Oceans (GEBCO) and Earth TOPOgraphy $1'$ (ETOPO1) is gathered and interpolated on the model grid. Higher bathymetric resolution of the coastal areas is obtained with the information provided by nautical charts. Numerical and physical settings of the wave model are set as default. The default settings in SWAN are based on empirical values from the literature.

The Bohai Sea and the city of Yantai

Geographic and hydrodynamic features

The Bohai Sea is a semi-enclosed continental sea located in the north of China (Figure 1.2). It is connected to the Yellow Sea through the extremity of the Shandong peninsula (Figure 1.2). The Bohai Sea is composed of the Laizhou Bay in the south, the Bohai Bay on the west and the Liaodong Bay in the north (Figure 1.2). The maximal length of this sea is 480km and the maximal width is 300km. The Bohai Sea is a relatively shallow semi-enclosed sea. It has an average depth of 18m and a maximal depth of 83m [Yang et al., 2014].

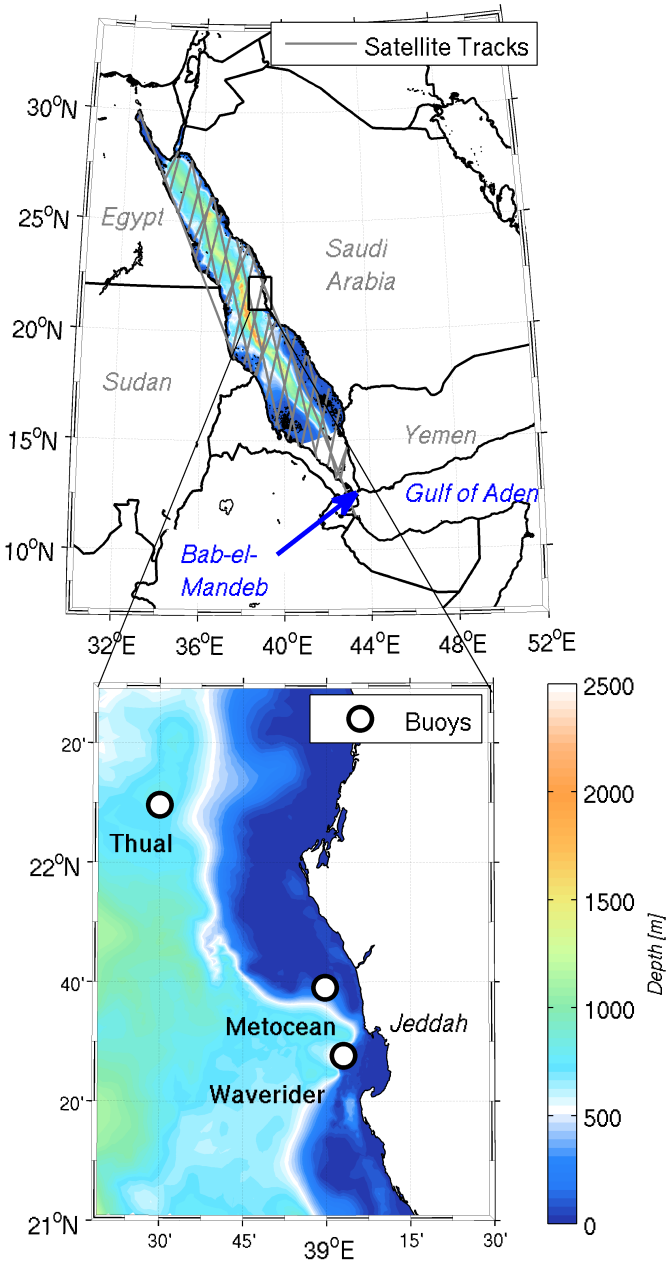

Figure 1.1: Study area : the Red Sea and the coastal waters of Jeddah.

In the Bohai Sea, the annual climate can be divided into two main seasons: summer and winter. This is due to the East Asian Monsoon climate. During the summer period (from April to September) which is warm and wet, extra-tropical storms coming from the south strike the region. During the winter which is cold and dry, storm surges with a northern dominant direction produced by cold-air outbreak hit the region [Huang et al., 2007, Zhang et al., 2012]. The reversal monsoon regime in the Bohai Sea triggers northeasterly and northwesterly winds in winter while it induces southern winds summer [Hainbucher et al., 2004]. Southeasterly winds blow as well during all seasons. The annual mean wind speed is less than 7m/s with higher wind speeds in winter and lower ones in summer [Chen et al., 2012, Gao et al., 2015].

Although tides are relatively small in the Bohai Sea, they have an important effect on the hydrodynamic processes. The tidal regime in the Bohai Sea is a mixed type where semi-diurnal tides are dominant over the diurnal tides [Fang, 1994]. Pelling et al. [2013] found out that the average tidal amplitude is 0.49m with a maximum of 1.4m in the north of the Liaodong Bay.

Surface currents in the Bohai Sea are stronger in summer than in winter and follow a specific gyre dynamic in each of the three bays of the Bohai Sea [Wang et al., 2010]. Still according to Wang et al. [2010], the seasonal winds induced by the Asian Monsoon and the water density have an important effect on the flow circulation in the Bohai Sea.

Waves in the Bohai Sea are the smallest waves of the chinese coasts. They are mainly wind-driven and fetch limited. The maximal fetch that can be reached is about 300km when associated to northwesterly winds. The waves follow the monsoon seasonal variations and as a consequence, northern waves prevail in winter and southern waves prevail in summer [Li and Guo, 1986]. Swell from the Pacific Ocean also enters in the Bohai Sea in summer [Li and Guo, 1986]. Higher waves are generated more often in winter than in summer. High waves can occur in summer during typhoon events [Li and Guo, 1986]. According to Fang and Duan [2014], wind-generated waves are the main forcing in the Bohai Sea.

Yantai is a coastal city located at the north of the Shandong Peninsula, at 37.48°N and 121.44°E (Figure 1.2). Yantai counts about 7 millions inhabitants. With its advantageous location on the shore of the Bohai Sea and the Yellow Sea, the city is a leader in terms of coastal tourism, marine engineering and aquatic production. Indeed, Yantai is the second largest aquatic producer in China. The bathymetry in Yantai's coastal waters is very smooth and does not include any coral reefs.

Wave modelling in the Bohai Sea

Spectral wave models have been implemented in several modelling studies of the Bohai Sea. Long-term and short-term simulations have been carried out with the spectral wave models SWAN and WW3 to understand the wave behaviour and characteristics within the Bohai Sea [Baoshu and Dezhou, 2004, Wang et al., 2012, Yanling et al., 2012, Liang et al., In-Press, Lv et al., 2014].

In this work, a nesting strategy for modelling waves in the Bohai Sea was selected. To account for swell from the Northern Bohai Sea and from the Yellow Sea, a coarse rectangular grid with a constant resolution of 5km that covers the entire Bohai Sea and a part of the Yellow Sea is built (Figure 1.2). A second grid is built around the Shandong Peninsula that is nested within the above-mentioned grid. This small grid is a curvilinear grid whose resolution increases from 1500m at the open boundary to 100m in the coastal waters of Yantai to describe accurately the wave conditions near Yantai. No wave boundary information is passed into the open boundary of the coarse model. It is assumed that the swell develops within the large domain under the influence of the wind only. Wind fields used to drive the wave models are wind reanalyses from the German Weather Service global model. The

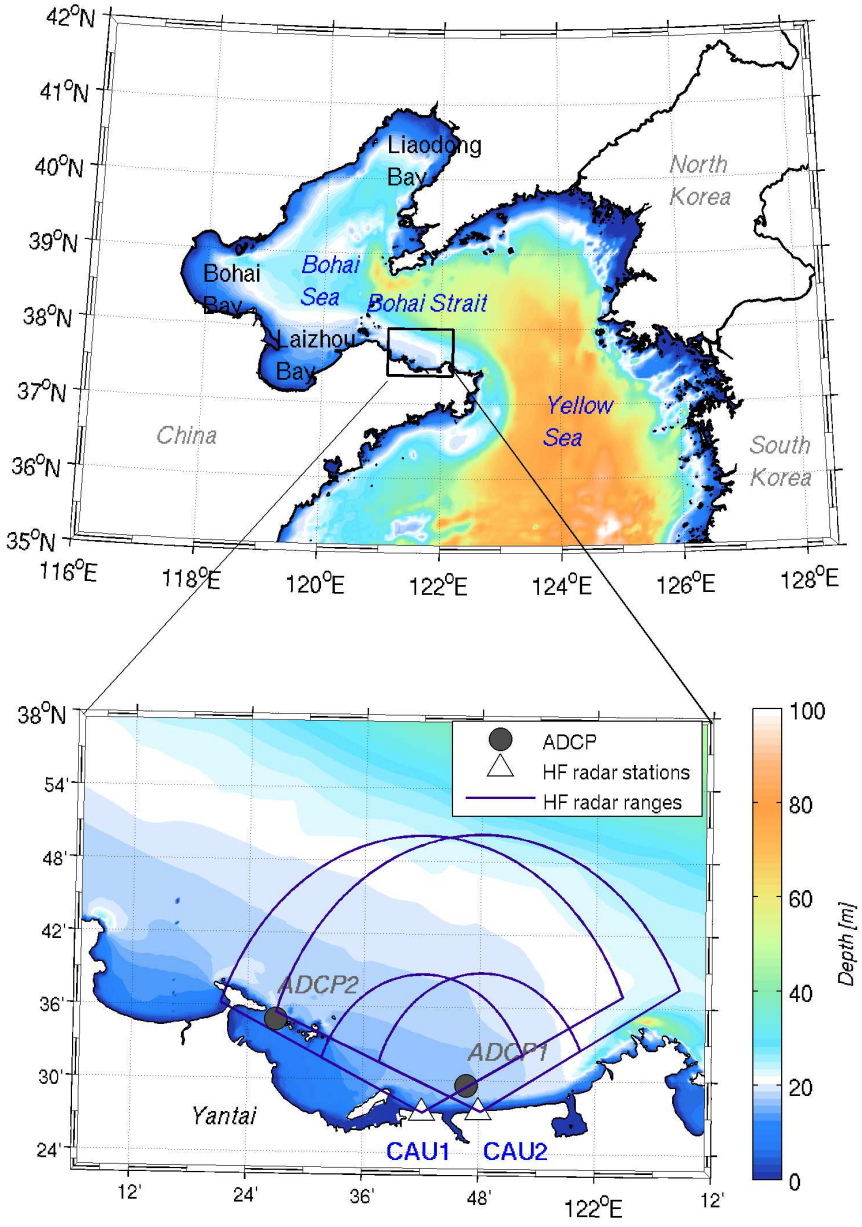

Figure 1.2: Study area : the Bohai Sea and the coastal waters of Yantai. CAU1 and CAU2 are the deployed HF radar stations. ADCP1 and ADCP2 are the locations of the deployed Acoustic Doppler Current Profilers.

bathymetry of the two domains is retrieved from nautical charts and bathymetric measurements. Default settings are applied to the numerical settings of SWAN.

Chapter 2

The Red Sea and the coastal waters of Jeddah

Numerical study of wind-generated waves in the Red Sea

Natacha Fery, Gerd Bruss, Abdullah Al-Subhi and Roberto Mayerle

Proceedings of the 4^{th} International Conference of the Application of Physical Modelling to Port and Coastal Protection
Ghent, Belgium
September 2012
pp 446-555

Numerical study of wind-generated waves in the Red Sea

Natacha Fery(1), Gerd Bruss(2), Abdullah Al-Subhi(3) & Roberto Mayerle(4)

(1) Research and Technology Centre, Christian Albrecht University, Otto-Hahn-Platz 3, Kiel, D-24118, Germany. fery@corelab.uni-kiel.de

(2) Research and Technology Centre, Christian Albrecht University, Otto-Hahn-Platz 3, Kiel, D-24118, Germany. bruss@corelab.uni-kiel.de

(3) Marine Physics Department, Faculty of Marine Sciences, King Abdulaziz University, P.O. Box 80207, Jeddah, 21589, Saudi Arabia. amalsubhi@kau.edu.sa

(4) Research and Technology Centre, Christian Albrecht University, Otto-Hahn-Platz 3, Kiel, D-24118, Germany. rmayerle@corelab.uni-kiel.de

Abstract

The results of simulated wave conditions are used to assess the spatial and temporal variability of wind-generated waves in the Red Sea. Simulations using the fully spectral wave model SWAN show a high sensitivity to the wind input and the dissipation of wave energy through white-capping. During the course of this investigation it was found out that longer and higher waves from north west prevail in spring and summer in the entire Red Sea. The wave climate in autumn and winter is characterized by short waves from north west and south east meeting at the centre of the Red Sea.

Introduction

The knowledge about wave conditions in both nearshore and offshore regions, is of major importance for human activities such as fishing, fish farming, navigation or harbour operations. The presented study aimed at developing a fully spectral wave model for the Red Sea with focus on coastal waters of Jeddah, Saudi Arabia. The work was conducted within the framework of the research project 'The Jeddah Transect' based on a scientific cooperation between the King Abdulaziz University of Jeddah, Saudi Arabia and the Research and Technology Centre of the University of Kiel in Germany.

The Red Sea extending from ca. 12°N to 30°N and ca. 33°E to 40°E is a semi-enclosed sea that is connected in the south to the Gulf of Aden through the narrow strait of Bab Al Mandeb. Its average length and width are 2300km and 350km, respectively. According to Al-Barakati [2004] the Red Sea is exposed to distinctive wind regimes. The northern part is generally exposed to north western winds. In the southern region western winds prevail in summer and spring while south eastern winds are frequent in autumn and winter. Consequently as Jeddah is located in the centre of the Red Sea it is characterized by prevailing winds from north/north west as well as low frequency south eastern winds.

Measured data of waves are scarce throughout the Red Sea and only few wave modelling studies have been published, so far Abdelrahman [1995]. To fill the gaps of wave information and improve the understanding of the spatial and temporal/seasonal variability of sea states within the Red Sea a wave model is set up. In the present study the spectral wave model SWAN (Simulating WAves Nearshore) is used. In the course of the model development a quality assessment of the wind forcing data as well as sensitivity analyses were conducted

on the physical and numerical parameters of the wave model. Measurements of wind and waves in the vicinity of Jeddah were used in association with the developed wave model to analyse the wave system.

State of knowledge

Bathymetric information from GEBCO (General Bathymetric Charts of the Oceans) of 0.5′ resolution and ETOPO1 (Earth TOPOgraphy 1′) gridded datasets supplemented by data from digitized nautical charts 2577, 2599 and 2659 (British Admiralty) were processed. The global bathymetry Earth TOPOgraphy 1′ (ETOPO1) is unsuitable to capture the complex bathymetric structures outside the bay of Jeddah. It is indeed less detailed and smoother than GEneral Bathymetric Charts of the Oceans (GEBCO) while approaching the coast. Therefore the latter is used to complement the bathymetry of the entire Red Sea. In the vicinity of Jeddah nautical charts were digitized and interpolated on a 50m to 100m rectangular grid to obtain a high resolved bathymetry in the coastal zone. Recorded wave data from a met-ocean buoy located in deep water at 22.2°N and 38.5°E were downloaded from the National Data Buoy Centre (NDBC) for the period October 6$^{\text{th}}$, 2008 to September 18$^{\text{th}}$, 2010. The met-ocean buoy also provided wind data for the same period. In the present study, modelled wind fields from the Global Meteorological Model (GME) of the German meteorological service (DWD) were used to force the wave model. The GME has a spatial resolution of 30 kilometres and an output time step of 3 hours. Comparisons with the wind measurements for two months of the recording period of the King Abdulaziz University of Science and Technology (KAUST) buoy show a correlation of 0.79 and 0.92, respectively between the two sets of data both in wind magnitude and wind direction (Figure 2.1).

The analysis of wave measurements between October 6$^{\text{th}}$, 2008 and September 18$^{\text{th}}$, 2010 showed an average significant wave height of 0.9m and an averaged peak period of 4.3s for wave propagating towards south to south-east. The highest waves (Hs) and periods (Tp) were found to be Hs=4.5m and Tp=7.2s, respectively. For the 2 month analysis, i.e. between March 1$^{\text{st}}$, 2010 and May 1$^{\text{st}}$, 2010 the prevalence of northern winds was established. The wind during this two month period also shows the strongest magnitude out of the two year available data. However, measured wind magnitudes are cut at 11m/s as a result of a possible limited range of the measurement device. Figure 2.2 which represents the monthly average of wave height and wave period for the years 2008, 2009 and 2010 shows higher and longer waves in spring and summer than in autumn and in winter.

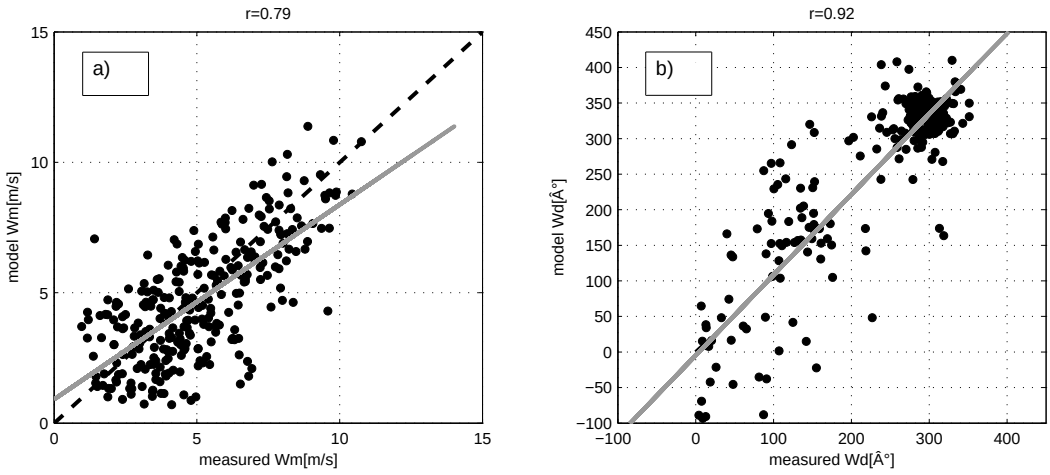

Figure 2.1: Correlation between the GME model and the KAUST wind measurements in terms of wind magnitude W_m (a) and wind direction W_d (b).

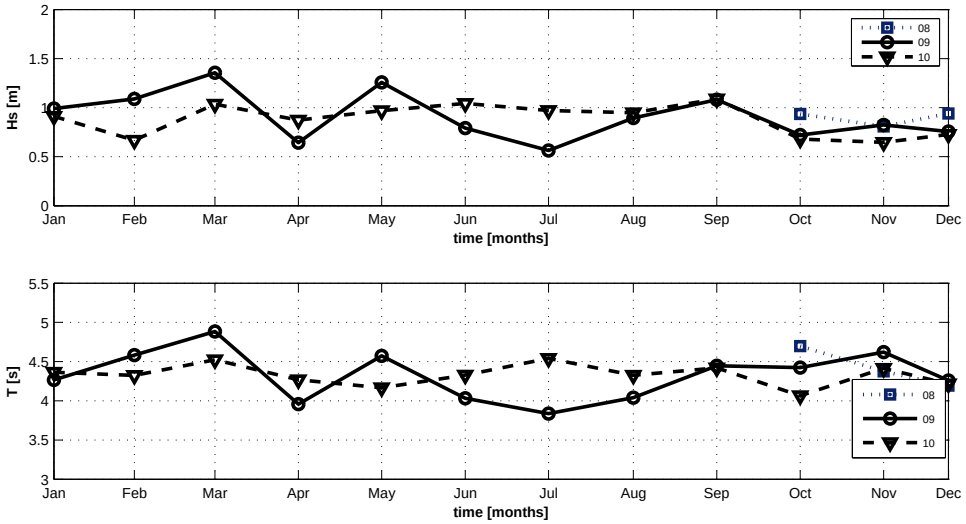

Figure 2.2: Monthly mean of wave height H_s (m) and wave period T (s) for 2008, 2009 and 2010.

The model SWAN developed at the Delft University of Technology, is a spectral model based on the conservation of the wave action density ([Booij et al., 1999, Ris et al., 1999]. The source term for wind growth in SWAN consists of the sum of a linear and an exponential expression (Equation (2.1)). It is essential to note that the expressions of wind growth terms and dissipation terms are empirical.

$$S_{in} = A + BE(\sigma, \theta) \tag{2.1}$$

With A the linear wind growth term and BE the exponential growth as a function of the wave frequency σ and the wave direction θ. The linear growth of waves by wind acting at the early stages of wave formation is described in Equation (2.2). It is brought through resonance between the free surface and pressure fluctuations over it under local wind, usually called Phillips resonant model (Phillips [1957] in Cavaleri and Malanotte-Rizzoli [1981]).

$$A = \frac{1.5e-03}{2\pi g^2}(U^*_{max}[0, \cos(\theta - \theta_w)])^4 H \tag{2.2}$$

Where U^* is the friction velocity and H a filter eliminating low wave growth frequencies as initial growth takes place at high frequencies ([Tolman, 1992]). The exponential growth is explained by the feed-back mechanism described by Miles [1957]. Once linear growth of the wave is reached, further energy due to pressure movements is transferred to the wave. Waves keep growing exponentially as they get larger. The exponential growth term can be expressed differently according to the work realised on wave growth by some authors. Snyder et al. [1981] formulation modified by Komen et al. [1984] proposed the following equation (Equation (2.3)) to describe the exponential growth of waves with the wind.

$$B_{KOMEN} = max[0, 0.25\frac{\rho_a}{\rho_w}(\frac{28U^* \cos(\theta - \theta_w)}{\frac{\sigma}{k_w}} - 1)]\sigma \tag{2.3}$$

Where ρ_a and ρ_w are the air and the water density respectively, k_w is the wave number and σ the wave frequency. Janssen [1991] presented the exponential growth of waves as following in Equation (2.4).

$$B_{JANSSEN} = max(0, \beta\frac{\rho_a}{\rho_w}(\frac{k_w U^*}{\sigma})^2 \cos^2(\theta - \theta_w)\sigma) \tag{2.4}$$

A third possibility for the wind input in SWAN is the wind formulation according to Yan [1987]. This formulation is however not extensively studied in this paper. The white-capping process included in the source/sink term of the action density equation of SWAN depends on the above-mentioned wind input formulation. Generally, this term is formulated as in Equation (2.5).

$$S_{ds}(\sigma,\theta) = -C_{wc}\tilde{\sigma}\frac{k}{\tilde{k}}E(\sigma,\theta) \tag{2.5}$$

Where

$$C_{wc} = C_{ds}[(1-\delta)+\delta\frac{k}{\tilde{k}}][\frac{\tilde{s}}{s_{\tilde{P}M}}]^4 \tag{2.6}$$

In Equation (2.6) k is the wave number, $\tilde{k}$ is the mean wave number, $\tilde{s}$ is the overall wave steepness $\tilde{s}_{PM}$ is the overall wave steepness defined for the Pierson-Moskowitz spectrum ($\tilde{s}_{PM}$=$\sqrt{3.02e-03}$).

C_{ds} is a coefficient used in the determination of the white-capping dissipation rate while δ is a parameter correlated to the dependency of the white-capping on wave number. In SWAN the coefficients for white-capping formulation vary between the wind growth terms according to Janssen [1991] and to Komen et al. [1984]. The coefficients to tune are generally a function of C_{ds} and of the wave steepness.

Applying Janssen wind formulation the tunable coefficient C_{ds1} is introduced such as $C_{ds1} = \frac{C_{ds}}{\tilde{s}^4_{PM}} = 4.5$ for a default parametrization (where C_{ds}=4.1e-05). The second tunable coefficient is δ which has a value of 0.5 in the default parametrization of the SWAN model.

If the wind input after Komen et al. [1984] is applied then the constant C_{ds} can be tuned (C_{ds}=2.36e-05 by default) as well as the wave steepness for a Pierson-Moskowitz spectrum (stpm=$\tilde{s}^2_{PM}$=3.02e-05 by default). If the wind input of Yan [1987] is selected, an alternative formulation for the white-capping is proposed by Van der Westhuysen et al. [2007] that is a non-linear saturation-based form of white-capping adapted from Alves and Banner [2003].

Sensitivity studies

To test the models sensitivity to variations of specific key parameters, the time period March 1st, 2010 to May 1st, 2010 which showed the highest wave activity was selected. Sensitivity was carried out to determine which parameters in the model physics are of great influence. During the investigation SWAN is run in a standalone non-stationary mode taking into account the effect of wind and swell. The non-stationary mode was chosen to reproduce adequately the higher residence time of waves generated by a wind varying in time and space in the computational area. The propagation scheme Backward Space Backward Time (BSBT) is chosen.

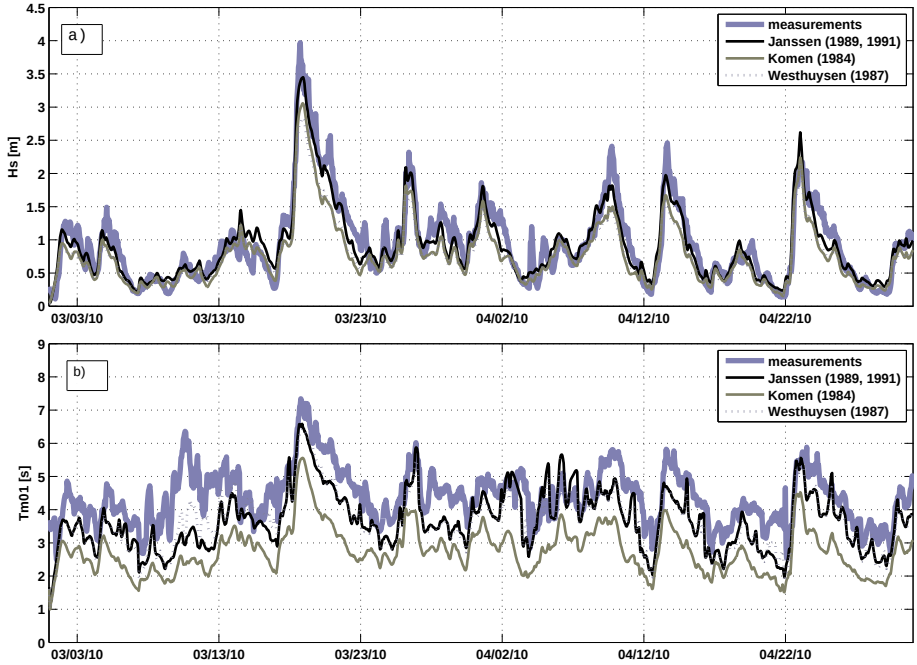

Figure 2.3: Time series of a) significant wave height in meters and b) mean wave period in seconds between 1st March 2010 and 1st May 2010. Comparison between the measurements of the KAUST buoy (grey thick line) and the three formulations of wave growth by wind in SWAN.

The sensitivity of the model to physical and numerical parameters in SWAN was investigated focusing on the wave growth by wind, on the dissipation of wave energy through white-capping, and on the time step.

During sensitivity analyses, the main effect could be assigned to the formulation of the wind growth and the white-capping term. Calculation of the Root Mean Square (RMS), bias and Scatter Index (SI) were used to estimate the effect of these parameters. The linear growth by Cavaleri and Malanotte-Rizzoli [1981] can be activated in SWAN adding the tunable Phillips constant α. Different values of α for each of the three formulations of the wind input of SWAN were tested (see Table 2.1). No effect on the wave parameters was perceived after changing the value of the proportionality coefficient. The modification of this coefficient does not reduce the errors. In the studied area linear wave growth by wind do not dominate the wave growth. Figure 2.3 a) and b) compare simulations' results with the measured significant wave heights and the measured mean wave periods respectively for 6 weeks between 1st March and 1st May 2010. It shows that the trends of significant wave heights are well captured by the model though single events of high waves are underestimated. Wave periods are generally underestimated especially if the default wave growth by wind after Komen et al. [1984] or the formulation after Van der Westhuysen et al. [2007] is applied.

Table 2.1: Statistical parameters of the sensitivity analysis [RMS, bias and SI]. The parameter α of the linear growth is first tested for each wave growth by wind formulation. The coefficients C_{ds} and δ of the white-capping term, as well as the time step are also tested using Janssen wave growth formulation.

		Hs			Tp		
		rms[m]	bias[m]	SI[-]	rms[s]	bias[s]	SI[-]
Formulation	α						
Komen et al. [1984]	0.0007	0.29	0.17	24.5	1.72	1.64	11.9
	0.003	0.29	0.17	24.5	1.72	1.64	12.0
Van der Westhuysen et al. [2007]	0.0007	0.28	0.15	24.6	0.88	0.74	10.9
	0.003	0.28	0.15	24.5	0.88	0.74	10.9
Janssen [1991]	0.0007	0.21	0.04	21.3	0.94	0.73	13.7
	0.003	0.20	0.04	21.0	0.95	0.72	13.8
C_{ds}(Janssen)	δ(Janssen)						
4.1e-05	0.05	0.53	0.38	38.1	2.12	2.01	15.4
1.82e-05	0.5	0.42	-0.34	25.9	0.65	0.28	13.8
4.1e-05	0.5	0.21	0.04	21.3	0.95	0.73	13.7
8.21e-05	0.5	0.44	0.36	28.9	1.50	1.38	13.3
2.74e-05	1	0.29	-0.19	22.4	0.69	-0.09	15.5
3.19e-05	1	0.24	-0.12	21.4	0.95	0.73	13.7
4.1e-05	1	0.20	-0.03	21.2	0.68	0.06	15.5
Time step[min]	Janssen						
6		0.23	0.09	21.9	0.69	0.35	13.4
12		0.21	0.04	21.3	0.95	0.73	13.7
60		4.60	-4.23	189.5	2.60	-2.11	34.5

White-capping is often used as a tunable closure mechanism and is based on empirical experiments implying uncertainties in this term. In this study, efforts on tuning the white-capping were concentrated on the coefficients C_{ds1} and δ (Equation (2.6)). Runs keeping δ as a constant and varying C_{ds} were first realised. It was applied the values of 2, 3, 3.5, 4.5 and 9 for C_{ds1} (corresponding respectively to values for C_{ds} of 1.82e-05, 2.74e-05, 3.19e-05, 4.10e-05 and 8.21e-05). In following runs C_{ds} was kept constant while values of 0.05, 0.5 and 1 were successively attributed to δ. While increasing the dependency of the white-capping on the wave number δ the wave height was slightly improved and the wave period could be improved significantly. Decreasing the value of the coefficient C_{ds} (which depends on the white-capping rate improved generally the results and the effect on wave height was even more substantial. To summarize the effects of modifications of the coefficients C_{ds} and δ, it was found that wave periods were improved by changing δ whereas wave heights reacted more sensitively to C_{ds}.

The influence of the time step was also tested during the sensitivity analysis. Unrealistic results were obtained using one hour time step with Janssen formulation in terms of both significant wave height and wave period. While using a time step of 12min a good agreement with the measurements was found. A 6min time step increased the model accuracy in terms of wave period but increased also the discrepancy with the measurements in terms of significant wave height.

Calibration

Wave heights and wave periods computed by the wave model are calibrated to wave measurements from the met-ocean buoy in deep water between March 1st, 2010 and May 1st, 2010. As no general standard for the calibration procedure of a wave model is known parameters determined as significant during sensitivity are tuned to match to the measurements.

According to the sensitivity results the wind-over-waves coupling theory of Janssen [1991] and Janssen [1989] significantly improved the reproduction of higher waves so it was applied in the parametrization of the model. The second physical parameter that was calibrated is the white-capping term. A combination of adapted values δ of and C_{ds} (δ=1, C_{ds}=4.1e-05) yielded to the best results in terms of both, wave height and wave period. These values are in the range of values used in other studies (Alves and Banner [2003]; Baoshu and Dezhou [2004]; Rogers et al. [2003]; Rusu et al. [2006]).

Figure 2.4 shows the correlation in terms of significant wave height (4a) and 4c)) and mean wave period (4b) and 4d)) before and after calibration of the white-capping term considering the wave growth after Janssen [1989] and Janssen [1991]. Significant wave heights are improved by 11% and wave periods by 15% in the two month simulation.

According to Tolman [1992] the smaller the time step the smaller the number of numerical errors. Time steps between 5min and 15min are considered as a good compromise to obtain reasonable results. In our study a time step of 12min was found out to be a good compromise between numerical errors and computing time.

The difficulty of the model in capturing high wave events as seen during the calibration phases may be related to the specific topography of the Red Sea which is fetch-limiting for certain wind directions. Also the wave model performance is closely related to the wind input. When the wind accuracy of the German Weather Service (DWD) model is high, the tendency of wave parameters is well captured. However it can largely differ when the wind input does not fit well to the measurements. The realization of a correct wind wave growth analysis is restricted here by the cut-off of the wind measurements at the location of interest. Adaptation of the wave growth formulation to capture wave heights at higher wind speeds is necessary.

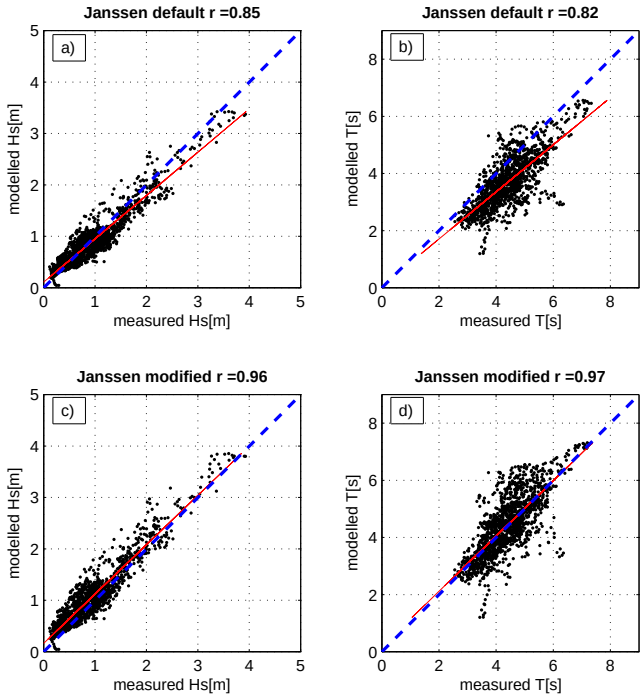

Figure 2.4: Correlation plots before and after calibration of the wave model in deep water for a two month period. The dotted line is the line of perfect correlation, the solid line is the linear fit to the scatter points. a) and b) are the correlation curves for the significant wave height and the wave period respectively before calibration of the white-capping term; c) and d) are the correlation curves for the significant wave height and the wave period after calibration of the white-capping term.

Application

The calibrated wave model was run for two periods within the year 2010. One month in spring 2010 (March 2010) and one month in autumn 2010 (October 2010) were simulated to evaluate the annual seasonality of wave processes in the Red Sea.

Figure 2.5a shows the spatial distribution of the mean significant wave height over one month in spring 2010 (Figure 2.5a) and in autumn 2010 (Figure 2.5b).

In spring wave heights are homogeneously distributed over the Red Sea with maximal values exceeding 1m. On the contrary wave heights and absolute values spatially vary in autumn. In autumn 2010 two wave patterns with a maximum wave height of 70cm facing each other are visualized. These results are closely related to the wind patterns that are observed in the Red Sea. Spring and summer are characterized by a strong wind blowing from the north west along the entire Red Sea. As a direct result the fetch and duration towards the south east increase so that wave height and period increase as well. On the other hand during autumn and winter north western winds over the northern Red Sea face south eastern winds in the south. This particular phenomenon reflects in the wave patterns observed in Figure 2.5b. The obtained results are in agreement with the 3 years wave measurements analysis (Figure 2.2).

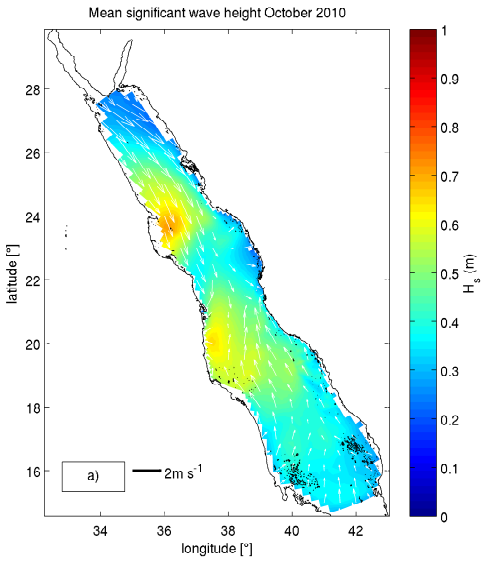

(a)

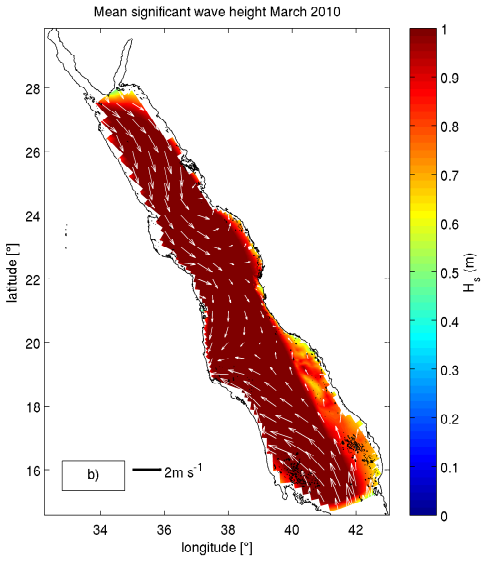

(b)

Figure 2.5: Spatial distribution of the wave height and wind fields (white arrows) averaged over 30 days in (a) spring 2010 and (b) autumn 2010.

Conclusion

In this study, SWAN model was used to simulate waves in the Red Sea. It was found that the default parametrization of SWAN is not entirely suitable for the Red Sea. Therefore modifications of the wind growth formulation and adjustments of the white-capping rate and the wave number have been investigated. Changes in the empirical white-capping dissipation term had a higher effect on the computed wave parameters than changes made in the wind growth term. The model was then calibrated by applying Janssen wind input

formulation [Janssen, 1989, 1991] and adjusting the white-capping term in deep water. The comparison of the model results for a two month period to wave measurements from a Met Ocean buoy revealed a good model accuracy.

Through the application of the calibrated wave model it was possible to assess the seasonality of regional wave characteristics. Higher and longer waves propagate to the south east in summer and spring while smaller and shorter waves from north west and south east face each other at the centre of the Red Sea. In the Red Sea wind patterns clearly influence wave propagation in deep water.

Additional work will include the validation of the wave model in shallow water as well as the online coupling of the wave model with a flow model to evaluate the effect of wave-current interactions. It is envisaged to integrate the final wave model within a coastal information system for the city of Jeddah.

Acknowledgements

Acknowledgements are addressed to the King Abdullah University (KAU) Saudi Arabia for funding the Jeddah Transect project and to the KAUST for providing meteorological and oceanographic data.

Evaluation of the sea state near Jeddah based on recent observations and model results

N. Fery, A.M. AL-Subhi, K.M. Zubier and G. Bruss

Journal of Operational Oceanography
Published online : 02 April 2015
ID: 1014636 DOI:10.1080/1755876X.2015.1014636

Evaluation of the sea state near Jeddah based on recent observations and model results

N. Fery, MSc, Research and Technology Centre Westcoast, Coastal Research Laboratory, Christian Albrecht University of Kiel, Germany
AM. Al-Subhi, PhD, Faculty of Marine Sciences, King Abdulaziz University, Jeddah, Kingdom of Saudi Arabia
KM. Zubier, PhD, Faculty of Marine Sciences, King Abdulaziz University, Jeddah, Kingdom of Saudi Arabia
G. Bruss, PhD, Research and Technology Centre Westcoast, Coastal Research Laboratory, Christian Albrecht University of Kiel, Germany

Abstract

This paper presents the analysis of recent wave measurements and results of the application of a wave model in the Red Sea with focus on the coastal waters of Jeddah in Saudi Arabia. Waves are simulated using Simulating WAves Nearshore within the Delft3D modelling package. Wind fields from the global model of the German Meteorological Service are used to drive the wave model. The model is extensively calibrated and validated with the measured data and satellite altimeters. The influence of the formulation of the wave growth by wind on the model results in the nearshore and offshore zones of Jeddah is investigated. It is also shown that the model reproduces well the refraction occurring over the sharp bathymetric variations in the bay of Jeddah. The analysis of the waves in this bay reveals periodic patterns, on both short and longer time scales. The wave climate follows a seasonality that is characterized by an increase in the wave action in May and a decrease in November. This longer term trend is superimposed by a distinct diurnal variation. It is also found that waves near Jeddah that are generated from northern wind are shorter and smaller than waves generated under westerly wind conditions.

Introduction

So far, knowledge about wave conditions throughout the Red Sea is limited to only a few studies and even fewer wave measurements. This study aims at to analyse recent wave measurements and apply a wave model to improve the understanding of the characteristic wave climate within the Red Sea, focusing on the coastal waters of Jeddah. In the framework of The Jeddah Transect - Sub Project 4 (2010-2013), a Coastal Monitoring System (CMS) was implemented to assist in sustainable coastal planning. The CMS incorporates real-time measurements and hydrodynamic, i.e. flow and wave, models of the Red Sea and the coastal area of Jeddah. The area of interest is characterized by complex features such as small islands and reef structures and thus fetch-limiting. In 2012, two monitoring buoys were installed in the vicinity of Jeddah to measure waves. One buoy also recorded meteorological and water quality parameters. These recent measurements of waves and wind are analysed together with previous data from a deep-water buoy deployed by the King Abdulaziz University of Science and Technology (KAUST) and used to validate the wave model. The model was also validated by means of altimeter measurements from the satellites ENVISAT and JASON-2. Finally, the model was used to hindcast waves for a 3-year

period between 2008 and 2011 to evaluate the characteristic wave climate in the coastal waters of Jeddah.

The growth of waves in the Red Sea is limited owing to the dimensions of this semi-enclosed sea (maximal width 350km) and due to the narrow connection to the Indian Ocean that limits the entrance of large waves and swell. Wave conditions within the Red Sea are mainly generated by regional winds. On the scale of the Red Sea, two wind regimes are dominant [Al-Barakati, 2004]. The northern part is exposed to northwestern winds. In the southern part of the Red Sea, western winds prevail in summer and spring, while southeastern winds blow in autumn and winter. In Jeddah (Figure 2.6), prevailing winds blow from north/northwest with weaker winds as well from the southeast.

The wave model of the CMS is based on the spectral model Simulating WAves Nearshore (SWAN) implemented within the Delft3D software from Deltares. SWAN has been successfully used to simulate waves in lakes, lagoons, and semi-enclosed seas. Generally, the model is able to capture wave conditions in these areas rather well. However, overestimation of the significant wave height and underestimation of the peak spectral period were observed in some studies (Kang-Ren and Zhen-Gang [2001a]; Moeni and Etemad-Shadidi [2009]; Jouon et al. [2009]). In coastal areas where the depth changes rapidly ,greater model errors appear in shallow water where refraction and diffraction have to be taken into consideration (Rogers et al. [2007]; Gorrell et al. [2011]; Mazarakis et al. [2012]).

Studies using SWAN-based wave modelling in the Red Sea have been carried out by Zubier et al. [2008], Gharbi [2012], Fery et al. [2012], and, more recently, Ralston et al. [2013]. In their work, Zubier et al. [2008] used the SWAN model to simulate the wave heights observed in the Red Sea during the summer of 2006 by a local wave gauge and two satellite altimeters (JASON-1 and ENVISAT). Considering the low resolution of the wind field obtained from US Navy's Operational Global Atmospheric Prediction System (NOGAPS), the simulation was able to capture the observed wave patterns reasonably well. In his work, Gharbi [2012] simulated waves in the Red Sea over an approximately 3-month period in 2010 using wind fields from the meteorological models NOGAPS, GFS3 and GFS4 (Global Forecast analysis). The wave model outputs were compared with observations from the Met-Ocean buoy Thual of KAUST as well as satellite data from ENVISAT along 36 tracks within the Red Sea. The model driven with the wind fields from GFS4 predicted the wave parameters well in comparison with GFS3 and NOGAPS meteorological fields, indicating a strong influence of the resolution of the atmospheric model. Fery et al. [2012] simulated surface waves in deep water in the Red Sea driving the model with wind fields from the global model of the German Weather Service (DWD). The performance of the wave model used in the study of Fery et al. [2012] was improved using the wave growth by wind formulation after Janssen. The wave model was used to assess wave seasonality over the Red Sea during the year 2010. Ralston et al. [2013] used a coupled version of SWAN and ADvanced CIRCulation (ADCIRC) models to simulate wave conditions over an approximately 2-year period (2007 - 2009). The coupled models were driven by wind fields obtained using the Weather Research and Forecasting Model with advance Research (WRF-ARW) to dynamically downscale the Centres for Environmental Prediction's Global Final Analysis (NCEP FNL) to a Red Sea subdomain. Both Thual Met-Ocean buoy observations and satellite altimeters data were used to evaluate the coupled models' performance. Initially, wave heights and periods were overpredicted by the coupled models at the buoy location owing to excessive refraction by the complex bathymetry. When this excessive refraction problem was solved by applying a modest smoothing of the bathymetry grid, better agreement between the predictions and observations was obtained. Similar to Gharbi [2012]'s findings, Ralston et al. [2013]'s results also showed strong model dependency on the atmospheric model resolution.

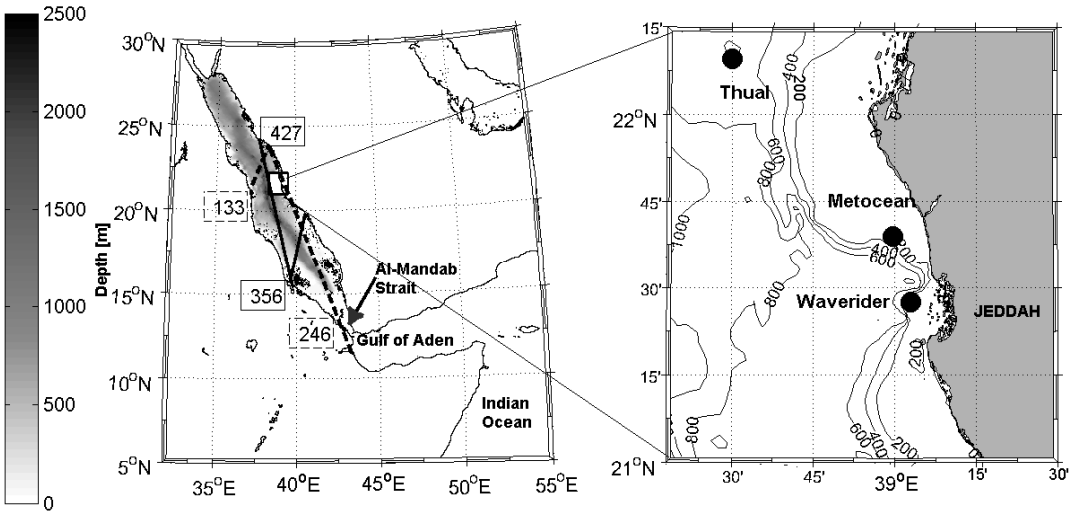

Figure 2.6: Map of the Red Sea with a zoom on the bay of Jeddah and locations of the oceanographic buoys and satellite tracks used in the study. Tracks from the satellite ENVISAT are shown in full dark line; tracks from the satellite JASON-2 are shown in dotted dark line.

Wave and wind data

Wind data

Wind fields from the reanalysis cycle of the global meteorological model of the DWD [Majewski et al., 2002] were used to drive the wave model. The DWD model has a spatial resolution between 20km (for wind data after 2012) and 60km (before 2008). The time resolution is 3h. In this study, we used local measurements of wind speed and wind direction from two meteorological and oceanographic buoys (buoy Thual and Met-Ocean buoy, which are described in Table 2.2) to validate the wind fields from DWD. A filter was applied to the buoys' data to remove noise and inconsistent values. It was found that wind magnitude and direction from DWD are in reasonably good agreement with the measurements.

A frequency analysis was performed for the available wind-speed data. All spectra show a distinct peak at a period of around 24h and another, smaller peak at 12h (Figure 2.7). The reproduction of these patterns in the DWD model again confirms the adequacy of the wind fields for use within the wave model. The main reason for the existence of a regular variation of diurnal period is assigned to circulations owing to larger-scale heat capacity differences between land and sea within the region. The 12h peak might be related to more local breeze effects appearing twice a day (morning and evening). The wind measured offshore by the buoy Thual shows qualitatively the same peaks but with a much smaller amplitude. This indicates the decrease of the land/sea effect with increasing offshore distance.

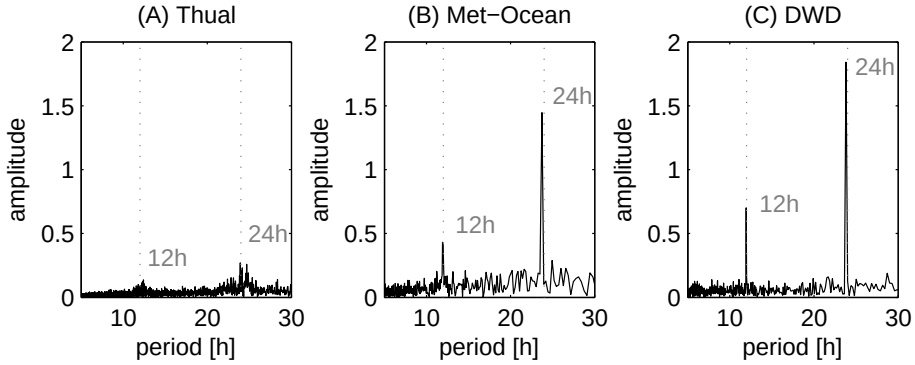

Figure 2.7: Frequency spectrum of the wind speed measured by the buoy Thual (A), the Met-Ocean buoy (B) and modeled by DWD (C).

Wave data

Wave data were obtained from three oceanographic buoys. One waverider and one Met-Ocean buoy were deployed in the coastal waters of the bay of Jeddah in 2012 whereas a second Met-Ocean buoy was formerly deployed in deep water 50km off Jeddah by the KAUST (Figure 2.6 and Table 2.2). Locations, wave parameters, recording periods, mean and maximal values of significant wave height, and wave period are given in Table 2.2. In addition to buoy wave measurements satellite-based wave data, more precisely the ku-band of the significant wave height, is used in this study. Satellite information was obtained from Technical University of Delft using web-based Radar Altimeter Data Acquisition Service (RADS). Significant wave height and wind speed from the satellites ENVISAT and JASON-2 are measured at spatial resolution of 7.50km and 6.25km respectively. The temporal resolutions are 1.11s and 1.02s, respectively. The tracks followed by the two satellites are also shown in Figure 2.6.

The analysis of the buoy data shows that dominant waves at the location of the buoy Thual are coming from north/northwest, whereas waves at the Met-Ocean buoy and at the waverider come mostly from west/northwest as shown in the wave roses in Figure 2.8. Significant wave heights and mean wave periods are higher at the buoy Thual, which is moored offshore in deep water. The mean significant wave height and mean wave period are 0.90m and 4.34s respectively (see Table 2.2). At this location, wave heights reach a maximum of 4.46m and 8.98s for the wave periods. In the nearshore region, waves are globally lower than at the offshore location. Waves are higher at the waverider (mean of 2.42m and maximum of 3.75m) in comparison with the Met-Ocean buoy (mean of 1.15m and maximum of 3.55m). This is explained by the presence of islands and coral reefs at the north of the Met-Ocean that dissipate wave energy before reaching the buoy.

Considering the diurnal variations of the wind speed as discussed above, the wave measurements were also analysed with regard to periodicity. Figure 2.9 shows the average daily variation of the significant wave height at the three buoys. The 24h peak of the wind spectrum (Figure 2.7) is visible at all three buoy locations. Generally the waves are highest around 5pm±2h, whereas low wave conditions occur mostly in the early morning hours. The waves at the Thual buoy show the smallest diurnal variations, whereas the waves at the Met-Ocean buoy show the most pronounced diurnal variations. Owing to the sheltered location, the waves at the Met-Ocean buoy are strongly influenced by local wind and react more directly to a drop in wind. At the locations of the waverider and Thual buoy, after a drop of local wind, swell is sometimes still apparent leading to an increase in the wave period and also keeping the significant wave height high.

Table 2.2: Buoys and measured wave parameters. Hsig : significant wave height, Tmean : mean wave period, Dmean : mean wave direction, Dpeak: peak wave direction, Tz : zero crossing period, Smax : maximal wave spectral density, spd : spectral power density, Tsig : wave period associated to the significant wave height, Tp : wave period at the peak of the wave spectrum.

	Thual	Waverider	Met-Ocean
Longitude	38.05E	39.05E	38.99E
Latitude	22.16N	21.46N	21.65N
Depth [m]	694	20	50
Recording period	10.2008-09.2010	12.2012-present	04.2012-07.2012
Parameters	Hsig	Hsig	Hsig
	Tmean	Tz	Tsig
	Dmean	Smax	Tp
		spd	Dmean
		Dpeak	
Sampling rate	20min	20min	1h
mean Hsig [m]	0.90	0.64	0.42
max Hsig [m]	4.46	2.21	1.15
mean T [s]	4.34	3.75	3.55
max T [s]	8.98	6.20	8.90

Wave model

Description of the wave model

The model SWAN included in the Delft3D WAVE package was used in this study. SWAN is a third-generation spectral wave model based on the conservation of the wave action density (Booij et al. [1999]; Ris et al. [1999]) developed at the Technical University of Delft. Numerical and physical parameters were selected according to the results of extensive sensitivity studies and previous studies [Fery et al., 2012]. The sensitivity analyses focused on the choice of a computational grid and on the numerical and physical parameters affecting the significant wave height and the mean wave period. Waves were computed on a radial grid with a resolution decreasing from 50m in the bay of Jeddah to 43km at the northwestern extremity of the Red Sea. The settings selected for the simulations of waves in this study are presented in Table 2.3. SWAN is run for three periods related to the measuring periods of the three buoys described in the section wave data.

In the bathymetry of the coastal waters of Jeddah, there are many coral reefs with steep gradients down to 900m depth. Bathymetric information from GEneral Bathymetric Charts of the Oceans (GEBCO)GEBCO of $0.5'$ resolution was integrated into the model bathymetry of the entire Red Sea. Further input to the bathymetry was provided from the nautical charts 2577, 2599, and 2659 from the British Admiralty and from echosounding measurements in the framework of the Jeddah Transect Project to adequately capture the complex bathymetry of the coastal waters of Jeddah (Figure 2.6). The final bathymetry of the wave model resulted in a combination of these extensive bathymetric measurements with digitized nautical charts and the global bathymetric data from GEBCO.

Table 2.3: Numerical and physical parameters of SWAN model applied in this study.

Numerical parameters	
Computational mode	Non-stationary
Time step	15min
Frequency space	17 bins between 0.03Hz and 0.58Hz
Directional space	36 bins of 10°
Physical parameters	
Generation by wind	Komen et al. [1984]; Janssen [1991]
White-capping	Komen et al. [1984]
Refraction	activated
Triads	not activated
Quadruplets	Discrete Interaction Approximation (Hasselmann and Hasselmann [1985])
Bottom friction	Jonswap model (Hasselmann et al. [1973])
Depth induced breaking	Model after Battjes and Janssen [1978]

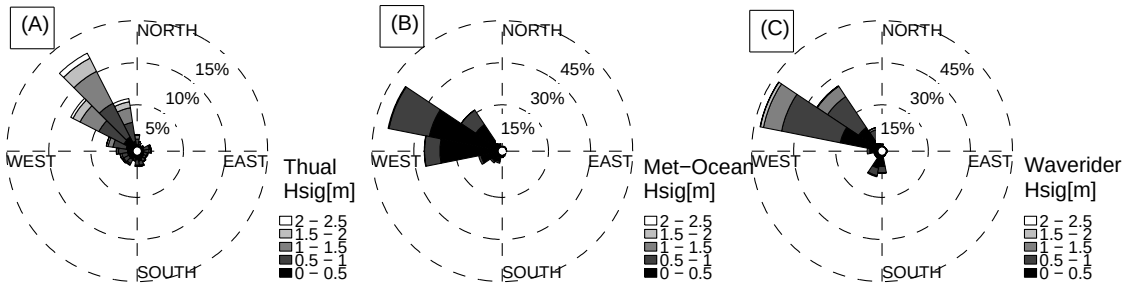

Figure 2.8: Wave roses of significant wave height (Hsig) at Thual (A), at the Met-Ocean buoy (B) and at the waverider (C).

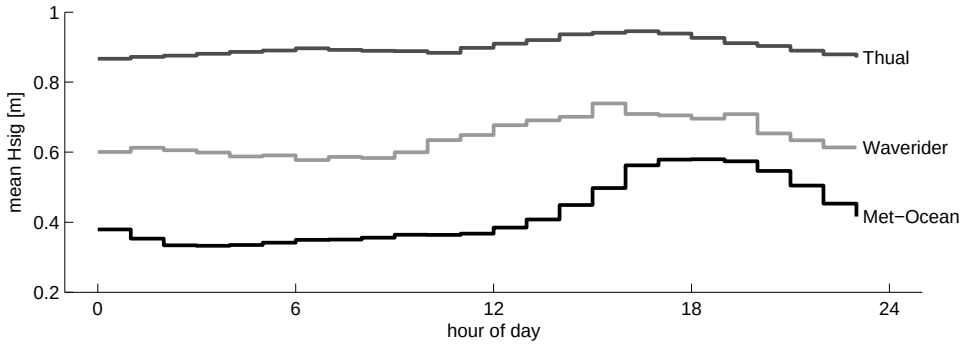

Figure 2.9: Mean daily variation of the significant wave height (Hsig). Shown are averages over the entire measuring period for each hour of the day.

Comparison of model results and measurements

The model SWAN was calibrated in a previous study [Fery et al., 2012]. Different formulations of the wave growth by wind were tested. The formulation after Janssen [1991] gave the best results in terms of significant wave height and mean wave period compared with the measurements of the buoy Thual, moored offshore in deep water. In the present study the two formulations of wave growth by wind after Komen et al. [1984] and Janssen [1991] are investigated. The main difference between the two formulations is that the wind-over-waves coupling theory of Janssen [1991] accounts for the interaction between wind and waves.

Figure 2.10 shows the time series of the significant wave height [Figure 2.10 (A)], the mean wave period [Figure 2.10 (B)] and the mean wave direction [Figure 2.10 (C)] from the wave model compared with the measurements of the buoy Thual, the waverider, and the Met-Ocean buoy. In Figure 2.11 the values of the statistical comparison of the modelled and measured time series are plotted. Mean values, representing temporal averages, and standard deviations of the model errors are considered.

From the time series plots, it becomes obvious that the general trends of significant wave height, mean wave period, and wave direction are well captured by the model at all considered locations. Modelled periods of high and low waves follow the patterns of the measurements. Significant differences appear only in the wave direction at the Thual buoy around 13^{th} March 2010. These deviations from the measured wave directions are assigned to inaccuracies in the applied wind fields.

Looking at the results, the model performance has to be differentiated between the offshore location of the buoy Thual and the two nearshore locations where the bathymetry is influencing the local wave patterns. Similar to the results of Fery et al. [2012], the wave growth by wind formulation after Janssen [1991] gives the best results of the significant wave height at the offshore location. At the nearshore locations, Janssen [1991] leads to an overestimation of the wave height. By using Komen et al. [1984], the reproduction of the absolute wave height values at the two nearshore locations could be substantially improved. For the mean wave period, there is a general tendency of underestimation in the model. This tendency is more pronounced if the wave growth by wind formulation after Komen et al. [1984] is used and at the offshore location. In Fery et al. [2012], the differences in the mean wave period at Thual between model with Janssen [1991] and measurements could be further reduced by reducing the dissipation due to white-capping. Since this approach leads to an overestimation at the two nearshore locations, it was not applied in this study. Considering the wave direction, the applied wave growth by wind formulation seems to be of minor importance [Figure 2.10 (C)]. The standard deviation of the model error is around 20cm for the wave height and between 0.5s and 0.8s for the wave period. The scatter of the model error is generally, apart from the wave height offshore, lower if the wave growth by wind formulation after Komen et al. [1984] is used.

Significant wave heights recorded by the altimeter of the satellites ENVISAT and JASON-2 were compared with the SWAN model results along the tracks followed by the satellite during the periods of analysis. The model results were interpolated on the tracks 356 and 427 from ENVISAT and the tracks 133 and 246 from JASON-2. The paths of the tracks are shown in Figure 2.6. The trends of significant wave height are well captured by the wave model for both formulations of the wave growth by wind. However, it can be seen in Figure 2.12 that absolute values of significant wave height are better reproduced with the formulation after Janssen [1991]. This observation agrees with the local comparisons of the significant wave height at the offshore location of the buoy Thual.

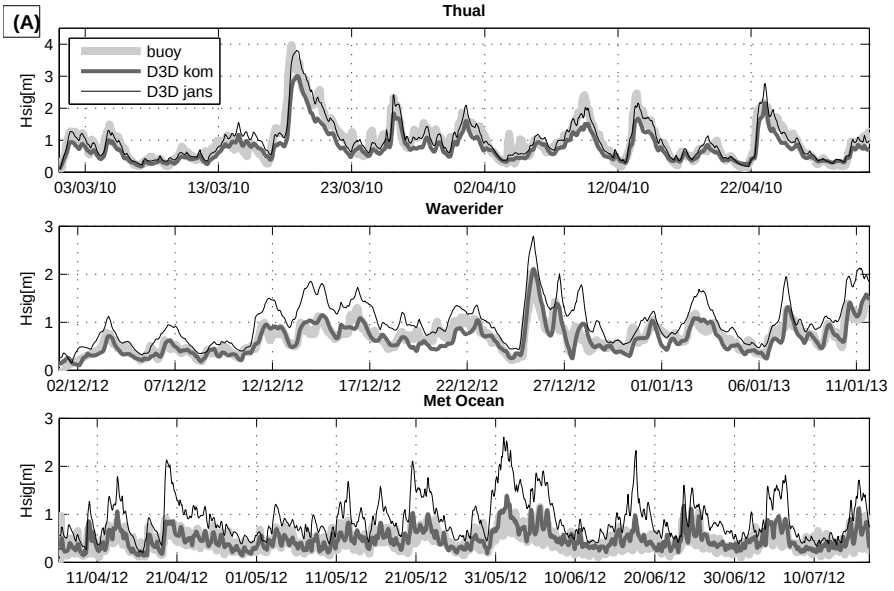
(A)
Thual
buoy
D3D kom
D3D jans
Hsig[m]
03/03/10
13/03/10
23/03/10
02/04/10
12/04/10
22/04/10
Waverider
02/12/12
07/12/12
12/12/12
17/12/12
22/12/12
27/12/12
01/01/13
06/01/13
11/01/13
Met Ocean
11/04/12
21/04/12
01/05/12
11/05/12
21/05/12
31/05/12
10/06/12
20/06/12
30/06/12
10/07/12

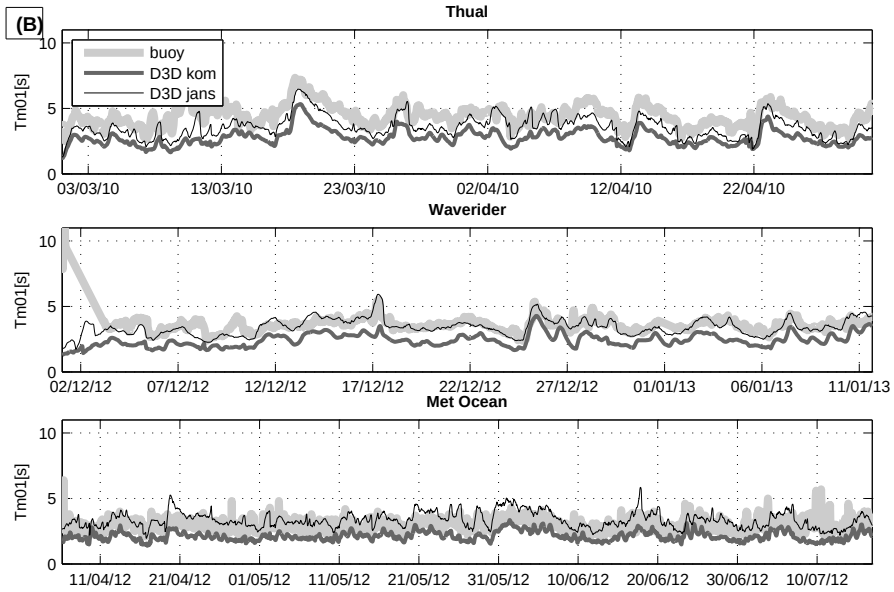
(B)
Thual
buoy
D3D kom
D3D jans
Tm01[s]
03/03/10
13/03/10
23/03/10
02/04/10
12/04/10
22/04/10
Waverider
02/12/12
07/12/12
12/12/12
17/12/12
22/12/12
27/12/12
01/01/13
06/01/13
11/01/13
Met Ocean
11/04/12
21/04/12
01/05/12
11/05/12
21/05/12
31/05/12
10/06/12
20/06/12
30/06/12
10/07/12

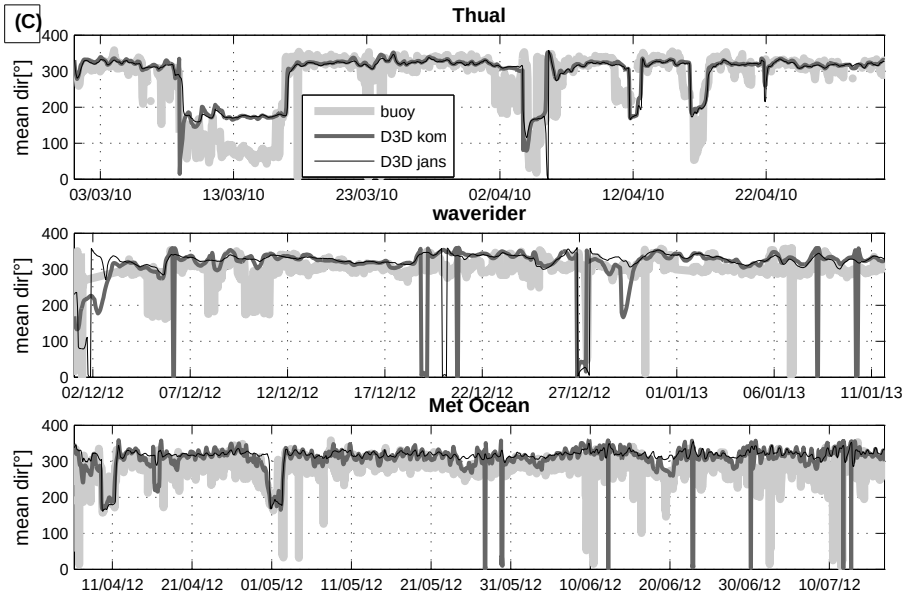

Figure 2.10: Significant wave height (A), mean wave period (B) and mean wave direction (C) measured by the buoy Thual, the waverider and the Met-Ocean buoy in thick grey line versus the SWAN model results with the formulations after Komen (D3D kom) and Janssen (D3D jans).

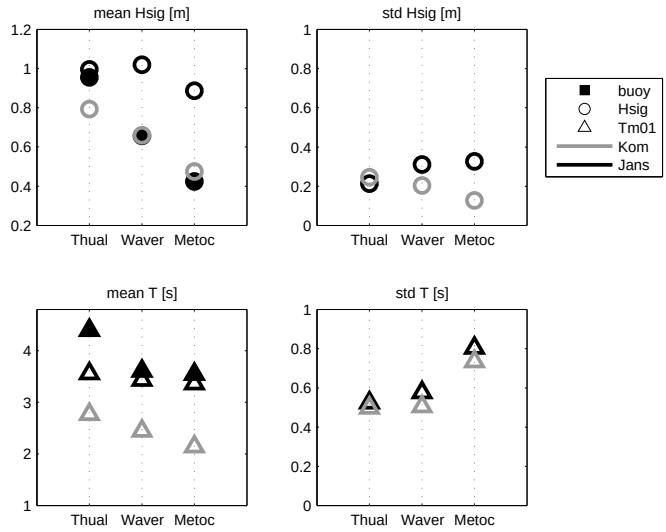

Figure 2.11: Mean significant wave height (Hsig) and wave period (T) at the buoy Thual, the waverider(Waver) and the Met-Ocean buoy (Metoc) on the left side. On the right side, the standard deviation of the model error (std) at each station for Hsig and T. Hsig is defined by circles, T is defined by triangles. Full markers show the measured data, empty grey markers show the model results with Komen and empty black markers show the model results with Janssen.

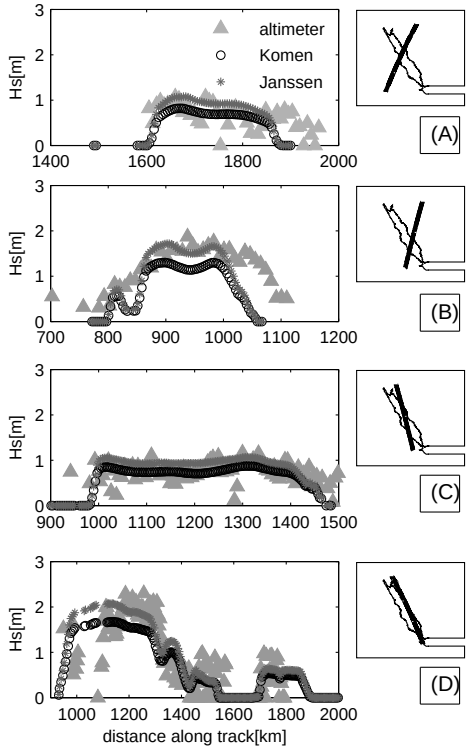

Figure 2.12: Comparison of significant wave heights between the altimeter measurements (in grey triangles) and the wave model (circles for the formulation after Komen; stars for the formulation after Janssen) along the tracks (A) 133 from JASON-2, (B) 356 from ENVISAT, (C) 427 from ENVISAT and (D) 246 from JASON-2.

Summary of model performance

It was shown earlier in this paper that the wave model reproduces well the wave conditions at the two locations in the vicinity of Jeddah and offshore. At offshore locations, applying the wave growth by wind formulation after Janssen [1991] gives the best results. At the two nearshore locations, wave heights are better captured with Komen et al. [1984], whereas the period is still better reproduced using Janssen [1991]. This means that for different focus locations and parameters, different set-ups of the model should be used. Since there is a high correlation between the modelled parameters using Janssen [1991] and Komen et al. [1984], it can also be practical to use one model set-up and perform correction to the disadvantaged locations/parameters by applying linear factors. In the study described in the next section, the formulation after Komen et al. [1984] was used. The significant wave height at the location of the buoy Thual was corrected by a factor of 1.3, which was determined by linear regression.

Long-term wave modelling in the region of Jeddah, Red Sea

Seasonal and monthly variations of wind and wave parameters

The SWAN model was run for a period of 3 years and 8 months between 1st January 2008 and 1st August 2011 to analyse the wave climate in the bay of Jeddah. The model was run using the wind reanalyses from DWD. The examination of the wave parameters was carried out spatially and locally at the locations of the three buoys (see locations of the buoys in Figure 2.6).

Monthly and daily variations of the significant wave height for the 3-year simulation are shown in Figure 2.13 (A) and (B), respectively. The smallest waves are found at the Met-Ocean buoy where the modelled mean wave height is 0.45m. Conversely, waves are higher at the buoy Thual where the modelled mean wave height is 0.70m. The mean values obtained with the wave model coincide with the mean observed values described in Table 2.2 of the section wave data.

Wave heights reach a maximum in May and a minimum in November Figure 2.13 (A). Modelled average diurnal variations are similar to the observed average diurnal variations. The significant wave height increases at around 5:00 pm. The seasonality is similar at all considered locations, i.e. nearshore and offshore.

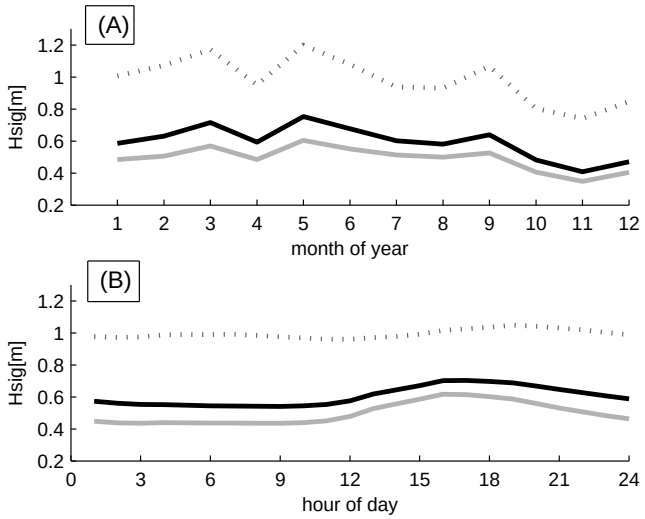

Figure 2.13: Seasonality of the significant wave height (Hsig) using SWAN between 2008 and 2011 at the buoy Thual (dotted grey line), at the waverider (black full line) and at the Met-Ocean buoy (light grey full line). (A) monthly average over a year and (B) hourly average over a day.

Figure 2.14 shows the seasonality of the mean wave direction during the same period of analysis at the Met-Ocean buoy [Figure 2.14 (A)], at the waverider [Figure 2.14 (B)] and at the Thual buoy [Figure 2.14 (C)]. The mean wave direction are compared with the mean wind direction from DWD at one grid cell. The main wave and wind directions vary between 270° and 360°, i.e. between west and north. Waves and wind propagate similarly at the offshore station Thual (Figure 2.14 (C)). At the two stations that are geographically close to each other located near the coast of Jeddah, there is an offset between the wave direction and the wind direction. The wind direction shows larger amplitude variations in the vicinity of the waverider and the Met-Ocean buoy that is not seen offshore at the buoy Thual. The largest offsets between the wind and the wave direction occur at the end of each year at the Met-Ocean buoy and at the waverider (Figure 2.14 (A) and (B)). This phenomenon occurs only inside the bay, where the water depth decreases. Larger offsets are visible when northern winds are blowing. Wave refraction inside the bay is thus stronger than for western wind conditions. Similar patterns are found in the variations of the significant wave height and the mean wave period (Figure 2.13). In the last months of a year (from October until January), the significant wave height and the mean wave period decrease and reach the lowest values of the year.

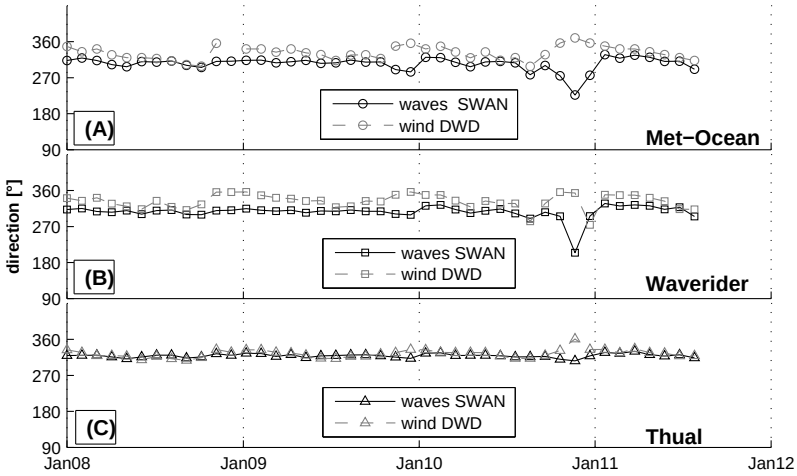

Figure 2.14: Monthly averages of the wind and wave directions between January 2008 and August 2011 at the Met-Ocean buoy (A), the waverider (B) and the buoy Thual (C).

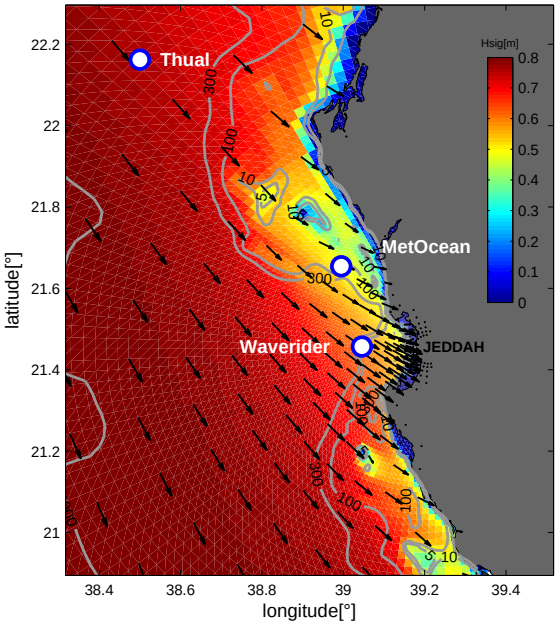

Figure 2.15: Mean significant wave height and wave direction (arrows) in front of the city of Jeddah between 2008 and 2011. Isobaths are showed in grey lines.

Figure 2.15 shows the modelled mean significant wave height and associated wave direction over 3 years near Jeddah. It can be seen that prevailing waves come from northwest. The significant wave height and the wave direction are modified in the bay of Jeddah where refraction occurs. Waves get smaller and turn anticlockwise at an angle of 45° from the offshore wave direction. The sheltering geography of the bay of Jeddah and the presence of coral and island reefs clearly affect wave conditions and limit the impact of large waves.

Conclusions

Recent wave measurements and results of a wave model were used to evaluate the characteristic sea state near Jeddah in Saudi Arabia. From the analysis of the measurements, it was

found that the wave patterns near Jeddah show a distinct diurnal variation. Lower waves in the early morning are followed by higher waves in the late afternoon. At the two observed locations of the waverider and the Met-Ocean buoy, the average wave heights range around 0.6m and 0.4m with maxima of 2.2m and 1.2m, respectively. The prevailing direction of waves at these locations is west/northwest.

The model SWAN was used to simulate waves in the coastal waters of Jeddah. A long-term simulation was realized to evaluate characteristic wave patterns in this region. The model was run with the wind reanalysis from the German Meteorological Service. Wind-input fields were in good agreement with the observed wind from the meteorological buoys. The wave model was calibrated and validated by means of two meteorological and oceanographic buoys and one waverider deployed in the vicinity of Jeddah. Significant wave heights from the altimeters of the satellites ENVISAT and JASON-2 were also considered. A generally good agreement between the simulated waves and the observed data was found.

However, the modelled wave parameters show significant sensitivity to the applied wave growth formulation. At offshore locations and generally for the wave period, better performance is achieved using the formulation after Janssen [1991]. At the two onshore locations the wave height is better reproduced with Komen et al. [1984]. Owing to the high correlation between the modelled parameters using the two formulations, it can be practical to perform linear model correction.

The analysis of the long-term model hindcast reveals a picture of high influence of the local bathymetric patterns on the average wave conditions near Jeddah. There are sheltered areas and areas that are more exposed to wave action according to the spatial configuration of the local coral reef structures. The prevailing offshore wave direction of north/northwest is refracted to west/northwest approaching the coast of Jeddah. The 3-year simulation furthermore reveals that the wave conditions regularly vary on daily and monthly timescales. A clear dependence of wave conditions on seasons is observed. The patterns of this seasonality are similar to the seasonal variations of the wind in the Red Sea. Waves are generally higher and longer in spring and summer with a maximum wave height in spring around May and lower waves in November. The diurnal variations and general average values of the 3-year simulation coincide with the observed data.

Acknowledgements

The authors acknowledge with thanks King Abdullah University (KAU) for technical and financial support.

Funding

This collaboration of the Jeddah Transect Project between KAU and Helmholtz-Centre for Ocean Research (GEOMAR) was funded by KAU Jeddah, Saudi Arabia [grant number T-065/430-DSR].

Chapter 3

The Bohai Sea and the coastal waters of Yantai

Validation experiment of wind and wave properties from High Frequency radar in the vicinity of Yantai, China

N. Fery, C. Tang and R. Mayerle

submitted to Regional Studies in Marine Science
2017

Validation experiment of wind and wave properties from High Frequency radar in the vicinity of Yantai, China

N. Fery, MSc, Research and Technology Centre Westcoast, Coastal Research Laboratory, Christian Albrecht University of Kiel, Germany
C. Tang, PhD, Yantai Institute of Coastal Zone Research, Chinese Academy of Sciences, China
R. Mayerle, Professor, Research and Technology Centre Westcoast, Coastal Research Laboratory, Christian Albrecht University of Kiel, Germany

Abstract

Wave information measured by a High Frequency (HF) radar in the coastal waters of Yantai in China at low and high sea state conditions is presented and compared with the in-situ measurements of a bottom-mounted Acoustic Doppler Current Profiler (ACDP) and with the results of the numerical wave model Simulating WAves Nearshore (SWAN). Wind information measured by the radar is compared with the wind measurements of a coastal station near Yantai and with the results of the German Weather Service global meteorological model. The HF radar performs well in reproducing the significant wave heights during both, calm and stormy conditions. Poor agreement is observed for the directional data at low sea state. The wave model SWAN performed well in capturing the wave parameters. Similarly, we found a high accuracy of the wind fields from the meteorological model used to force the wave model. The wave climate along the north of the Shandong peninsula with a focus near Yantai is assessed with the validated wave model between 2008 and 2014.

Introduction

The city of Yantai is located on the Shandong peninsula along the Bohai Sea in China. The Bohai Sea is a semi enclosed sea that is connected to the Yellow sea through the Bohai strait (Figure 3.1). Like many coastal regions in China, the Shandong peninsula is going through demographic and economic growth. The coastal regions are vulnerable to wave conditions both over the short term through storms and over a longer term through wave action. Dominant and stronger waves reaching the northern coast of the Shandong peninsula are fetch-limited waves coming from north/northeast. A second wave system from the south, i.e. from the Yellow Sea is reaching the northern coast of the peninsula. Waves from the south are refracted and are of lower energy than northern waves.

Studies on wave conditions in the Bohai Sea are so far mainly based on numerical wave models because of a lack of in-situ wave measurements. The spectral wave model Simulating WAves Nearshore (SWAN) was used to simulate waves in the Bohai Sea. Wang et al. [2012] used the wind fields from the Regional Atmospheric Modelling System (RAMS) and the water level from the Princeton Ocean Model (POM). A good agreement between the wave observations and the wave model was found. In other studies, the model SWAN was forced with the wind fields from the European Centre for Medium range Weather Forecasts (ECMWF) [Wang et al., 2012, Liang et al., In-Press] and the water levels of a 2D hydrodynamic model [Wang et al., 2012]. The above-mentioned authors assessed the wave climate in the Bohai Sea over the last 20 years. Several studies showed that modifications of the parametrization of SWAN are necessary to improve the hindcasting of the waves.

Namely, a tuning of the white-capping, the bottom friction and the coefficients related to the wind and wave growth improved the performance of the wave model [Baoshu and Dezhou, 2004, Wang et al., 2012, Lv et al., 2014]. According to the same authors, the highest and longest waves occur in winter while the lowest and the shortest waves occur in summer. The waves are influenced by the East Asian monsoon that triggers northern cold-air outbreaks in winter and southern winds in summer.

High Frequency radars are powerful instruments usually deployed along the coast to derive surface current, wave and wind information over a spatial domain. Electromagnetic and hydrodynamic properties of the HF radar are used to obtain the surface currents and wave parameters such as the significant wave height and the wave direction, and wind parameters such as the wind magnitude and the wind direction. Along the Chinese coasts, the HF radar OSMAR2000 developed by the Wuhan University in China provided wind and wave measurements up to 200km of the coast. In their study, Huang et al. [2002] found a good agreement between HF radar measurements and ship measurements. Differences between the sets of information were due to influence of the inappropriate use of linear equations in shallow water and to interferences with external targets. The accuracy of HF radar measurements and their application has been demonstrated in numerous studies. HF radar wave measurements validation studies can be found in Graber and Heron [1997], Wyatt et al. [1999, 2005], Wyatt and Green [2009], Wyatt et al. [2011].

The present study is the result of co-operation between the Yantai Institute of Coastal zone research (YIC) in China and the Coastal Research Laboratory of the University of Kiel. Its purpose is to verify the accuracy of a High Frequency radar in measuring wave and wind parameters in a coastal area at low and high sea state conditions. The present measurements are used to validate the wave model that is used to assess the wave conditions over 6 years in the coastal waters of the Shandong peninsula in China. The considered region is not well investigated due to its location close to the Bohai straits and is often not included in hydrodynamic studies within the Bohai Sea. In a first section, we describe the different datasets used for the verification of the HF radar data. The accuracy of the HF radar wave data is assessed by means of comparisons with the measurements of an Acoustic Doppler Current Profiler (ADCP) and with the results of the numerical wave model Simulating WAves Nearshore (SWAN) within the area covered by the HF radar. Similarly, comparisons of wind parameters measured by HF radar with measurements of a coastal station and a meteorological model are realised. As an example of application, we describe in a last section the wave patterns in the coastal waters of the Shandong peninsula between 2008 and 2014.

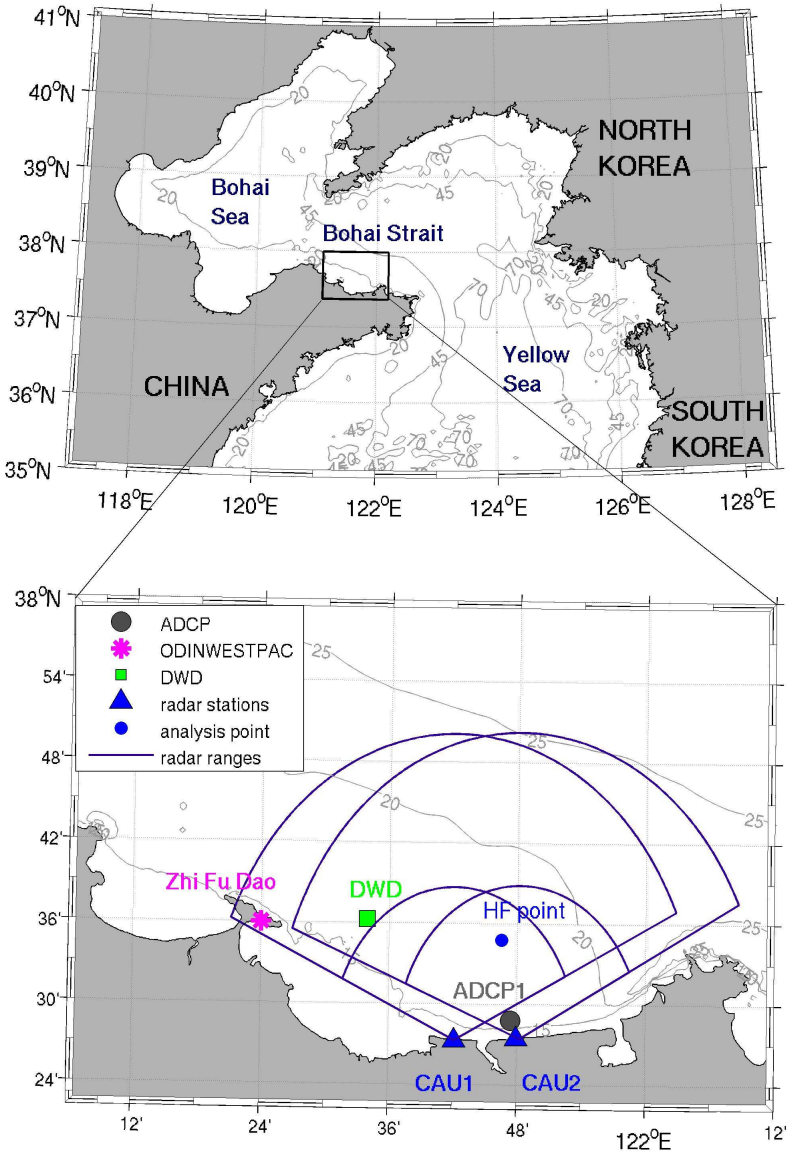

Figure 3.1: The Bohai Sea (top figure) and the coastal waters of Yantai (bottom figure) with the locations of the deployed ADCP and the HF radar. Blue lines correspond to the measurement ranges of surface currents and waves by the stations of the HF radar CAU1 and CAU2. Measured and modelled wind data are retrieved at the station Zhi Fu Dao (ODINWESTPAC) and DWD, respectively.

Description of the wave and wind measurements

High Frequency radar

Wind and wave parameters were recorded by a WEllen RAdar (WERA) deployed along the coast of Yantai in China between June and September 2013. The WERA is a High Frequency (HF) radar developed at the Technical University of Hamburg. The HF radar transmits a Frequency Modulated Continuous Wave (FMCW) of 27.26MHz. The 100kHz bandwidth of the radar allows a measurement cell size of 1500m and a maximum measure-

ment range of 38km. The radar system consists of a shore based phased array system of 4 transmitting antennas and 12 receiving antennas. Each system is deployed at two stations, CAU1 (121.7°E, 37.5°N) and CAU2 (121.8°E, 37.5°N) separated from 9km (Figure 3.1). The transmitting antennas are deployed in a rectangular shape while the receiving antennas are aligned along the coast over 20m. This geometry is required in the beam forming technique that is used to obtain the full backscattered Doppler spectrum [Gurgel et al., 2001]. Indeed, the retrieval of ocean information by HF radar is based on the processing of the power spectrum that is backscattered by the ocean waves having half the wavelength of those from the radar. The first-order Bragg peaks of the backscattered power spectrum are used to determine surface currents. The wave data is extracted from the second order regions of the power spectrum which are caused by a combination of double electromagnetic scattering satisfying the Bragg relation and non-linear effects. Barrick et al. [1977] established theoretical equations between the backscattered spectrum and the ocean wave directional spectrum. In the present study, the WERA algorithm described by Essen et al. [1999] and Gurgel et al. [2006] is used. The algorithm proposes an empirical solution based on the regression with measurements of a buoy to derive the significant wave height and the wave direction. The outputs are averaged every 20min and are interpolated onto a regular grid of 500m resolution inside the HF radar measurement area. This area expands to 81km in longitude and 39km in latitude in front of the coast of Yantai. The radar configuration for saving the outputs was switched from a continuous acquisition mode (June to end of August 2013) to a permanent acquisition mode (September 2013). The permanent acquisition mode is preferred as the acquisition is faster. Another advantage is that the output data can be cut into specific sections during post processing procedures.

Acoustic Doppler Current Profiler

A 600kHz bottom mounted Acoustic Doppler Current Profiler (ADCP) from Teledyne RD Instruments was deployed during a measurement campaign in the coastal waters of Yantai between July, 23^{rd} 2013 and September, 26^{th} 2013. The ADCP is used to validate the HF radar data. It was hence was deployed close to the overlapping area of the two HF radar stations 2.75km from the shore at 121.8°E and 37.5°N and moored at a depth of 17m (Figure 3.1). Wave parameters such as the significant wave height, the peak period, peak direction and the directional spectra were recorded. The vertical resolution of the ADCP is 0.5m and the outputs were stored every 30min. The device has a precision of 0.14m.

Coastal station Zhi Fu Dao

In-situ wind measurements used for the validation of the HF radar wind data are provided by the coastal station Zhi Fu Dao (ZFD) located on an island connected to the city of Yantai.at 121.4°E and 37.6°N (Figure 3.1). The data was retrieved from the online platform of Ocean Data and Information Network for the Western Pacific Region (ODINWESTPAC). The wind magnitude and the wind direction are continuously measured at a sampling rate of 1hour since 1999.

Numerical models

The spectral wave model SWAN [Booij et al., 1999, Ris et al., 1999] integrated into the Delft3D modelling suite is used in this study to simulate waves in the Bohai Sea (Deltares, the Netherlands). Computations were realised on two grids where a finer grid is nested into a coarser grid. We used a nesting strategy to capture with a higher accuracy the bathymetric and waves structures in the coastal waters of the Shandong peninsula. The coarser grid

is a rectangular grid of 2.5km resolution that covers the entire Bohai Sea while the finer grid is a curvilinear grid which resolution decreases from 500m at the open boundary to 100m near the coast of the city of Yantai, a city located along the Shandong peninsula. The resolution of the finer grid was chosen so as to be similar to the grid of the High Frequency radar measurements. The bathymetry used in the model is obtained from the digitization of nautical charts and from the interpolation of nearshore bathymetry measurements (personal communication). The wave model was driven by the wind fields derived from the German Weather Service (DWD). The global model of DWD has a spatial resolution of 30km and a time resolution of 3hours [Majewski et al., 2002]. SWAN is run in a non stationary mode with a time step of 15min and the outputs are saved every hour. The wave spectrum is discretized into 24 directional bins and into 25 frequency bins from 0.05Hz to 1Hz, which corresponds to wave periods from 1s to 20s. Additional numerical parametrization of the wave model includes the use of the wave growth by wind formulation after Janssen [1991]. This formulation showed real improvements in capturing strong variations of significant wave height in deep water and in areas free of bathymetric obstacles [Fery et al., 2012]. Figure 3.2 provides details about the effect of the formulation on significant wave heights at the location of the ADCP in the coastal waters of Yantai. The two formulations give similar results and a good agreement with the measurements for wave heights smaller than 0.7m (root mean squared error below 0.40m). A slight improvement is however observed for these small waves when the formulation after Komen et al. [1984] is used. Above this value, this same formulation leads to an underestimation of the significant wave height and at this point, the formulation after Janssen [1991] is more appropriated to capture the peaks of significant wave height. For the validation experiment, the waves were modelled for a period of 3 months between June 2013 and September 2013. Besides, the wave climate assessment is based on a simulation of 6 years between 2008 and 2014.

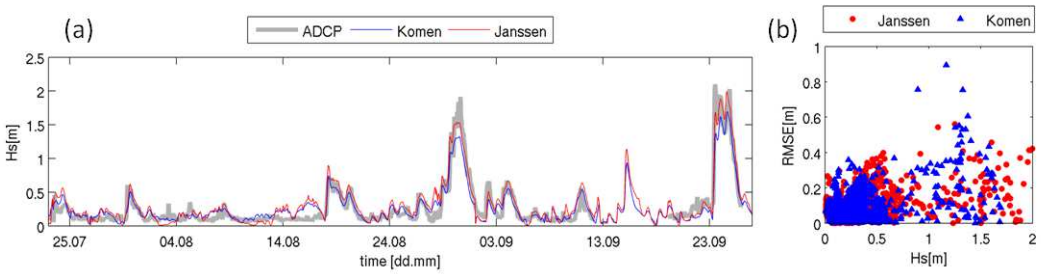

Figure 3.2: Comparison of the modelled significant wave height obtained with the formulation of the wave growth by wind after Komen et al. [1984] and after Janssen [1991](a), Root Mean Squared Errors with the ADCP measurements against the significant wave height for the two formulations (b).

Validation of High Frequency radar data at low sea state

Analysis of the significant wave height, the wave and the wind direction

Low sea state conditions in the coastal waters of Yantai are characterized by significant wave heights smaller than 1m. The study was split into two analyses, i.e. at low and high sea states to evaluate the performance of the HF radar under these two conditions. Indeed, according to the literature, a HF radar operating at a frequency of 26.27MHZ provides reliable wave information for wave heights comprised between 0.58m and 3.63m [Helzel et al., 2010]. Below and above this range, the HF radar data is limited and/or not reliable any more. The time period between the 23^{rd} July, 2013 until the 22^{nd}, August, 2013 was

selected to analyse the low wave and wind conditions.

The analysis of the significant wave height and the wave direction measured by HF radar was realised at the analysis point whose location is showed in Figure 3.1. This point is located within the overlapping area of the two radar stations, area where the directional data of the waves is available. It is important to note that the range of the wave measurements is reduced to 50% of the total range measured with the HF radar which is reached for the measurement of surface currents. Indeed, the calculation of waves is based on the amplitude of the second-order scattering of the HF signal which is lower than the first-order scattering signal used for the calculation of surface currents. The radar analysis point was selected to be close to the moored ADCP (6km between the two points) to proceed accurate comparisons of the wave parameters. Outputs of the numerical wave model SWAN were as well retrieved at the nearest point from the location of the ADCP. It is assumed that the wave conditions are similar at the different analysis and measurement points because the bathymetric variations in the coastal waters of Yantai are smooth. At low sea state, no wind direction was recorded by the HF radar. Only a validation of the wind forcing used in SWAN could be performed comparing the wind direction and the wind speed modelled by DWD with the wind parameters measured by the coastal station Zhi Fu Dao. Similarly, the wind fields from DWD were extracted at the closest grid cell to this station (11km separate the two comparison points).

The HF significant wave height was filtered over the time to remove spurious noise. A low-pass filter that consists in selecting the local minima was applied to remove unrealistic high wave heights recorded by the HF radar. In addition, the data was discarded from the dataset when the differences between two consecutive values was greater than 1m [Wyatt and Green, 2009]. Finally, the signal was smoothed by means of a moving average of 4 hours. The difference between raw and filtered HF significant wave heights is shown in Figure 3.3. The same smoothing procedure was applied on the wave heights measured by the ADCP to remove the outliers. At low sea state, the filter reduced significantly the noise within the raw data but it lead to a total percentage reduction of 69% of the original wave height data at the considered analysis point. No filter was applied to the directional data.

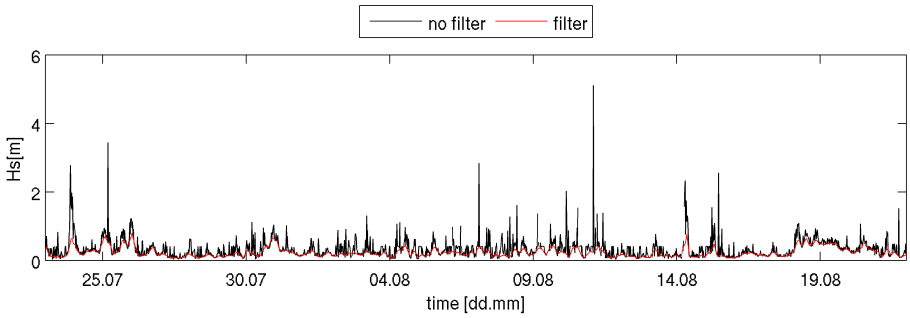

Figure 3.3: HF radar significant wave height before (black line) and after filtering (red line) at low sea state at the analysis point in the HF radar domain.

During low sea state conditions, small waves with a mean wave height of 0.17m and a maximum wave height of 0.87m propagate near Yantai. Figure 3.3 shows the wave distribution at low sea state conditions near Yantai based on the ADCP measurements (Figure 3.4 (a)) and on the SWAN outputs (Figure 3.4 (b)). Similar wave conditions are observed in the ADCP measurements and in the model outputs. According to the figure, the small amplitude waves are associated to weak south/southwestern winds. It can be seen that the wave and the wind directions coincide. The wind blows with a wind speed smaller than 10m/s during normal conditions. Waves generated by southern winds have a low fetch

which explains the low characteristics waves that are observed. Not only the short fetch is a reason for the generation of the low waves. Southern waves that propagate from the Yellow Sea refract at the eastern part of the Shandong peninsula. These waves reach the shallow waters of Yantai with a low height and period.

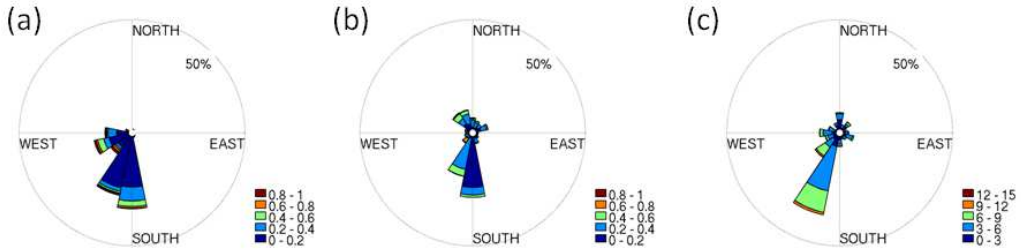

Figure 3.4: Wave roses from the data measured by the ADCP (a), modelled by SWAN near the ADCP (b) and wind rose from the data measured at the coastal station Zhi Fu Dao (c) at low sea state.

Error estimation

The purpose of the present analysis is the validation of the HF radar data by means of comparison with in-situ measurements and numerical model outputs at low sea state. The Root Mean Square Error (RMSE) is used here to estimate the accuracy of the HF radar measurements and to represent the performance of the wave and the meteorological models whose outputs are used to force the latter. Formulation in Equation (3.1) was used to quantify the errors of the linear and directional data.

$$RMSE = \sqrt{\frac{1}{N}\sum_{i=1}^{n}(x_i - y_i)^2} \tag{3.1}$$

Where N is the total number of samples, x_i and y_i are the vectors of data being compared.

Comparisons between the significant wave heights recorded with the HF, the ADCP and the outputs of SWAN at low sea state are shown in Figure 3.5 (a). Though the HF radar and the wave model tend to slightly overestimate the significant wave height, a good agreement between the model and the observations was found. A RMSE of 0.16m is found between the significant wave heights of the HF radar and the model SWAN. An error of 0.12m is found between the significant wave height measured by the HF radar and the ADCP. The results are listed in Table 3.1. Figure 3.5 (b) shows a comparison of the wave direction between SWAN outputs, the HF radar and the ADCP measurements. The wave model reproduced well the wave direction measured by the ADCP expect during the first week of measurements period (total RMSE of 72.6°). The HF radar could not capture reliable directional wave data, an error greater than 124° with the ADCP measurements and the model results was found. The HF radar did not record any wind direction data during the considered period. As a result, only the comparison between the wind direction measured at the coastal station Zhi Fu Dao and modelled by the meteorological model of DWD is shown in Figure 3.6. A good agreement was found between the two sets of data in terms of wind speed, i.e. RMSE of 1.62m, and of wind direction, i.e. RMSE of 62°. The wind fields from DWD are accurate enough to provide reliable wave predictions at low sea state.

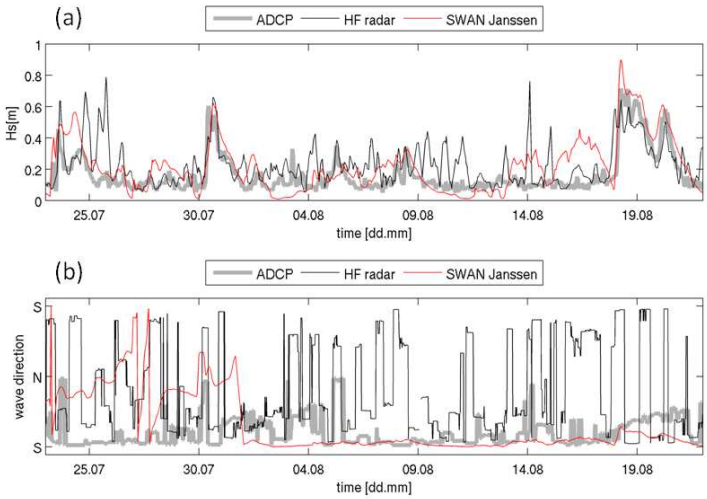

Figure 3.5: Comparison of significant wave height (a) and wave direction (b) between the numerical model SWAN and the field measurements from HF radar and ADCP at low sea sate.

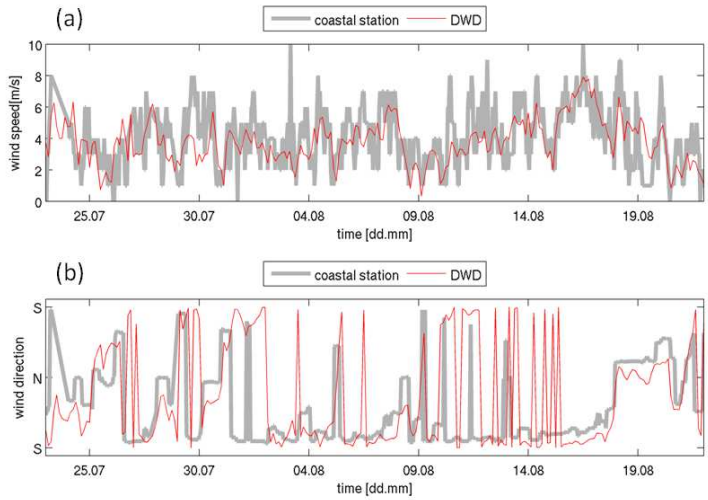

Figure 3.6: Comparison of wind speed (a) and wind direction (b) between the numerical model DWD and the field measurements of the coastal station Zhi Fu Dao at low sea sate.

Table 3.1: Root Mean Square Errors for the significant wave height, the wave direction, the wind direction and the wind speed at low sea state.

	HF radar	**SWAN**	**ADCP**	**DWD**	**ZFD**
Hs					
HF radar	-	0.16	0.12	-	-
SWAN	0.16	-	0.11	-	-
Wave direction					
HF radar	-	125.9	124.7	-	-
SWAN	125.9	-	72.6	-	-
Wind direction					
DWD	-	-	-	-	62.0
Wind speed					
DWD	-	-	-	-	1.62

Validation of High Frequency radar data at high sea state

Analysis of the significant wave height, the wave and the wind direction

Similarly to the validation of HF radar data during low sea state conditions, wave and wind conditions are analysed during high sea conditions. A period of 7 days from the 20^{th}, September 2013 to the 27^{th}, September 2013 during which a storm occurred was taken into account.

The analysis of the significant wave height and the wave direction was proceeded at the locations described in a previous section. The signal backscattered from the waves during stormy conditions has a higher amplitude and the HF radar could record wind direction data. In such conditions, the backscattered signal is stronger and the second-order regions of the Doppler spectra are less sensitive to external noise. As a result, less errors occur during the extraction of the wave parameters at high sea states. The HF radar did not record the wind magnitude. We upscaled the HF radar wind direction data to enable realistic comparison with the outputs of the global meteorological model DWD. In more details, the average of the dominant wind direction over the radar measurement grid was evaluated and was compared to the 30km spatial data of the meteorological model. The measurements of the wind direction at the coastal station Zhi Fu Dao are used as a benchmark for the following statistical analyses.

The filtering of the data is described in the section above. For high sea state, 25% of significant wave height measured by HF radar remains exploitable after filtering. The significant wave heights measured by HF radar before and after the filter are visualised in Figure 3.7. A maximum significant wave height of 2.6m was recorded by the HF radar during the storm.

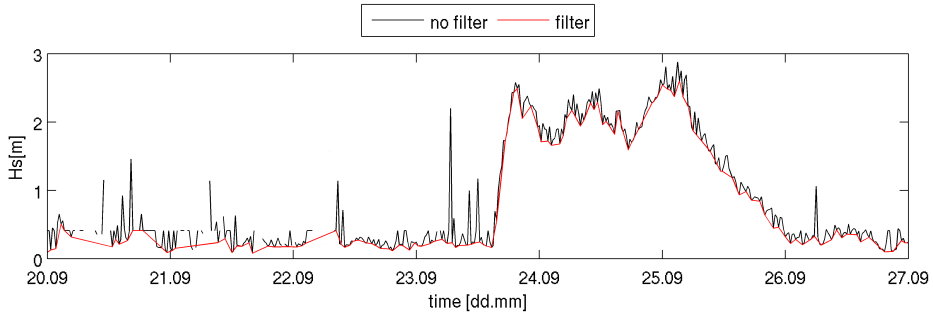

Figure 3.7: HF radar significant wave height before (black line) and after filtering (red line) at high sea state at the analysis point in the HF radar domain.

Considering the data measured by the ADCP during the storm of September 2013 near Yantai, the waves reach a maximum significant wave height of 2.10m and propagate from the north and northeast (Figure 3.8). The average wave height is 0.65m. These high and long waves are generated by strong northeastern winds whose maximal magnitude is 15m/s (Figure 3.8 (c)). Steady northeastern winds blowing over maximum fetches of 300km within the Bohai Sea during cold outbreaks can generate high and long waves. The measurements of the ADCP (Figure 3.8 (a)) coincide with the outputs of the wave model SWAN (Figure 3.8 (b)) in terms of wave height and wave direction.

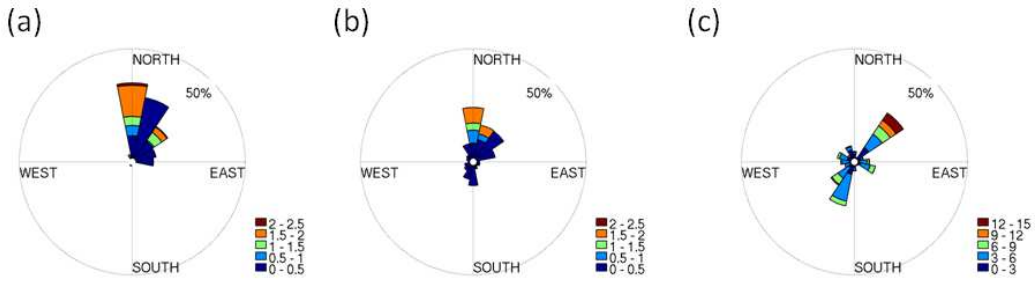

Figure 3.8: Wave roses from the data measured by the ADCP (a), modelled by SWAN near the ADCP (b) and wind rose from the data measured at the coastal station (c) for high sea state conditions.

Error estimation

The estimation of the HF radar accuracy during stormy conditions is based on the comparisons of wave and wind parameters between the different sources of data. The Root Mean Square Errors are evaluated for each parameter (Equation (3.1)) and are listed in Table 3.2. Also, the performance of the wave model SWAN and the meteorological model of DWD during stormy conditions could be evaluated. The comparisons of the significant wave height measured by the HF radar, by the ADCP and modelled by SWAN are shown in Figure 3.9 (a). RMSE around 0.20m are found which indicates that the significant wave heights recorded by HF radar are in good agreement with the ADCP measurements and the SWAN outputs. The RMSE are higher during stormy conditions than during calm conditions. This could be explained on the one hand, by the difference of time length be-

tween the two considered periods (one month of calm conditions versus one week for stormy conditions). On the second hand, the differences in wave height from the different data are stronger at the peaks of the storm. While the HF radar overestimates the significant wave height, the model SWAN reproduces well the measured significant wave height (RMSE of 0.15m). The wave direction measured by the ADCP and the HF radar are in good agreement with the model outputs. Errors lower than 25° were found (Table 3.2). The performance of the HF radar in reproducing the wind direction pattern is however low (error of 140°). The accuracy of the driving wind fields from DWD during stormy conditions was assessed as previously in Figure 3.10, namely in comparing modelled winds with the wind measurements of the coastal station. Higher wind speeds could not be well reproduced by DWD. It explains why the modelled wave height is slightly underestimated in comparison to the ADCP and the HF radar wave height measurements. A better agreement is found for the comparison of the wind direction (69.4°).

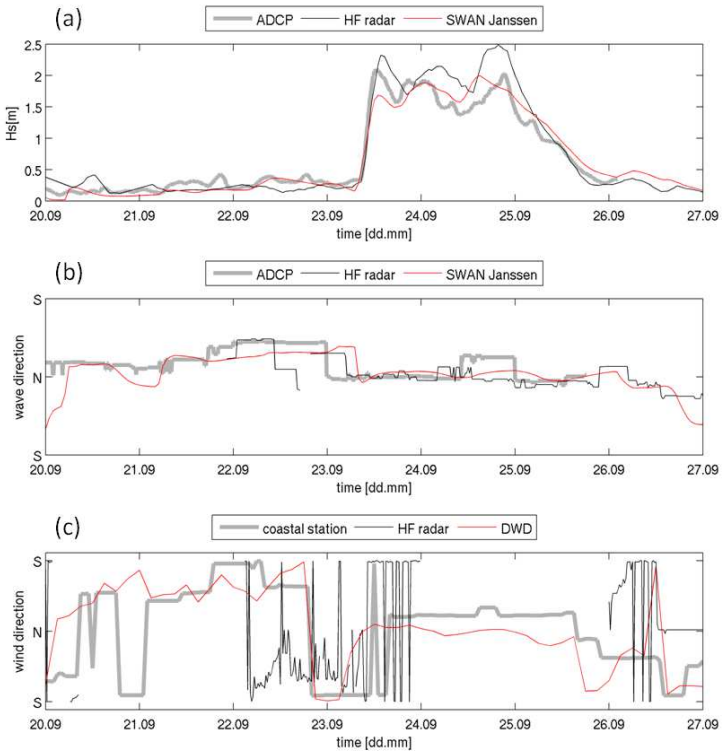

Figure 3.9: Comparison of significant wave height (a), wave direction (b) and wind direction between the numerical models (SWAN and DWD) and the field measurements (HF radar, ADCP and coastal station) at high sea sate.

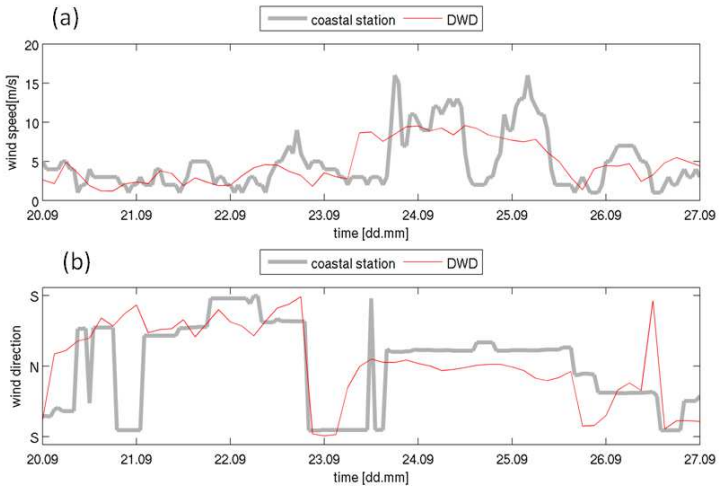

Figure 3.10: Comparison of wind speed (a) and wind direction (b) between the numerical model DWD and the field measurements of the coastal station Zhi Fu Dao at high sea sate.

Table 3.2: Root Mean Square Errors for the significant wave height, the wave direction, the wind direction and the wind speed at high sea state in the vicinity of the ADCP.

	HF radar	**SWAN**	**ADCP**	**DWD**	**ZFD**
Hs					
HF radar	-	0.22	0.25	-	-
SWAN	0.22	-	0.15	-	-
Wave direction					
HF radar	-	19.9	22.3	-	-
SWAN	19.9	-	25.1	-	-
Wind direction					
HF radar	-	-	-	141.7	131.2
DWD	141.7	-	-	-	69.4
Wind speed					
DWD	-	-	-	-	2.94

Wave climate in the coastal waters of the Shandong peninsula and Yantai

The waves were simulated with the model SWAN for a period of 6 years between 2008 and 2014 to determine the wave climate in the north of the Shandong peninsula and near Yantai. The distribution of the maximum and mean wave heights over the 6 years in the coastal waters of the Shandong peninsula are showed in Figure 3.11. The average maximum and mean values of the significant wave height are 2.95m and 0.40m for the considered region. These results are in agreement with the work of Lv et al. [2014] who found an annual mean significant wave height of 0.47m in the Bohai Sea. Highest waves are found at the east of the peninsula where an extreme event can trigger waves of 7m. This region is less sheltered by the land and is prone to higher wave activity. On the contrary, lower maximum wave heights are found at the west of the peninsula. The distance from the open sea, i.e. the Yellow Sea and the the Bohai strait that is characterized by many islands dissipate and intercept high waves. The seasonality of the waves in the coastal waters of Yantai are shown

in the wave roses of Figure 3.12. We considered the following seasons : spring (April-May), summer (June-August), fall (September-October) and winter (November-March). Highest waves occur in winter (Figure 3.11 (d)), propagate from the west and reach a maximum of 5.20m between 2008 and 2014. An average wave height of 0.90m was found near Yantai in winter. Smallest waves (average wave height of 0.40m) are observed during the summer (Figure 3.12 (b)) and propagate mainly from the southwest or from the east. These results support the work of Wang et al. [2012], Lv et al. [2014]. Highest waves in summer reach a height of 3.50m during typhoons. During fall and spring that are transition seasons between the northeast and the southwest monsoon, the mean and maximum wave heights are similar. The dominant wave direction varies however from one season to another due to the East Asian monsoon.

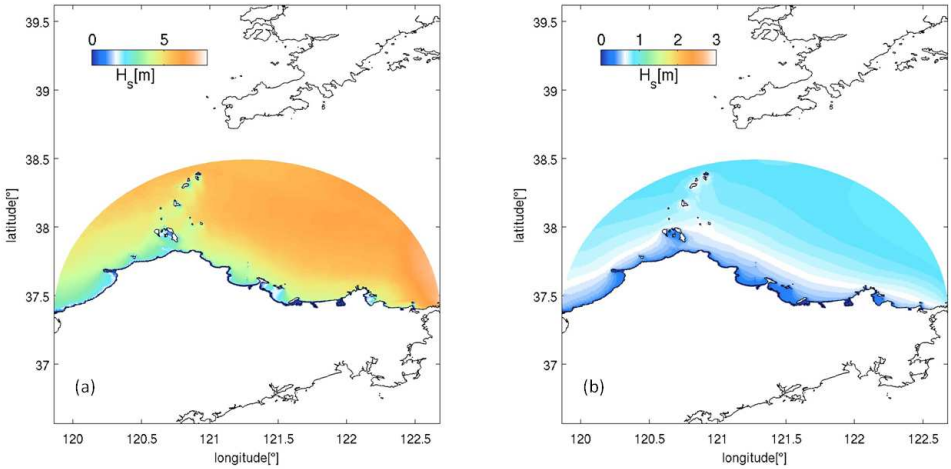

Figure 3.11: Maximum (a) and mean (b) significant wave height in the Shandong peninsula between 2008 and 2014.

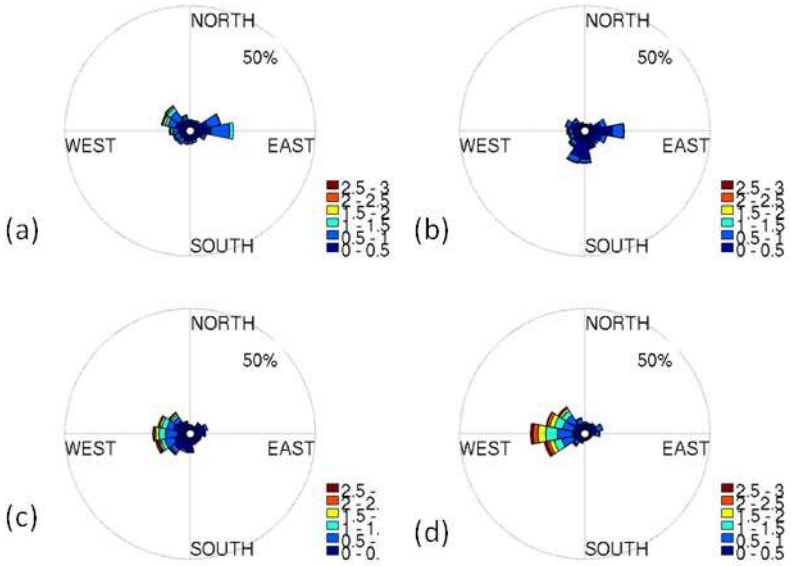

Figure 3.12: Wave roses in spring (a), summer (b), fall (c) and winter (d) between 2008 and 2014 in the vicinity of Yantai.

Conclusions

The goal of this work was to validate the data recorded by a HF radar, a remote-sensing technology recently deployed along the coast of Yantai in China. An important advantage of the HF radar is the simultaneous acquisition at a single time of data over a large surface. The wave data of the HF radar was compared to the in-situ wave measurements of a bottom-mounted Acoustic Doppler Current Profiler and the outputs of the numerical model SWAN. Similarly, the wind data measured by the HF radar was compared to the measurements of a coastal station in Yantai and the outputs of the meteorological global model of the German Weather Service. This study aimed as well at the evaluation of the performance of the numerical models SWAN and DWD which is used to force the wave model.

To assess the performance of the HF radar under different wave conditions, analyses were conducted at low and high sea state conditions. The HF data contained spurious noise, at both calm and stormy conditions and a low pass filter was used to smooth the signal. The main drawback of such a filter is the loss of data, until 75% of the total raw data in some cases. The HF radar captured well significant wave heights at low and high sea states, provided that the analysis point is located within the overlapping area of two HF radar stations. A Root Mean Square Error of 0.12m was found between the wave height measured by the radar and the ADCP at low sea state. The HF radar overestimated however the peaks of significant wave height but reproduced well the wave direction during stormy conditions. The HF radar performed less accurately for the measure of the wave and the wind direction during calm conditions. This is due to the low amplification of the radar backscattered signal. As a result, the device recorded sparse and poor quality directional wind data.

The numerical wave model SWAN reproduced well the wave characteristics for all sea state conditions. The role of the formulation of the wave growth by wind for the wave

predictions in the Bohai Sea and in the coastal waters of Yantai was investigated. The formulation after Janssen [1991] was preferred to capture waves higher than 0.7m. Small discrepancies at high sea state in the modelled wave height were induced by inaccurate wind forcing. Indeed, an underestimation of the wind speed in the DWD wind fields lead to a slight underestimation of the significant wave height at high sea state. At low sea state however, the modelled wind parameters were in good agreement with the measurements of meteorological parameters of a coastal station in Yantai. Results of the simulations showed that large waves were generated by strong north to northeastern winds whereas small waves were generated by weak south to southwestern winds during the summer of 2013.

The validated wave model was run over a period of 6 years, more precisely between 2008 and 2014. The wave characteristics were assessed in the north of the Shandong peninsula and in the coastal waters of the city of Yantai. The East Asian Monsoon highly influences the wave seasonality in the area of interest. Near Yantai, southern waves with a mean wave height of 0.40m are dominant in summer. During the winter, the waves are higher and propagate from the west. A mean wave height of 0.90m with a maximum wave height of 5.20m were found for this season. Fall and spring correspond to transition seasons between the two monsoon systems. These seasons are characterized by similar wave heights (0.50m in average) with opposite directions. The mean wave height in the north of the Shandong peninsula between 2008 and 2014 is 0.40m. Highest waves propagate at the east of the peninsula. They are generated within the Yellow Sea and refract into the Bohai Sea through the peninsula. On the contrary, due to the sheltering effect of the islands forming the Bohai Strait, the west of the peninsula is hit by waves with a lower amplitude.

Acknowledgements

The authors wish to thank the experts from Helzel Messtechnik GmbH, Kaltenkirchen for the profitable discussions in the field of radar data processing. We are also grateful to the German Weather Service (DWD) for providing the global wind data..

Funding

This work was supported by the German Ministry of Education and Research (BMBF) [grant number 03F0632A].

Decision Support System for the management of the Shandong Peninsula, China

G. Dalledonne, X. Zheng, N. Fery, C. Tang and R. Mayerle

35^{th} International Conference on Coastal Engineering
Antalya, Turkey
November 2016

Decision Support System for the management of the Shandong Peninsula, China

Guilherme Dalledonne(1), Xiangyang Zheng(2), Natacha Fery(3), Cheng Tang(4) and Roberto Mayerle(5)

(1) Research and Technology Centre, University of Kiel, dalledonne@corelab.uni-kiel.de
(2) Research and Technology Centre, University of Kiel, xyzheng@corelab.uni-kiel.de
(3) Research and Technology Centre, University of Kiel, fery@corelab.uni-kiel.de
(4) Yantai Institute of Coastal Zone Research, Chinese Academy of Sciences, ctang@yic.ac.cn
(5) Research and Technology Centre, University of Kiel, rmayerle@corelab.uni-kiel.de

Abstract

A Decision Support System (DSS) for supporting decision makers in the management of the Shandong Peninsula has been developed. Emphasis has been given to coastal protection and coastal cage aquaculture. The investigations were done in the framework of a joint research project funded by the German Ministry of Education and Research (BMBF) and the Chinese Academy of Sciences (CAS). In this paper a description of the DSS, the development of its components, and results of its application are presented.

The system integrates in-situ measurements, process-based models and a database management system. Models for simulation of flow, waves, sediment transport and morphodynamics covering the entire Bohai Sea were developed. The grid resolution ranges from about 1000m on the Bohai Sea to less than 200m along the coast [Dalledonne and Mayerle, 2016, Fery et al., 2017]. The Delft3D modelling suite (Deltares) is used. Calibration and validation were done using water levels at several stations, current velocities and waves from moored Acoustic Doppler Current Profiler (ADCP) and High Frequency (HF) radar in the vicinity of Yantai. In order to enable cost-effective and scalable applications, a database management system was developed. It enhances information processing, data evaluation and supports the generation of data products.

Results of the application of the Decision Support System (DSS) to the management of coastal protection, coastal cage aquaculture and harbours are presented here. Model simulations covering the most severe storms observed during the last decades were carried out leading to an improved understanding of hydrodynamics and morphodynamics [Dalledonne and Mayerle, 2016]. Results helped in the identification of coastal stretches subjected to higher levels of energy and to improved coastal protection measures.

Introduction

The Bohai Sea is a shallow water region situated in the northern part of China. The sea and its surrounding provinces are rich in natural resources and are subject to stringent marine environment preservations. The sea covers an area of approximately $79000 km^2$ with average depths of about 18m. It is rather shallow except for the submerged valley near the north of the Bohai Strait, the only connection with the Yellow Sea (Figure 3.13).

The Shandong Peninsula is located between the Bohai Sea and the Yellow Sea in the east of China. It is the largest peninsula in China with 3000km of coastline. The Shandong province is an important fishery and fish farming area, and it holds the first place in marine food production in China. However, during the last decades, harbours and industries have been expanding rapidly, which might threaten the water quality. In addition, storm surges, green tides and coastal erosion are big concerns in this area.

In order to assess coastal environment hazards in terms of hydrodynamic conditions, a Decision Support System (DSS) was developed for the Shandong Peninsula. The DSS provides more comprehensive information to decision makers and enables to link model results (e.g. water level, currents and waves) with practical applications (e.g. suitability map for aquaculture). Model results are assessed by defining specific criteria and thresholds for hydrodynamic parameters. The DSS is considered to be a helpful tool to assist decision makers in finding solutions for the management and preservation of the Shandong coast.

Modelling studies in the Bohai Sea and in the Yellow Sea began in the mid 1980's. According to Huatong and Wang [1985], the flow circulation in the Bohai Sea is mainly due to the combined effect of tidal forcing and winds. Although northerly winds prevail in winter, during flood season (summer/autumn) river discharges affect tidal currents to a certain extent. Fang and Yang [1985] used a two dimensional shallow water equation to compute the diurnal and semi diurnal tide; the authors found a new current amphidromic point. Yu and Zhang [1987] simulated the water level and tidal current with a three dimensional model; their result agreed well with observations. They pointed out that the tidal residual current is usually very weak. Zhao and Shi [1993] modelled the wind-driven current in summer and winter. They discussed the current velocity on different layers and the current on the profile of Bohai Strait. Wang used a three dimensional model with an unstructured mesh to study the seasonal circulation in Bohai Sea and found that the density structure due to the temperature stratification of sea water is an important factor in summer, but can be negligible in winter [Wang et al., 2010]. Ding and Ding [2014] simulated a storm surge which occurred in October, 2003 over the Bohai Sea and they concluded that the nonlinear combination of wind and tide is necessary for accurate simulation of the surge.

Several studies about wave modelling in the Bohai Sea and in the Yellow Sea are also available. Yanling et al. [2012] used the model WAVEWATCH-III (WW3) to study wind-wave characteristics in the Bohai and Yellow Sea. Liang et al. [In-Press] simulated waves with the model Simulating WAves Nearshore (SWAN) over 22 years to analyse the variations of wave height on a long-term scale. Lv et al. [2014] also used the model SWAN to simulate waves over 20 years.

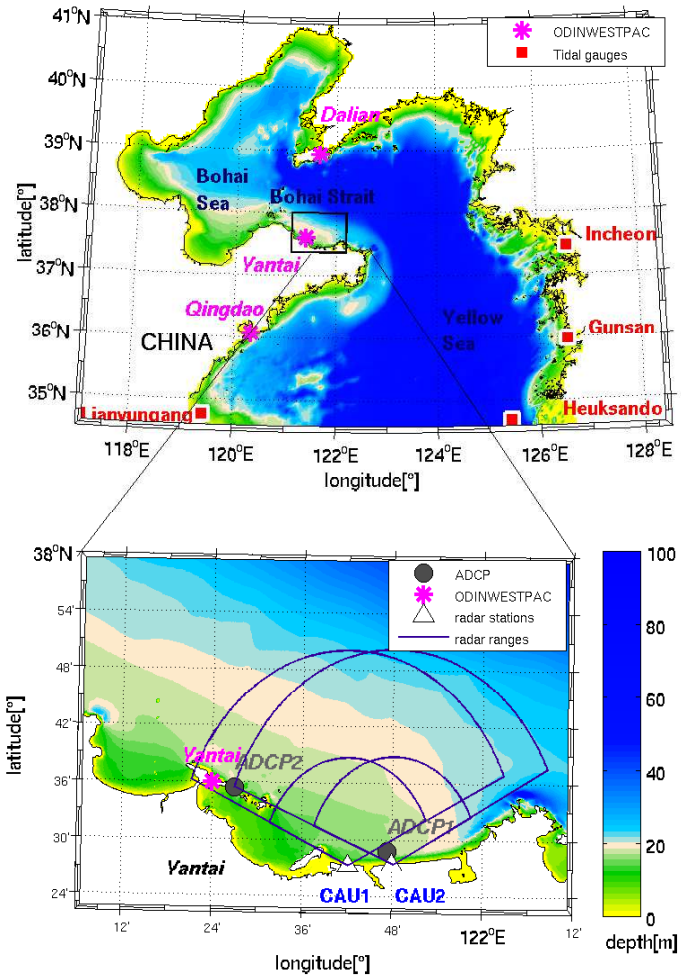

Figure 3.13: Area of interest, locations of recording devices and bathymetry.

The current study consists in the development of a Decision Support System. The system is based on the results of a hydrodynamic model, which must be first set up. After that, the definition of criteria and respective thresholds related to relevant coastal activities is followed. At last, the combination and analysis of model results with all selected criteria is presented in graphical form (maps). All modules are integrated into a database management system and an operational system.

Numerical model description

The numerical model used in this study was set up based on the Delft3D suite, developed by Deltares. The model is composed by several modules that can be combined. In the present study modules of flow and wave have been implemented. The flow module solves the continuity, motion and transport equations under shallow water assumption. The wave module solves the discrete spectral action balance equation using the 3^{rd} generation spectral wave model SWAN [Booij et al., 1999, Ris et al., 1999]. The interaction between the flow and wave modules takes into account the effect of waves on current via forcing, enhanced turbulence and bed shear stress. In return, the effect of the waves on currents via wave set-up, current refraction and enhanced bottom friction is as well taken into account.

Grid

A nesting sequence was applied to study the currents and waves at the northern coast of the Shandong Peninsula (Figure 3.14). A coarser rectangular model grid (BYS) covers the Bohai/Yellow Seas above the parallel of 34.5° with ca. 5km grid resolution. This coarser grid is used to provide boundary conditions (water level, currents and waves) to a finer circular model grid (SNS), centred close to the Yantai urban area. The finer grid covers the northern part of the Shandong Peninsula with a horizontal grid resolution varying from 0.2km onshore up to 1km offshore. Both model grid are shown in Figure 3.14.

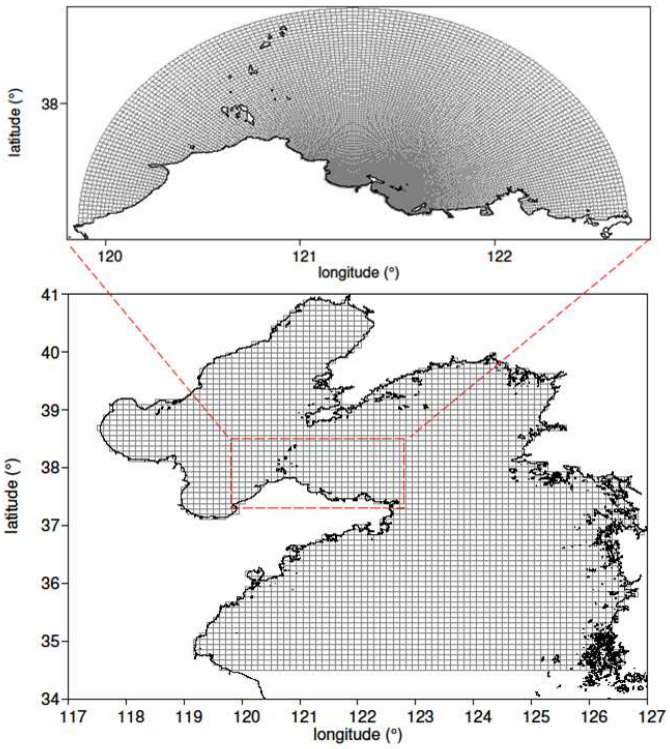

Figure 3.14: BYS (below) and SNS (above) model grids.

Bathymetry

The model bathymetry in the model is based on the digitization of nautical charts and on data from the GEneral Bathymetric Charts of the Oceans (GEBCO) with a resolution of about 1km. Nearshore bathymetric data from a measuring campaign was also taken into account (personal communication).

Driving forces

The BYS model has an open boundary in the south, where tidal forcing is imposed based on the Global Model of Ocean Tides (TPXO). Water levels and wave spectrum information from the coarser model is imposed at the open boundaries of the finer model as time series. Wind and pressure fields available from the global model of the German Weather Service (DWD) with spatial and temporal resolution of ca. 30km and 3h, respectively, are imposed on the model free surface [Majewski et al., 2002].

The model is forced with open boundary condition and sea surface boundary condition. Nine tidal constituents (M2, S2, N2, K2, K1, O1, P1, Q1, M4) provided by the TPXO were interpolated to the open boundary of the larger model. The resolution of the TPXO data is 1/30° in the China Seas. The open boundary condition of temperature and salinity were from HYbrid Coordinate MOdel (HYCOM), which a global model with resolution of 1/12°.

Calibration and validation of the hydrodynamic model

Sensitivity analysis results showed that a two-dimensional depth-integrated approximation (2DH) can be assumed for describing flow and transport processes in the region reasonably well. Only in summer, when density currents are stronger, monthly averaged currents cannot be used for the current profile approximation.

Tides

The BYS flow model was calibrated on the basis of tidal components at the stations Dalian and Lianyungang. Figure 3.15 shows good agreement of measured and simulated tidal components at the two stations. At Dalian, in the north, the correlation coefficient between measured and modelled values is 0.99 whereas at Lianyungang, close to the open boundary, the correlation is 0.93.

Currents

Depth-averaged values measurements from a stationary ADCP deployed in the Yantai Bay in September 2013 at a water depth of about 17m have been used as depth-averaged values. The comparison of water levels and current velocities in Figure 3.16 shows a good agreement between measured and computed values.

The modelled surface current was also compared to HF radar surface currents and to ADCP currents. In Figure 3.17 it can be seen that the east component agrees much better than the north component of surface current. The reason is that the tidal current is flowing along the coastline and its north component is very weak; the model cannot simulate the small scale wind-induced current velocity due to the relatively coarse temporal resolution. According to a previous study [Chapman et al., 1997], the accuracy of HF radar measured is about $7cm/s$, which is closer to the order of the north component of the surface current. Thus, the model can reproduce reasonably well current velocities in this area.

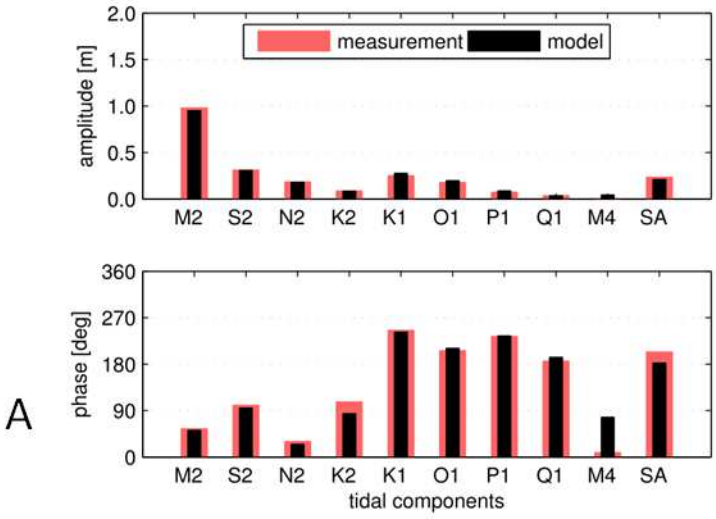

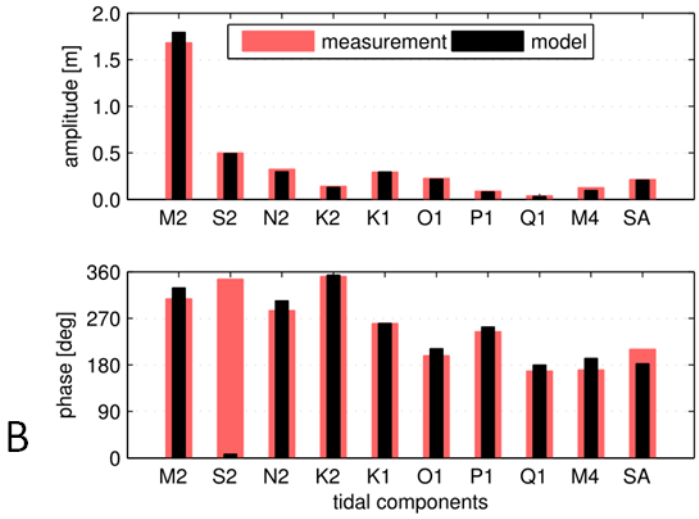

Figure 3.15: Comparison of tidal harmonics obtained on the basis of measured and modelled values at stations (A) Dalian and (B) Lianyungang.

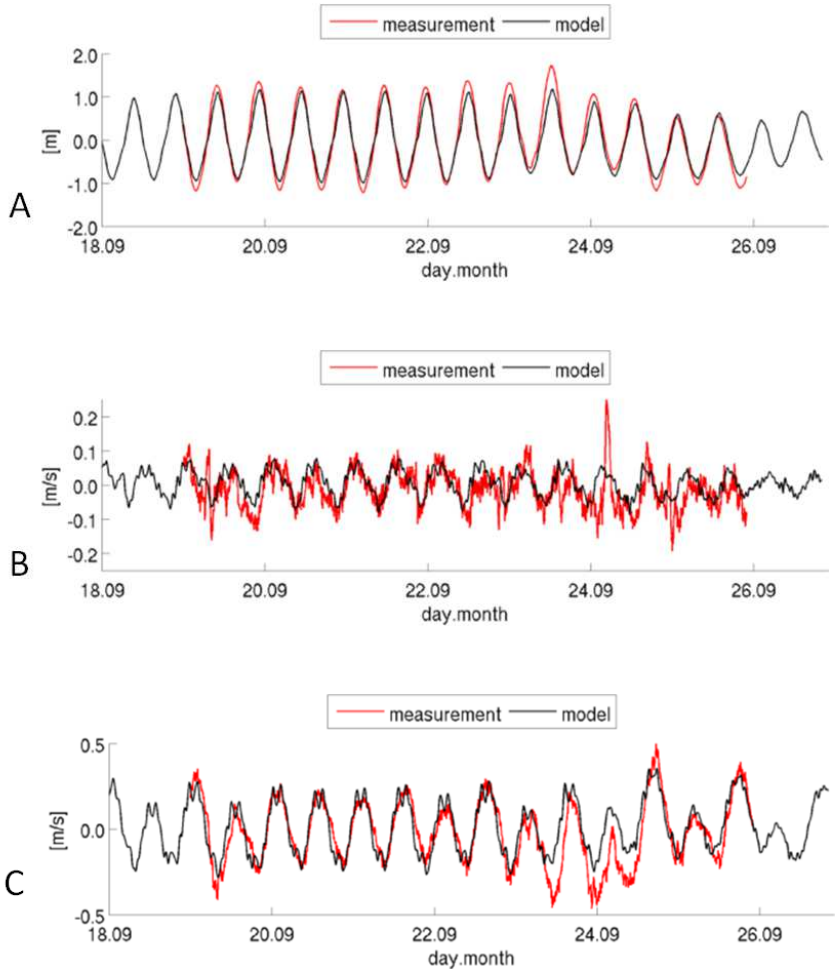

Figure 3.16: Measured versus computed (A) water levels, (B) east-west currents and (C) north-south currents.

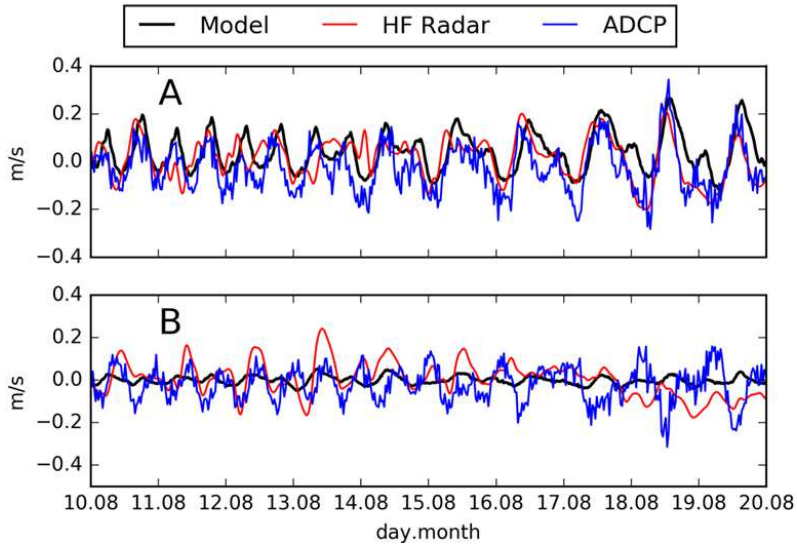

Figure 3.17: Surface current velocity comparison of model, HF radar and ADCP in the early August 2013. (A) east-west component; (B) north-south component.

Waves

For calibration and validation of the wave model measurements from the ADCP and from the HF radar have been used. Best settings of the wave model were found by comparing the model outputs to these measurements. A good agreement is found between the significant wave modelled by SWAN and the in-situ measurements (Figure 3.18). A correlation of 0.83 is found between the model and the ADCP measurements, and 0.70 between the model and the HF radar wave height.

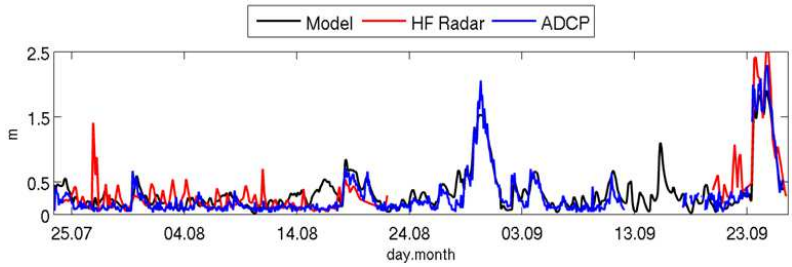

Figure 3.18: Comparison of the significant wave height measured by the ADCP, the HF radar and modelled by SWAN.

Decision Support System

A Decision Support System (DSS) can be defined as a computer-based information system that supports decision-making activities. DSSs serve the management, operations, and planning levels of an organization and help people making decisions about problems that may be rapidly changing and not easily specified in advance, and also problems that require information from different fields of expertise to be translated into actions and practical results.

The DSS developed for the Shandong Peninsula has been conceived to provide available real-time hydrodynamic information, to identify suitable areas on the coast according to coastal activities, and to determine vulnerable coastal zones to extreme weather events.

The system relies on hydrodynamic results from numerical models, i.e. currents, waves and sediment dynamic. A five-year period and 21 storm events are included in the simulations.

The DSS includes an operational module responsible for executing the simulations and update the results in the database, a suitability module in which criteria for each selected activity are defined and applied in the evaluation of results, and a vulnerability module in which physical characteristics are defined, classified and then also applied in model evaluation.

Operational module

The numerical model is integrated into a Nowcast/Forecast System (NFS) for the Shandong Peninsula. The system consists of a numerical model, an automatic measuring network, a database and a website for visualizing the forecasts. The database is the central component of the NFS system, as other components work independently and exchange data only with the database. Usage of the database standardizes data format and facilitates system development and maintenance. In addition, users have immediate access to graphical model results via the website.

A forecast cycle starts from downloading forecasted meteorological data and, open boundary data and storing them in the database. The two sets of data, provided by the Global Forecast System (GFS) and HYbrid Coordinate MOdel (HYCOM) respectively, force Delft3D over the sea surface and on the open sea boundaries. Once the NFS detects updated forcing data, it will prepare boundary conditions using Global Forecast System (GFS) and HYCOM data and generate initial conditions from the last forecast cycle for the BYS model. Then the BYS model will run and provide a 6-hour forecast of water level, 3D current velocity, salinity, temperature and wave. As the general model in the nesting system, the BYS model also generates open boundary conditions for the SNS model and stores it in the database. The SNS model will run in the same way as the model BYS. All the model results are stored in the database for display, for the following forecast cycle and for other applications in the DSS system. The forecast results are made available in a website as shown in Figure 3.19.

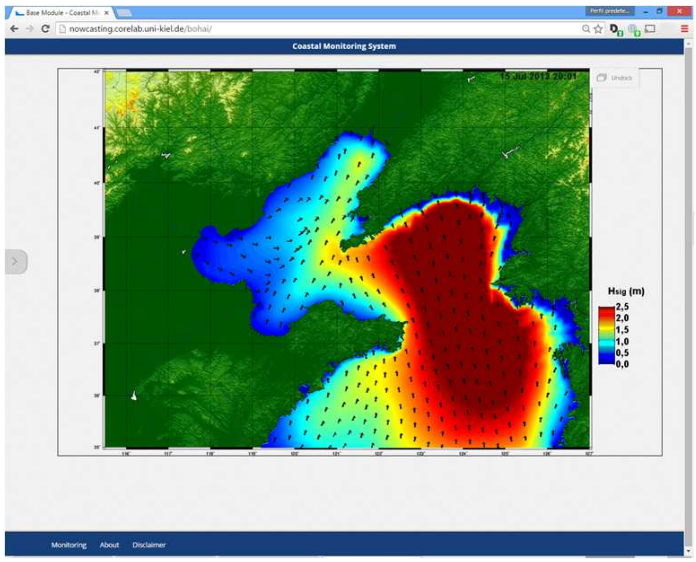

Figure 3.19: The nowcasting website.

Suitability module

Coastal activities along the Shandong Peninsula are very diverse and range from fish farming (offshore cage culture, mussels and sea cucumber culture), going through harbours and industrial activities (mineral and energy), to tourism (recreation as well). Finally, the DSS has been used to determine the suitability of coastal activities planned by the Chinese government (Figure 3.20).

The coastal planning of the peninsula is used for comparison with the results of the DSS. Indeed the DSS is used to evaluate the allowed spatial distribution of the coastal uses found in the planning taking the hydrodynamic conditions of the area into consideration.

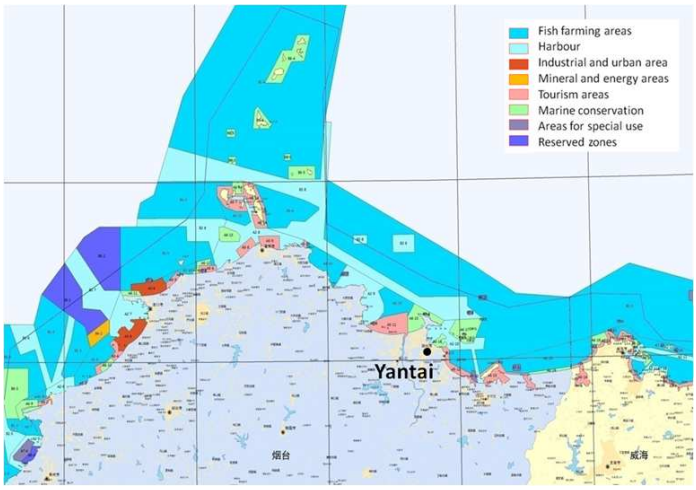

Figure 3.20: Coastal activities plan from 2011 to 2020 in Shandong Province according to the Government of Shandong Province (2012).

Each coastal use is affected by different environmental parameters. A set of parameters is thus selected for each activity based on recommended values found in the literature. As an example, the offshore cage farming requires a minimum and a maximum water depth, current velocities and significant wave height to enable optimal conditions for fish production. Thresholds have been set for those parameters that define allowable and optimal ranges. A value is considered allowable when it does not contribute to harm the environment or a given coastal use. A value is considered optimal when it fits the best conditions required for a given coastal use. The values of the thresholds are based on the literature or on simple assumptions when references cannot be found.

Table 3.3 and Table 3.4 show the parameters and their corresponding thresholds for offshore cage culture and harbours respectively, the two most important activities identified in the vicinity of Yantai.

Table 3.3: Criteria for offshore cage culture [Chen et al., 2008].

Parameter	**unit**	**statistic**	**allowable**	**optimal**
min water depth	m	min	>10	>10
max water depth	m	max	<30	<30
min current velocity	m/s	min	$\geq$ 0.0	>0.5
max current velocity	m/s	max	<1.2	<1
wave height	m	max	<2	<1

Table 3.4: Criteria for harbours [Liu and Burcharth, 1999].

Parameter	**unit**	**statistic**	**allowable**	**optimal**
min water depth	m	min	>4	>4.5
max water depth	m	max	<31.2	<31.2
anchorage depth	m	max	<60	<60
max current velocity	m/s	max	<1.5	<1
wave period	s	max	<12	<7
wave height	m	max	<3	<1
wind speed	m/s	max	<20	<10

In the next figures, the defined ranges for each criterion have been classified into optimal and allowable, as already explained. In order to facilitate visual interpretation, the suitability maps have been generated following the traffic light principle: above the optimal threshold was assigned the green colour, between the allowable and the optimal thresholds the yellow colour, and below the allowable threshold the red colour was assigned.

The following Figure 3.21 and Figure 3.22 show the resulting suitable sites for fish farming and harbours respectively, obtained from averaged conditions within five years of model results. Polygons show the Chinese coastal plan regarding each activity.

Fish farming is suited everywhere along the shore, apart from very shallow areas close to the coastline (where the depth is smaller than 10m), and the suitable areas are in good agreement with the current coastal plan. Harbour activities are more restricted to regions with moderate hydrodynamic conditions. Results show that the most northern part of the peninsula is more exposed to wave action and strong currents among islands, indicated by large red regions. Light blue triangles along the coast indicate existing harbours.

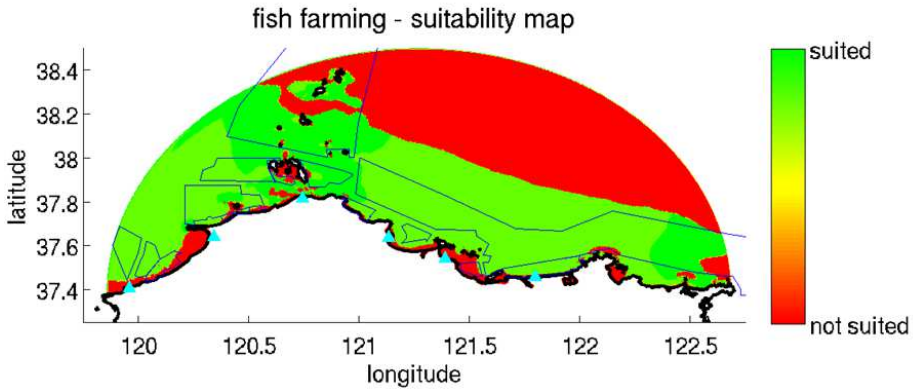

Figure 3.21: Suitability map for offshore cage culture.

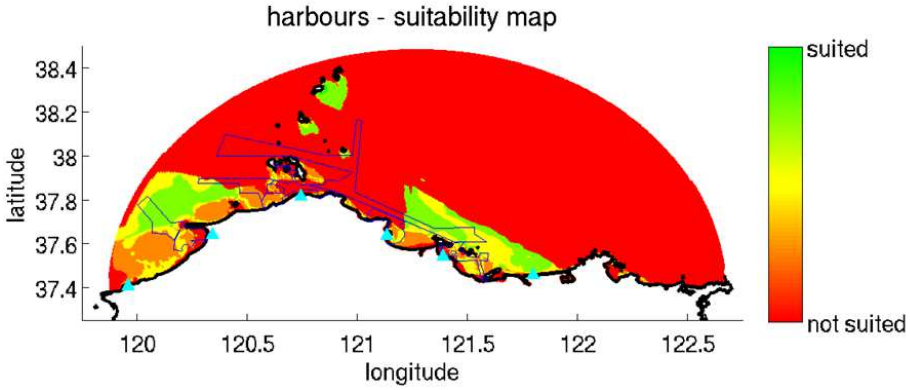

Figure 3.22: Suitability map for harbours.

Figure 3.23 and Figure 3.24 show the resulting suitable sites for fish farming and harbours respectively, obtained from averaged conditions within storm periods. Polygons show the Chinese coastal plan regarding each activity. Comparisons between the results and the existing coastal plan show in general good agreement. However, due to strong hydrodynamic conditions, offshore cage culture is not recommended on the east of the peninsula. Besides, care should be taken in the planning of floating fish cages in the north of the Bohai Strait. Apart from the long and thin polygons representing ship traffic routes, the ones connected to land (four areas in the figure) present allowable ranges for harbour activities, according to Table 3.4. Light blue triangles along the coast indicate existing harbours.

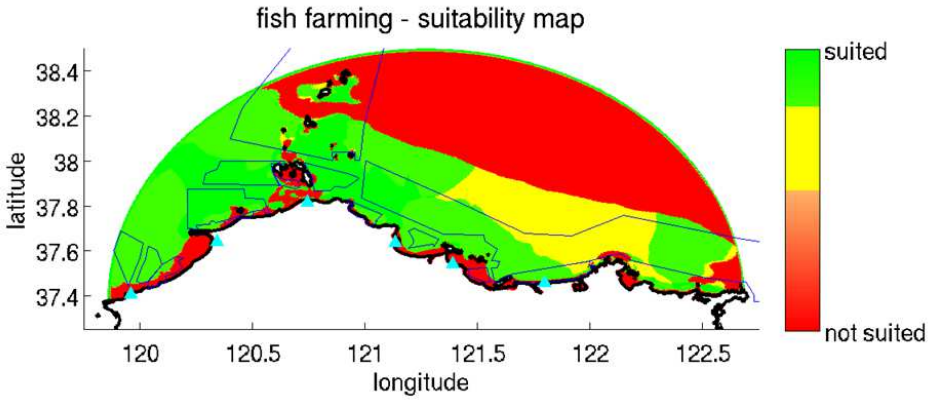

Figure 3.23: Suitability map for offshore cage culture under storm conditions.

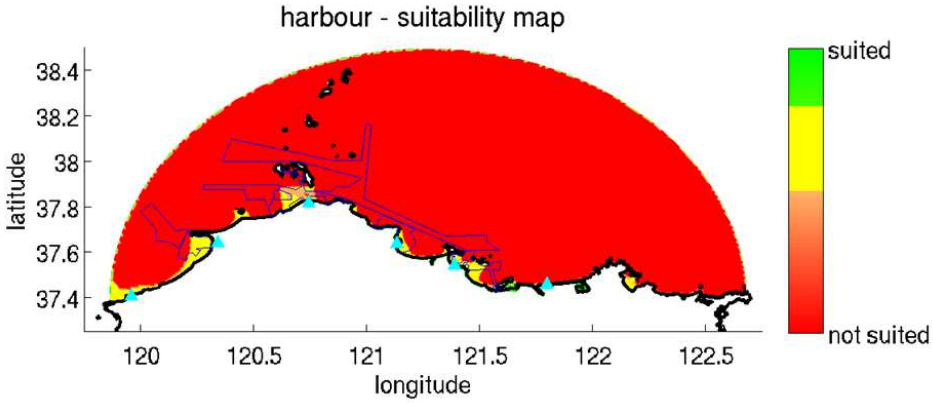

Figure 3.24: Suitability map for harbours under storm conditions.

Vulnerability module

According to the definition of the International Panel on Climate Change (IPPC) [McCarthy et al., 2001], vulnerability is the degree to which a system is susceptible to, or unable to cope with, adverse effects (of climate change for example). Vulnerability assessment is the process of identifying, quantifying, and prioritizing (or ranking) the vulnerabilities in a system. Vulnerability index is a measure of the exposure of a population to some hazard. Typically, the index is a composite of multiple quantitative indicators that delivers a single numerical result via a pre-defined relation.

Another application of the DSS is the assessment of coastal vulnerability. The vulnerability assessment in the coast of Shandong peninsula was based on hydrodynamic and meteorological conditions (storm events). Based on ranges given in the literature for each vulnerability criteria [Thieler and Hammar-Klose, 1999], model results have been analysed and evaluated.

The criteria have been narrowed down to five physical variables, which were divided into five classes. The final classification with the thresholds applied to the Shandong Peninsula is presented in Table 3.5.

Table 3.5: Root Mean Square Errors for the significant wave height, the wave direction and the wind direction at high sea state in the vicinity of the ADCP.

Variable	**very low**	**low**	**moderate**	**high**	**very high**
geomorphology	rocky coasts	-	alluvial plains	-	mud flats
coastal slope (%)	>0.2	0.2-0.7	0.07-0.04	0.04-0.025	<0.025
shoreline erosion/accretion (m)	>0.1	0.1-0.05	0.05-(-0.05)	-0.05-(-0.1)	<-0.1
mean tide range (m)	<0.2	0.2-0.733	0.733-1.267	1.267-1.8	<1.8
mean wave height (m)	<0.1	0.1-0.333	0.333-0.567	0.567-0.8	>0.8

The Coastal Vulnerability Index (CVI) is an index that allows the physical variables to be related in a quantifiable manner. This method yields numerical data that cannot be directly equated with particular physical effects. It does, however, highlight those regions where the various effects of intense hydrodynamic conditions may be the greatest.

Once each section of coastline is assigned a risk value based on each specific data variable, the coastal vulnerability index is calculated as the square root of the geometric mean, or the square root of the product of the ranked variables divided by the total number of variables as described in Equation (3.2).

$$CVI = \sqrt{\frac{a * b * c * d * e}{5}} \tag{3.2}$$

where a is geomorphology, b is coastal slope, c is shoreline erosion/accretion rate, d is mean tide range and e is mean wave height. In Figure 3.25, the coastal vulnerability index for the Shandong Peninsula under storm conditions is presented, where each colour was assigned to one vulnerability class.

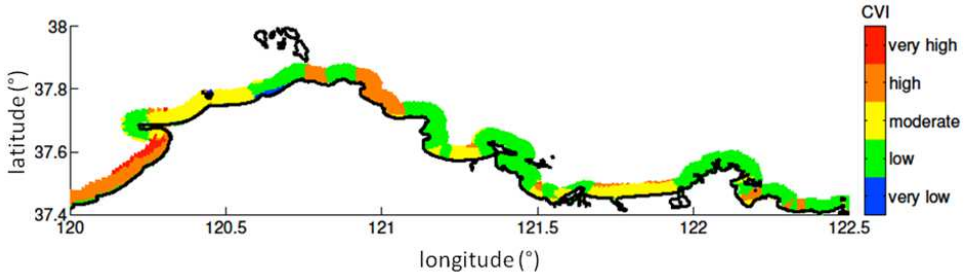

Figure 3.25: Coastal Vulnerability Index along the Shandong Peninsula under storm conditions.

The geomorphology factor has a rather important impact on the index in rocky capes; the mean tide range is higher in the central region; and the mean wave height is dominant in the Northwest, where the coast is more exposed to winds coming from the Bohai Sea. The influence from the coastal slope is apparently not so important, because the greatest slopes near the coast are found in front of rocky regions, where the vulnerability already is considered to be low. Erosion areas are not as common as deposition areas along the coast, and thus do not increase the CVI significantly.

Many areas that are more exposed to sea/weather conditions and are expected to be highly vulnerable presented a low CVI. The reason for that lies mainly on the geomorphology factor, where rocky coasts are located. Moderate to high CVI are mostly related to the mean wave height, where the coast is more exposed to north/northwestern waves during storms.

Conclusions

In the present paper the first steps for the development of a coastal modelling system for the Shandong Peninsula are described. The system consists of a hydrodynamic model, with possible extension to sediment transport and morphodynamics, suitability and vulnerability modules, and a database module. The output is presented in a graphical form and automated by an operational system.

The numerical model has been calibrated and validated by means of in situ measurements such as ADCPs and tidal gauges, and remote sensing technology such as the HF radar. Generally good agreement was found between measurements and model results. Model results have been integrated into a DSS, in which the identification of suitable locations to specific coastal activities, and the identification of vulnerable areas to different hydrodynamic and morphological conditions are possible.

A suitability analysis of fish farming and harbour activities was carried out for averaged long-term (five years) and storm conditions (21 events). Results showed that for averaged

long-term conditions fish farming is suited everywhere along the shore, apart from very shallow areas close to the coastline, and harbour activities are more restricted to regions with moderate hydrodynamic conditions. For averaged storm conditions, offshore cage culture is not recommended on the east of the peninsula and in the north of the Bohai strait due to strong hydrodynamic conditions, and specific areas along the coast fulfil allowable ranges for harbour activities and five out of six existing harbour locations are included.

Also, a vulnerability analysis was carried out based on hydrodynamic and meteorological conditions, and evaluated according to five physical variables. Low vulnerability areas are related to the geomorphology factor, where rocky coasts are located. Moderate to high CVI are mostly related to the mean wave height, where the coast is more exposed to north/northwestern waves during storms.

In addition, the presented DSS was integrated into an operational system to forecast currents and sea state conditions of the Bohai Sea. An immediate access to graphical model results is possible, as well as access to the suitability and to the vulnerability analysis results.

Acknowledgements

The authors would like to thank the German Ministry of Education and Research (BMBF) for the funding of the Project SPLASH (03F0632A), the University of Kiel (CAU), the Yantai Institute of Coastal Zone Research, Chinese Academy of Sciences (YIC), the company Helzel Messtechnik GmbH and the German Weather Service (DWD) for providing data access.

Chapter 4

Discussion and general conclusions

Discussion

Limits of the wave model SWAN

A current issue that is reported during the implementation of the wave model SWAN is the underestimation of the wave period and the significant wave height [Kang-Ren and Zhen-Gang, 2001a, Moeni and Etemad-Shadidi, 2009, Jouon et al., 2009]. This is a well known issue when the default formulations are used in SWAN. Similar results are observed with the wave model WAM. Indeed, Cavaleri and Bertotti [2003] reported an underestimation of the wave heights and the wind speeds in enclosed basins. The authors obtained better results in the open oceans using wind fields from European Centre for Medium range Weather Forecasts (ECMWF) and the wave model WAM. The quality of modelled wind fields in the oceans is higher than in enclosed and semi-enclosed basins. In SWAN, low frequency energy is underestimated and high frequency energy is overestimated. Most of the formulations in SWAN are empirical and stem from laboratory experiments. The wave behaviour might be different in the real field and formulations have to be re-adapted. In this work, a clear underestimation of the wave period was observed. The significant wave height was well captured by the wave model except for peaks of wave height especially during storms. Underestimations and overestimations of the wave period and the significant wave height in SWAN have been overcome differently according the source of error that was considered. Commonly, errors in capturing the right wave heights and the wave periods are attributed to uncertainties of the wind forcing [Group et al., 2007, Bolaños et al., 2007]. The wind fields used to drive the wave models are based on the predictions and hindcasts reanalyses from meteorological models (ECMWF, DWD). Errors in those fields would inherently lead to errors in the wave model outputs. Furthermore, the response of SWAN to strong and short variations in the wind input might be the reason of the underestimation of the significant wave height.

In this work, the underestimation of the wave period and the significant wave height was corrected by adjusting some physical parameters in SWAN responsible for the generation and the dissipation of the wave energy in the action balance equation of the model. First adjustments were done in the white-capping term. It was found that wave periods were sensitive to the coefficient δ whereas wave heights reacted more sensitively to the coefficient C_{ds}. Similarly, several studies overcame this issue by tuning the white-capping term [Rogers et al., 2003, Mulligan et al., 2008, Alomar et al., 2014]. These corrections are sometimes not sufficient to solve the underestimation or overestimation issue. As an example, Rogers et al. [2003] corrected the underestimation of the wave parameters by modifying the white-capping formulation and disabled as well the breaking of swell in the model. In this study, in addition to the corrections of the white-capping term, we found out that the model was

sensitive to the wave growth by wind formulation. In coastal areas, waves generated by local winds are confronted to waves generated offshore. Such a bimodal wave system is not included in the parametrization of SWAN. The default settings in SWAN implements the formulation after Komen et al. [1984]. This formulation gave good results in sheltered shallow waters where the wind mainly blows from the land. However, in deep and open shallow waters, this formulation leads to an underestimation of the wave parameters during strong wind events. Better results in this kind of areas were found using the wave growth by wind formulation after Janssen [1991].

Not only the tuning of the physical processes in SWAN but the numerical settings as well can be responsible for the underestimation and/or the overestimation of the modelled wave parameters. Bolaños et al. [2007] looked for other reasons than the wind forcing and other physical processes to explain the underestimation of the modelled wave height during storms and pointed out the importance of spatial resolutions of the wind and wave models in coastal areas. The sensitivity of the wave model to the time resolution was as well analysed. In theory, the time step in SWAN has to be chosen so as to be 1/20 or 1/40 of the characteristic length of the structures to be modelled [The SWAN Team, 2006]. A too large or a too small time step can trigger numerical instability within the model. Tolman [1992] found out that the the smaller the time step the smaller the number of numerical errors. However Makarynskyy et al. [2001] ran several simulations with different time steps and no significant differences were observed. In this work as well, we compared the results of simulations with different time steps. Time steps between 5min and 15min were considered as a good compromise between numerical errors and computing time.

The model SWAN can be run in two modes. In a stationary mode, it is assumed that waves propagate, grow and decay instantaneously. It is a time-independent mode. It is however only valid for small domains and for driving wind fields that are slowly varying. The second available mode is a non-stationary mode. This mode should be implemented in areas where the wind forcing is locally and strongly varying. Settelmaier et al. [2011] investigated differences between stationary and non-stationary modes in SWAN. The non-stationary mode showed a better accuracy in capturing local events. In this study, we ran the models in a non-stationary mode because of the short variations in the model inputs, namely in the wind driving forces and in the bathymetry.

A part of the underestimation can be solved with the hotstart option in SWAN. With this option, the model saves the wave fields computed of a previous time step and uses it as initial conditions in the calculation of the next time step. Makarynskyy et al. [2001] highlighted the importance of the hotstart option for the first time steps in non-stationary simulations. This option is particularly important in non-stationary simulations that need some hours to warm up [Settelmaier et al., 2011]. In this work, we found out that this option is compulsory to obtain satisfactory results. Without this option, the modelled significant wave height and the wave period were largely underestimated. The main drawback of the use of the hotstart is the increase of the computing time. It requires as well more disk memory as each hotstart file is saved at each time step for the entire computational grid.

Computational costs can increase rapidly with the selected options in SWAN. Increasing the resolutions in time, space, frequencies and directions increases the computational time. The wave models for the Red Sea required in average 20 hours to be completed using 3 to 4 CPU threads for a simulation period of one month and a time step of 15min. For the Bohai Sea model and the same settings, it required 45hours due to the nesting strategy. In this work, the time required to compute waves was affected by the number of available processors. Indeed, increasing the number of CPU threads speeded up the simulation time.

At least, we analysed the model results in deep, shallow and nearshore areas. The model had a strong sensitivity to the bathymetric input, its resolution and the spatial resolution of the computational grid. Due to the lack of bathymetric data, the setting

of a realistic and reliable model bathymetry is in many cases a complicated task. Global relief models of the earth surface such as ETOPO1 or GEBCO combine global bathymetric measurements on a grid that has a resolution varying between $0.5'$ (0.9km) for GEBCO and $1'$ (1.9km) for ETOPO1. These resolutions are far too coarse for applications in coastal areas. Structures such as islands and coral reefs in the coastal areas might not be integrated into global bathymetric datasets. Similarly, it is important to adjust the resolution of the computational grid to the domain being modelled. That means that the smaller the coastal structures are, the higher the resolution of the computational grid must be. Coarse spatial resolution in sheltered areas might induce errors in the model predictions [Rogers et al., 2007]. Gorrell et al. [2011] analysed the performance of SWAN over a complex nearshore bathymetry and found that errors between the measurements and the model results increase with a decreasing depth. According to the authors, this observation is the result of wrong parametrizations of non linear wave interactions in shallow water. In the Aegean Sea , where many islands have to be taken into consideration, the model SWAN showed low performance [Mazarakis et al., 2012]. As a whole, it is reported that the increase of the grid size resolution leads to improvements of the wave predictions [Bolaños et al., 2007, Alomar et al., 2014].

Limits in the application of the wave models

Numerical wave models are largely implemented in the field of the operational oceanography. The wave models are often coupled to other models such as for currents, tides and more rarely sediment transport. Prediction of waves (and other hydrodynamic parameters) are realised in real-time or near real-time, known as nowcast, in the future, forecast and in the past, hindcast. The products of an operational system have to be provided rapidly to the concerned institutions or authorities. The wave models set up in this work are suitable for hindcasts and forecasts as far as accurate wind inputs are used. Wave models are also used in consultancy studies for coastal protection and engineering where the return period of extreme events are analysed. Coastal protection design parameters' calculation is based on 10 to 100 years wave simulation depending on the events to analyse. In this work, wave simulations were done for several months to several years. So the results obtained in this work should be used with caution when analysing past changes and trends.

Limits in the accuracy of the measurements

In addition to the wave model errors, we consider in this work errors due to the measurement techniques. Several techniques, direct or indirect, punctual or over a given area, were used to obtain wave measurements. Good quality data is required when the model prediction capabilities have to be assessed. Often, a quality check is done to correct the data and avoid the introduction of errors in any application of the data. In this section, we discuss the accuracy of the HF radar, the wave buoys, the ADCP and the altimeter wave measurements.

The accuracy of HF radar measurements is affected by the operation frequency of the radar and the interferences with other sources dealing with similar frequencies in the coastal zone. The HF radar deployed near Yantai emitted a frequency of 26.27MHz. The operation frequency affects both, the beamformed ranges of the radar and the measurement ranges of the wave parameters [Helzel et al., 2010, Wyatt et al., 2011]. In details, the range of the significant wave height achieved with a transmitting frequency of 26.27MHz varies from 0.58m to 3.625m. Only limited data is measured by the HF radar for significant wave heights with a value below 0.58m. The data becomes not reliable any more below 0.17m. The upper threshold of significant wave height is 3.63m. Above this value, the data becomes as well not reliable any more. The mean averaged significant wave height observed in front of Yantai is 0.36m and the maximum observed wave height is 2.61m. It

was evident that because of the low wave conditions measured by the HF radar, a lot of noise was superimposed to the measurements. During the stormy event recorded in September 2013, the HF radar was able to record accurately the significant wave height. Modifying the operation frequency, especially increasing the operating frequency could improve the accuracy of wave measurements for such sea conditions like in Yantai. A drawback of the increase of the operating frequency is the resulting decrease in the beamformed range. The range of measurements depends on the transmitted frequency, shorter measurements' ranges are reached with higher operation frequency of the radar [Gurgel et al., 1999b, Helzel et al., 2010]. The maximal or total beamformed range by the antennas of the HF radar is reached for measurements of the surface currents. The beamformed ranges for waves by the radar are reduced to half of this maximal range. The maximal range for currents measurements in this study is on average 55km. This range can however vary between 33km and 65km due to external parameters. As a consequence, the maximal range of wave measurements is comprised between 15km and 29km. Wind measurements by HF radar are done at 80% of the total range, that is to say 44km. This range can vary between 26km and 52km due to external parameters which trigger interferences within the backscattered signal. The electromagnetic waves emitted by the HF radar propagate over the horizon over the water surface which is conductive. The conductivity of the water surface varies with the salinity of the water masses. When the salinity of the water increases, the electromagnetic waves propagate farther and consequently, the measurement range increases [Meadows et al., 2013, Harlan et al., 2010]. The beamformed range is as well varying with the day and night cycles. Meadows et al. [2013] put some limits in the use of HF radar in fetch limited areas. Surface waves generated in fetch limited areas are characterized by shorter wavelengths that cannot always enter in resonance with the emitted signal from the HF radar. This is one reason to explain the noise contained in the wave measurement near Yantai for low wind conditions. Ships, ionosphere interferences and coastal activities using high frequency signals can as well introduce noise into the backscattered Doppler spectra and decrease the signal to noise ratio of the data.

Lower accuracy of the wave measurements is achieved with the satellite altimeters. First, the time and spatial resolutions of the satellite altimeters are much coarser than the other instruments used in this study for calibration and validation of the wave models in coastal areas. As an example, the satellite ENVISAT whose data was used to calibrate the wave model in the Red Sea has a spatial resolution of 7km. Records of the satellite altimeters are done at a rate of one measure per second. A track of 200km is covered in approximately 30seconds and a same track is measured every 35 days. Secondly, in coastal areas, satellite altimeters are not as accurate as in the open ocean [Vignudelli et al., 2006, Feneglio-Marc et al., 2007]. The tidal and atmospheric corrections applied to the altimetric data recorded over the open oceans are no more valid near the coasts. Also, the signal is contaminated by the land that has a different roughness than the water surface. In the case study of the Red Sea, higher correlation with the model was found in the centre of the sea. Unrealistic wave heights were found at the extremities of the tracks, that is to say at the boundary between land and sea. Reprocessing of the altimetric data is usually done to obtain more accurate data in coastal areas [Anzenhofer et al., 1999]. Such a work was not done here as it is beyond the scope of this study.

Higher accuracy of the wave measurements is achieved with the bottom-mounted ADCP and the wave buoys. The accuracy of measurements done with an ADCP is higher when a higher frequency of the the transmitted pings is used. However, like the HF radar, the range of measurements decreases when the emitting frequency is increased. Measurements with an ADCP can be contaminated by sidelobes near the water surface and the sea floor. These lobes are areas outside the main lobe where the pulses are transmitted. Another drawback of using high frequencies is that the battery is rapidly consumed. The ADCP deployed near

Yantai was set with an emitting frequency of 600kHz at a depth of 17m. It has an accuracy of 0.14m. According to Strong et al. [2013], the error sources of ADCP measurements are due to the uncertainties in the water depth, the height of the instrument above the bottom, the presence of currents, the turbulences such as bubbles in the water column and the signal to noise ratio. Miscalculations of the wave parameters can also be caused by biofouling on the instrument. The growth of benthic species or algae on the transducers can occur when the instrument is deployed over a long time period on the sea bottom or within the water column. The biofouling diminishes the performance of the instrument by interfering with the sensors of the ADCP [Alliance for Coastal Technologies (ACT) and NOAA, 2003].

Wave buoys are deployed at the water surface so the instruments are less affected by biological fooling than the bottom-mounted ADCP. The buoys deployed in the coastal waters of Jeddah recorded information during a period of one month for the met-ocean buoy and 2 months for the waverider. Due to maintenance and data transfer issues, a full record of the period was not possible. Contrary to the ADCP, the battery issue is here solved with the use of solar panels. The accuracy of the significant wave height and the wave direction with the waverider are 0.04m and 2° respectively [Datawell Oceanographic Instruments, 2009].

General Conclusions

This work provides new information about wind-generated wave conditions in two semi-enclosed sea with a focus on two coastal areas. To overcome the sparsity of wave measurements, a numerical wave model was set up to obtain wave information in each of the areas of interest. Surface waves were modelled by means of the third generation spectral wave model SWAN which is a numerical model developed for wave modelling purposes in coastal areas. The models were calibrated, validated and applied for coastal purposes.

The two semi-enclosed seas considered for analysis are the Red Sea and the Bohai Sea. Semi-enclosed seas have the particularity of not being influenced by large swell as a small entrance separates them from the open oceans. As a consequence, waves generated in this type of seas are mostly wind-generated. Hence, this work investigated the modelling of surface waves and their properties in the above-mentioned areas. The models were forced with the wind field reanalysis from the German Meteorological Service (DWD).

A first wave model was set for the Red Sea. The wave climate and the wave seasonality were assessed in the Red Sea over three years [Fery et al., 2012]. It was found that higher and longer waves propagate to the south east of the Red Sea in summer while in spring, smaller and shorter waves propagating from the north west and from the south east face each other at the centre of the Red Sea. The same model with an increased resolution was implemented within the coastal waters of Jeddah in Saudi Arabia [Fery et al., 2015]. Wave characteristics were evaluated on the short- and on the long-term. A diurnal wave pattern was observed in the coastal waters of Jeddah where low waves occur in the morning and high waves in the afternoon. Waves are mainly propagating from the northwest and reach a maximal height of 2m in front of the reef structures. Long-term simulations near Jeddah revealed clear seasonal variations that coincide to those of the Red Sea. Waves are higher and longer in May whereas they are lower and shorter in November. Regular daily and monthly variations of the wave parameters were as well observed. Another concluding result in this study is the importance of the wind and the bathymetry in the modelling of waves in coastal areas. In deep and in shallow water, waves closely followed the wind direction. In the whole Red Sea, the waves follow the direction of the Arabian monsoon wind fields. In deep water, the bathymetry does not affect the wave propagation. The wave propagation is modified in the coastal waters of Jeddah which are characterized by many local reef structures. The wave height decreases when approaching the nearshore area of

Jeddah because of the presence of coral reefs that produce a dissipation and sheltering effect on the waves. Additionally to the sheltering effect due to coral reefs, a refraction of the offshore prevailing waves from north/northwest to west/northwest was observed.

A second wave model based on a nesting strategy was set for the Bohai Sea and the coastal waters of Yantai. A nesting strategy was preferred here to take into account the large dimensions of the sea and the relatively large connection between the Bohai Sea and the Yellow Sea, i.e 200km, that allows larger waves to enter in the Bohai Sea, and consequently to avoid the underestimation of wave parameters. Wave conditions at the north of the Shandong peninsula over 6 years were evaluated. A maximum wave height of 2.95m and a mean wave height of 0.40m were found. Waves are higher and longer at the east of the peninsula. Theses waves are generated within the Yellow Sea and propagate into the Bohai Sea through the peninsula with a high energy. Lowest waves are found in the west of the peninsula. The Bohai Strait made of many small islands has a sheltering effect for northern and western waves. Contrary to the coastal waters of Jeddah, the bathymetry of the coastal waters of Yantai is characterized by a smooth sandy sea bottom. Waves are not refracted and the shore is less sheltered. The wave seasonality is influenced by the East Asian Monsoon. Highest waves with a prevailing direction of west occur in winter while they are the smallest during summer and propagate mainly from the southwest or from the east. High waves generated by typhoons or cyclones can however occur during the summer near Yantai. Characteristic waves observed during fall and spring have a similar average height (0.50m) but opposite directions due to the transition between the northeast and the southwest monsoons that occur at this time of the year [Fery et al., 2017].

The accuracy of the numerical wave models and their inputs were verified by means of direct and indirect measurements. The wind fields from the global meteorological model DWD used to force the model were validated using wind measurements from several coastal stations and meteorological buoys. In both case studies, a good agreement was found for both parameters, the wind speed and the wind direction. The calibration and the validation of the wave model in the Red Sea, in particular near Jeddah were based on wave data from two wave buoy and satellite altimeters. In the coastal region of Yantai, an ADCP and a HF radar provided the wave data required for the validation work of the wave model. Emphasis was given to assess the accuracy of the measurements of the HF radar deployed in Yantai. Indeed, wave measurements with HF radar are sensitive to external interferences and a quality control needs to be processed. An extensive study was realised on the wave parameters measured by HF radar. After processing and filtering of the HF radar data, a good agreement with other sources of measurements was found in terms of significant wave height. However, the analysis of the data showed a strong decrease of the accuracy of the measurements of wave and wind direction by HF radar.

Not only the validation of the measurements was of importance in this study, but as well the capability of the wave models to predict wave parameters with a high accuracy. It was found that the default parametrization of the model SWAN was not entirely suitable for the deep waters of the Red Sea. Indeed, the default settings lead to an underestimation of the predicted wave parameters. Improvements were obtained modifying the white-capping dissipation term and changing the wave-growth by wind formulation after Komen et al. [1984] to that after Janssen [1991]. The numerical study of waves in the coastal waters of Jeddah revealed similar conclusions in the parametrization of the wave model. The formulation after Janssen [1991] was suitable in the offshore part of the considered area. Onshore, where the bathymetry affects the wave propagation, it was found that the formulation after Komen et al. [1984] reproduced better the wave parameters. To avoid two different settings within a same model, we performed linear model correction of the wave parameters, i.e. the significant wave height and the wave period. The same model parametrization, that is to say using the wave growth by wind after Janssen [1991] was used in the parametrization of

the wave model for the Bohai Sea. Wave predictions with the formulation after Komen et al. [1984] showed that waves with a height smaller than 0.7m were well captured but higher waves were underestimated. Small waves were well captured with the two formulations even if smaller errors were found for the formulation after Komen et al. [1984]. In areas where incoming waves reach a significant wave height below 0.7m, the waves can be well predicted with the default formulation of SWAN. As soon as larger waves propagate, the use of the formulation after Janssen [1991] is recommended. In the studied semi enclosed seas, this formulation was required for the simulation of storm events and in offshore areas that are prone to a swell generated within the sea. The transfer of wind energy to the waves described in the equation after Janssen [1991] allows an exponential growth of the waves by wind which is stronger than those after Komen et al. [1984].A two way interaction between the wind an the wave energy explains the faster growth of waves with Janssen's formula. At the present, the two considered formulations cannot be used at the same time in a simulation. The establishment of such a new equation would be based on empirical assumptions related to the wave climate of the area under consideration. However, a way to overcome this step is to apply a coefficient to the calculated wave parameters. If a user implements the formulation after Komen et al. [1984], he would apply a coefficient to increase the highest waves and if he chooses to use the formulation after Janssen [1991], he would apply a coefficient to the lowest waves. These coefficients are set with linear regression and are empirical. Lastly it was shown in this study that the bathymetry significantly contributed to the wave climate conditions. Indeed, special care needs to be given to obtain an accurate representation of obstacles and other bathymetric structures within the model settings to avoid under- and/or overestimation of the wave parameters.

In the last part of this work, several applications of both wave models, for the Red Sea and for the Bohai Sea were given. Results of the wave models in the coastal areas were integrated into coastal planning systems. The wave model calibrated and validated for the coastal waters of Jeddah was integrated into a Coastal Monitoring System, the Jeddah-CMS, for supporting the sustainable environmental planning of coastal areas near Jeddah. The CMS aimed in helping decision makers for the management of the coastal area and related issues where the predictions of waves, water level, current velocities and water quality parameters are relevant [Mayerle et al., 2016].

The calibrated and validated wave model for the coastal waters of Yantai is coupled to a flow and a sediment model. A Decision Support System (DSS) for the Shandong Peninsula based on this coupled modelling system was developed to help decision makers in finding suitable locations for coastal activities [Dalledonne et al., 2016]. Relevant coastal activities along the peninsula are the harbour and industrial activities (mineral and gas exploitation), aquaculture (onshore and offshore fish farming) and at least, tourism. The numerical models were run for several environmental conditions including effects of the climate change such as the sea level rise and storms. Suitable locations for aquaculture and port activities found with the DSS were compared to the actual coastal planning of the Chinese government along the Shandong peninsula. Generally, a good agreement between the locations extracted from the DSS and the official coastal planning was found. Extended applications of the DSS include the evaluation of vulnerable coastal sections prone to erosion and the predictions in real-time of water level, flow and waves in the Bohai Sea.

The physics of the model SWAN were investigated to improve wave predictions on the global and local scales of semi-enclosed seas. Generation and dissipation terms of the wave action equation such as the white-capping and the wave growth by wind were successfully modified and adapted to several case studies. The idea of an operational system taking the above mentioned changes and as most wave data as possible is the matter of further research. Real time assimilation of wave measurements of different sources might be of interest in areas facing high environmental and anthropogenic pressures, mainly induced by

an increase of the demography and the water level. The operational use of SWAN to provide synoptic wave information might be as well relevant in the planning of coastal activities. The assimilation of wave data could as well increase the prediction capability of the wave model SWAN.

Bibliography

S.M. Abdelrahman. Statistical wave parameters offshore jeddah coast. *Journal of King Abdulaziz University*, 6:25–37, 1995.

A.M.A. Al-Barakati. Residual currents in coastal waters near jeddah desalinisation plants, red sea. *Journal of King Abdulaziz University*, 20:49–58, 2004.

S. Al-Hathoul and M.A. Mughal. Jeddah. *Cities*, 8(4):267–273, 1991.

Alliance for Coastal Technologies (ACT) and NOAA. Biofouling prevention technologies for coastal sensors/sensor platform. Workshop technical report, University of Maryland, Solomons, Maryland, 2003.

M. Alomar, A. Sánchez-Arcilla, R. Bolaños, and A. Sairouni. Wave growth and forecasting in variable, semi-enclosed domains. *Continental Shelf Research*, 87:28–40, 2014. doi: 10.1016/j.csr.2014.05.008.

J.H.G.M. Alves and M.L. Banner. Performance of a saturation-based dissipation-rate source term in modeling the fetch-limited evolution of wind waves. *Journal of Physical Oceanography*, 33:1274–1298, 2003.

M. Anzenhofer, C.K. Shum, and M. Rentsh. Coastal altimetry and applications. Technical report, Geodetic science and surveying, Department of civil and environmental Engineering and geodetic science, 1999.

Matthew R. Archer, Lynn K. Shay, and Jorge Martinez-Pedraja. Evaluation of WERA HF radar observations: Currents, winds and waves. *2015 IEEE/OES 11th Current, Waves and Turbulence Measurement, CWTM 2015*, 2015. doi: 10.1109/CWTM.2015.7098148.

Y. Baoshu and Y. Dezhou. Application study of shallow water wave model (swan) in bohai sea. In P.R. China National Marine Environment Forecasting Center State Oceanic Administration, editor, *The Twelfth Workshop on Ocean Models (WOM-12)*, Dalian, China, 2004.

D.E. Barrick, M.W. Evans, and B.L. Weber. Ocean surface currents mapped by radar. *Science*, 198:138–144, 1977.

J.A Battjes and J.P.F.M. Janssen. Energy loss and set-up due to breaking random waves. In *16th Conference on Coastal Engineering ASCE*, Hamburg, Germany, 1978.

R. Bolaños, A. Sánchez-Arcilla, and J. Cateura. Evaluation of two atmospheric models for wind-wave modelling in the nw mediterranean. *Journal of Marine Systems*, 65:336–353, 2007. doi: 10.1016/j.jmarsys.2005.09.014.

N. Booij, R. C. Ris, and L. H. Holthuijsen. A third-generation wave model for coastal regions 1- model description and validation. *Journal of Geophysical Research*, 104:7649–7666, 1999.

L. Cavaleri and L. Bertotti. The characteristics of wind and wave fields modelled with different resolutions. *Quarterly Journal of the Royal Meteorological Society*, 129:1647–1662, 2003. doi: 10.1256/qj.01.68.

L. Cavaleri and P. Malanotte-Rizzoli. Wind wave prediction in shallow water : Theory and applications. *Journal of Geophysical Research*, 86:10,961–10,973, 1981.

R.D. Chapman, L.K. Shay, H.C. Graber, J.B. Edson, A. Karachintsev, C.L. Trump, and D.B. Ross. On the accuracy of hf radar surface current measurements: Intercomparisons with ship-based sensors. *Journal of Geophysical Research*, 102(C8):18737–18748, 1997. doi: 10.1029/97JC00049.

J. Chen, C. Guang, H. Xu, Z. Chen, P. Xu, X. Yan, Y. Wang, and J. Liu. Marine fish cage culture in china. In A. Lovatelli, M.J. Phillips, J.R. Arthur, and K. Yamamoto, editors, *FAO/NACA Regional Workshop on the Future of Mariculture : a Regional Approach for Responsible Development in the Asia-Pacific Region*, pages 7–11. FAO Fisheries Proceedings, Guangzhou, China, 2008.

X. Chen, D. Pan, X. He, Y. Bai, Y. Wang, and Q. Zhu. Seasonal and interannual variability of the sea surface wind over the china seas and its adjacent ocean from quickscat and ascat data during 2000-2011. In *Proceedings of the International Society for Optics and Photonics (SPIE)*, volume 8533, 19 October 2012 2012. doi: 10.1117/12.974573.

P. Cipollini and Co-Authors. The role of altimetry in coastal observing systems. In *Proceedings of OceanObs09: Sustained Ocean Observations and Information for Society*, volume 2, Venice, Italy, 21-25 September 2009 2010. ESA Publication WPP-306.

D.D Crombie. Doppler spectrum of sea echo at 13.56mc/s. *Nature*, 175:681–682, 1955.

G.L Dalledonne and R. Mayerle. Modelling of storm impacts on the shandong peninsula coast. *Journal of Coastal Research*, 74:70–82, 2016.

G.L. Dalledonne, X. Zheng, N. Fery, C. Tang, and R. Mayerle. Decision support system for the management of the shandong peninsula, china. In *35th International Conference of Coastal Engineering (ICCE)*, Istanbul, Turkey, 2016.

Datawell Oceanographic Instruments. *Datawell Waverider Reference Manual*. Datawell Oceanographic Instruments, 2009.

Deltares The Netherlands. *Delft3D-WAVE Simulation of short-crested waves with SWAN User Manual*. Deltares The Netherlands, 2014.

Y. Ding and L. Ding. Extratropical storm surge and hydrodynamic response in the bohai sea. *Discrete Dynamics in Nature and Society*, 2014:8 pages, 2014. doi: 10.1155/2014/282085.

H.H. Essen, K.W. Gurgel, and T. Schlick. Measurements of ocean wave height and direction by means of hf radar : an empirical approach. *German Journal of Hydrography*, 51:369–383, 1999.

G.H. Fang. Tides and tidal currents in east china sea, huanghai sea and bohai sea. In D. Zhou, Y.B. Liang, C.K. Zeng, and C.K. Tseng, editors, *Oceanology of China Seas*, chapter Part I, pages 101–112. Springer, The Netherlands, 1994.

G.H. Fang and J.F. Yang. A two-dimensional numerical model of the tidal motions in the bohai sea. *Chinese Journal of Oceanology and Limnology*, 3(2):135–152, 1985.

H. Fang and M. Duan. Special problems in sea petroleum engineering for beaches and shallow sea areas. In *Offshore operation facilities : Equipment and procedures*. Gulf Professional Publishing, 2014.

L. Feneglio-Marc, A. Vignudelli, A. Humbert, M. Cipollini, M. Fehlau, and M. Becker. An assessment of satellite altimetry in proximity of the mediterranean coastline. In *3rd ENVISAT Symposium Proceedings*, page 5. ESA Publication Division, 2007.

N. Fery, G. Bruss, A. Al-Subhi, and R. Mayerle. Numerical study of wind generated waves in the red sea. In University of Ghent, editor, *Book of proceedings 4th International Conference Coastlab12*, Ghent, Belgium, 2012.

N. Fery, A.M. Al-Subhi, K.M. Zubier, and G. Bruss. Evaluation of the sea state near jeddah based on recent observations and model results. *Journal of Operational Oceanography*, 8(1):1–10, 2015. doi: 10.1080/1755876X.2015.1014636.

N. Fery, C. Tang, and R. Mayerle. Validation experiment of wind and wave properties from high frequency radar in the vicinity of yantai, china. manuscript submitted for publication in Regional Studies in Marine Science, 2017.

M. Gao, J. Ning, and X. Wu. Normal and extreme wind conditions for power at coastal locations in china. *PLoS ONE*, 10(8):26, 2015. doi: 10.1371/journal.pone.0136876.g007.

Gharbi. Numerical wave simulation in the red sea. Master's thesis, King Abdulaziz University, Saudi Arabia, 2012.

L. Gorrell, B. Raubenheimer, Elgar Steve, and R.T. Guza. Swan predictions of waves observed in shallow water onshore of complex bathymetry. *Coastal engineering*, 58:510–516, 2011. doi: 10.1016/j.coastaleng.2011.01.013.

H.C. Graber and M.L. Heron. Wave height measurements from hf radar. *Oceanography*, pages 90–92, 1997.

The WISE Group, L. Cavaleri, J.-G.M. Alves, F. Ardhuin, M. Babanin, M. Banner, K. Belibassakis, M. Benoit, M. Donelan, J. Groeneweg, T.H.C. Herbers, P. Hwang, T. Janssen, I.V. Lavrenov, R. Magne, J. Monbaliu, M. Onorato, V. Polnikov, D. Resio, W.E. Rogers, J. Sheremet, A. McKee Smith, H.L. Tolman, G. vanVledder, J. Wolf, and I. Young. Wave modelling- the state of the art. *Progress in Oceanography*, 75:603–674, 2007. doi: 10.1016/j.pocean.2007.05.005.

K-W. Gurgel, H-H. Antonischi, T. Essen, and T. Schlick. Wellen radar (wera): a new ground-wave hf radar for ocean remote sensing. *Coastal Engineering*, 37:219–234, 1999a.

K.W. Gurgel, H. Essen, and S.P. Kingsley. Hf radars : Physical limitations and recent developments. *Coastal Engineering*, 37:201–218, 1999b.

K.W. Gurgel, H.H. Essen, and T. Schlick. The university of hamburg wera hf radar - theory and solutions. In *Proceedings of the First International Radiowave Oceanography Workshop ROW 2001*, page 7, 2001.

K.W. Gurgel, H.H. Essen, and T. Schlick. An empirical method to derive ocean waves from second-order bragg scattering : prospects and limits. *IEEE Journal of Oceanic Engineering*, 31:804–811, 2006.

D. Hainbucher, W. Hao, T. Pohlmann, J. Sündermann, and S. Feng. Variability of the bohai sea based on model calculations. *Journal of Marine Systems*, 44(3-4):153–174, 2004.

J. Harlan, E. Terrill, L. Hazard, C. Keen, D. Whelan, S. Howden, and J. Kohut. The integrated ocean observing system high-frequency radar network: status and local, regional, and national applications. *Marine Technology Society Journal*, 44:122–132, 2010.

K. Hasselmann, T.P. Barnett, E. Bouws, H. Carlson, D.E. Cartwright, K. Enke, J.A. Ewing, H. Gienapp, D.E. Hasselmann, P. Kruseman, A. Meerburg, P. Mller, D.J. Olbers, K. Richter, W. Sell, and H. Walden. Measurements of wind-wave growth and swell decay during the joint north sea wave project (jonswap). *Ergenzungsheft zur Deutschen Hydrographischen Zeitschrift Reihe*, 12:95, 1973.

S. Hasselmann and K. Hasselmann. Computations and parameterizations of the nonlinear energy transfer in a gravity-wave spectrum. part i: A new method for efficient computations of the exact nonlinear transfer integral. *Journal of Physical Oceanography*, 15: 1369–1377, 1985.

T. Helzel, M. Kniephoff, and L. Petersen. Oceanography radar system wera : features, accuracy, reliaility and limitations. *Turkish Journal of Electrical Engineering and Computer Sciences*, 18:389–396, 2010.

M.L. Heron, P.E. Dexter, and B.T. McGann. Parameters of the air-sea interface by high-frequency ground-wave hf doppler radar. *Australian Journal of Marine and Freshwater Research*, 36:655–670, 1985.

S. F. Heron and M. L. Heron. A comparison of algorithms for extracting significant wave height from hf radar ocean backscatter spectra. *Journal of Atmospheric and Oceanic Technology*, 15:1157–1163, 1998.

L.H. Holthuijsen. *Waves in Oceanic and Coastal Waters*. Cambridge University Press, 2007.

R. Huang, J. Chen, and G. Huang. Characteristics and variations of the east asian monsoon system and its impacts on climate disasters in china. *Advances in atmospheric sciences*, 24(6):993–1023, 2007. doi: 10.1007/s00376-007-0993-x.

W. Huang, S. Wu, E. Gill, H. Biyang, and J. Hou. Measurements with a hf radar over the eastern china sea. *IEEE Geoscience and Remote Sensing*, 40:1950–1955, 2002.

W. Huatong and J.D. Wang. Modelling the hydrodynamics of the bohai sea in china. *Chinese Journal of Oceanology and Limnology*, 3(2):185–199, 1985.

P.A. Janssen. Wave-induced stress and the drag of air flow over sea waves. *Journal of Physical Research*, 19:745–754, 1989.

P.A. Janssen. Quasi-linear theory of wind-wave generation applied to wave forecasting. *Journal of Physical Oceanography*, 21:1631–1642, 1991.

H. Jeffreys. On the formation of water waves by wind. *Proceedings of the Royal Society of London*, [A] 107:189, 1925.

H. Jeffreys. Formation of water waves by wind. *Proceedings of the Royal Society of London*, [A] 110:241–247, 1926.

A. Jouon, J. P. Lefebvre, P. Douillet, S. Ouillon, and L. Schmied. Wind wave measurements and modelling in a fetch-limited semi-enclosed lagoon. *Coastal engineering*, 56:590–608, 2009.

J. Kang-Ren and J. Zhen-Gang. Calibration and verification of a spectral wind-wave model for lake okeechobee. *Ocean Engineering*, 28:571–584, 2001a.

Jin Kang-Ren and Ji Zhen-Gang. Calibration and verification of a spectral wind-wave model for lake okeechobee. *Ocean engineering*, 28:571–584, 2001b.

J.W. King, F.D.G. Bennett, R. Blake, D. Eccles, A.J. Gibson, G.M. Howes, and K. Slater. Oscr (ocean surface current radar) observations of currents off the coasts of northern ireland, england, wales, and scotland. In *Proceedings of the Conference on Current Measurement Offshore*, London, 17 May 1984 1984. Society for Underwater Technology.

J. Kohut and S. Glenn. Seasonde is integral to coastal flow model development. *Hydro International*, 3:32–35, 1999.

J.T. Kohut and S.M. Glenn. Improving hf radar surface current measurements with measured antenna beam patterns. *American Meteorology Society*, 20:1303–1316, 2003.

G.J. Komen, S. Hasselmann, and K. Hasselmann. On the existence of a fully developed wind-sea spectrum. *Journal of Physical Oceanography*, 14:1271–1285, 1984.

G. Li and J. Guo. *Progress in China's developmental research on wave energy*, pages 125–132. Springer Verlag Berlin, Heidelberg, 1986.

B. Liang, X. Liu, H. Li, Y. Wu, and D. Lee. Wave climate hindcasts for the bohai sea, yellow sea and east china sea. *Journal of Coastal Research*, In-Press.

Z. Liu and H. Burcharth. Encounter probability of individual wave height. *Coastal Engineering*, pages 1027–1038, 1999. doi: 10.1061/9780784404119.076.

X. Lv, D. Yuana, X. Maa, and J. Taoa. Wave characteristics analysis in bohai sea based on ecmwf wind field. *Coastal Engineering*, 91:159–171, 2014.

F. Madah, R. Mayerle, G. Bruss, and J. Bento. Characteristics of Tides in the Red Sea Region, a Numerical Model Study. *Open Journal of Marine Science*, 5:193–209, 2015. doi: 10.4236/ojms.2015.52016.

Per A. Madsen and David R. Fuhrman. *High-order Boussinesq-type modelling of nonlinear wave phenomena in deep and shallow water*, pages 245–285. Advances in Coastal and Ocean Engineering. World Scientific Publishing Co Pte Ltd, 2010. ISBN 978-981-283-649-6.

D. Majewski, D. Liermann, P. Prohl, B. Ritter, M. Buchhold, T. Hanisch, G. Paul, W. Wergen, and J. Baumgardner. The operational global icosahedral-hexagonal gridpoint model gme : Description and high-resolution tests. *Monthly Weather Review*, 130:319–338, 2002.

O. Makarynskyy, A.A. Pires Silva, D. Makarynska, C. Ventura Soares, and E. Ferreira Coelho. On the question of the swan model sensitivity to changes in time steps and initial conditions. In *Proceedings og XXIX International Association for Hydro-Environment Engineering and Research (IAHR) Congress*, Beijing, China, 2001. Tsinghua University Press.

R. Mayerle, A. Al-Subhi, J. Fernández Jaramillo, A. Salama, G. Bruss, K. Zubier, K. Runte, A. Turki, H. Hesse, K.and Jastania, N. Ladwig, and M. Mudarris. Development of a coastal information system for the management of jeddah coastal waters in saudi arabia. *Computers and Geosciences*, 89:71–78, 2016. doi: 10.2016/j.cageo.2015.12.006.

S. Mazaheri, B Kamranzad, and F. Hajivalie. Modification of 32 years ecmwf wind field using quickscat data for wave hindcasting in iranian seas. *Journal of Coastal Research*, 65:344–349, 2013. doi: 10.5194/nhess-12-3433-2012.

N. Mazarakis, V. Kotroni, K. Lagouvardos, and L. Bertotti. High-resolution wave model validation over the greek maritime areas. *Natural Hazards and Earth System Sciences*, 12:3422–3440, 2012.

J.J. McCarthy, O.F. Canziani, N.A. Leary, D.J. Dokken, and K.S. White. Climate change 2001 : Impacts, adaptation and vulnerability. Contribution of working group ii to the third assessment report, the Intergovernmental Panel on Climate Change, Cambridge, 2001.

L.A. Meadows, Whelan C., D. Barrick, R. Kroodsmac, C. Ruf, C.C. Teague, G.A. Meadows, and S. Wang. High frequency radar and its application to fresh water. *Journal of Great Lakes Research*, 39:183–193, 2013. doi: 10.1016/j.jglr.2013.01.002.

D. Medio, C.R.C Sheppard, and J. Gascoigne. *Chapter 8 - The Red Sea*, pages 231–251. Oxford University Press, Inc, 2000. ISBN 0-19-512596-7.

J.W. Miles. On the generation of surface waves by shear flow. *Journal of Fluid Mechanics*, 3:185–204, 1957.

J.W. Miles. On the generation of surface waves by turbulent shear flows. *Journal of Fluid Mechanics*, 7:469–478, 1960.

J.W. Miles. A note on the interaction between the surface waves and wind profiles. *Journal of Fluid Mechanics*, 22(4):823–827, 1965.

M. H. Moeni and A. Etemad-Shadidi. Wave parameter hindcasting in a lake using the swan model. *Civil engineering*, 16:156–164, 2009.

S.A. Morcos. Physical and chemical oceanography of the red sea. *Oceanography and Marine Biology Review*, 8:73–202, 1970.

R.P. Mulligan, A.J. Bowen, A.E. Hay, A.J. van der Westhuysen, and J.A. Battjes. White-capping and wave field evolution in a coastal bay. *Journal of Geophysical Research*, 113: 16, 2008. doi: 10.1029/2007JC004382.

J.C.J (Editor) Nihoul. *Hydrodynamics of semi-enclosed seas*, volume 34. Elsevier Scientific Publishing Company, The Netherlands, 1982. ISBN 0-444-42077-0.

O. Nwogu. Alternative form of boussinesq equations for nearshore wave propagation. *Journal of Waterway, Port, Coastal and Ocean Engineering*, 119:618–638, 1993.

T. Oguz and J. Su. *Semi-enclosed seas, islands and Australia pan-regional overview*, pages 83–116. Volume 14. A.R. Robinson AND K.H. Brink, 2004. ISBN 0-674.

J.D. Paduan and L.K. Rosenfeld. Remotely sensed surface currents in monterey bay from shore-based hf radar (coastal ocean dynamics application radar). *Journal of Geophysical Research*, 101:20,669–20,686, 1996. doi: 10.1029/96JC01663.

J.D. Paduan, K.C. Kim, M.S. Cook, and F.P. Chavez. Calibration and validation of direction-finding high-frequency radar ocean surface current observations. *IEEE Journal of Oceanic Engineering*, 31:862–875, 2006. doi: 10.1109/JOE.2006.886195.

W.C. Patzert. Wind-induced reversal in the red sea circulation. *Deep-Sea Research*, 21: 109–121, 1974.

H.E. Pelling, K. Uehara, and A.M. Green. The impact of rapid coastline changes and sea level rise on the tides in the bohai sea, china. *Journal of Geophysical Research*, 118: 3462–3472, 2013. doi: 10.1002/jgrc.20258.

D.H. Peregrine. Long waves on a beach. *Journal of Fluid Mechanics*, 27:815–827, 1967.

O.M Phillips. On the generation of waves by turbulent wind. *Journal of Fluid Mechanics*, 2:417–445, 1957.

D. Quadfasel and H. Baudner. Gyre-scale circulation cells in the red sea. *Oceanologica ACTA*, 16:221–229, 1993.

D. K. Ralston, H. Jiang, and J. T. Farrar. Waves in the red sea: Response to moonsonal and mountain gap winds. *Continental Shelf Research*, 65:1–13, 2013.

RD Instruments Acoustic Doppler Solutions. *Waves User's Guide*. RD Instruments Acoustic Doppler Solutions, 2001.

R. C. Ris, L. H. Holthuijsen, and N. Booij. A third-generation wave model for coastal regions 2- verification. *Journal of Geophysical Research*, 104:7667–7681, 1999.

W.E. Rogers, P.A. Hwang, and D.W. Wang. Investigation of wave growth and decay in the swan model : three regional-scale applications. *Journal of Physical Oceanography*, 33: 366–389, 2003.

W.E. Rogers, J.M. Kaihatu, L. Hsu, R. E. Jensen, J.D. Dykes, and K.T. Holland. Forecasting and hindcasting waves with the swan model in the southern california bight. *Coastal engineering*, 54:1–15, 2007. doi: 10.1016/j.coastaleng.2006.06.011.

A. Roland. *Spectral Wave Modelling on Unstructured Meshes*. PhD thesis, Institut für Wasserbau und Wasserwirtschaft, Technische Universität Darmstadt, Darmstadt, 2008.

E. Rusu, L. Rusu, and C.G. Soares. Prediction of extreme wave conditions in the black sea with numerical models. In *Proc. 9th International Workshop on Wave Hindcasting and Forecasting*, Victoria, B.C., Canada, 2006.

A. Saket, A. Etemad-Sahidi, and M.H. Moeni. Evaluation of ecmwf wind data for wave hindcast in chabahar zone. *Journal of Coastal Research*, special issue 65:380–385, 2013. doi: 10.2112/SI65-065.1.

R. Scharroo, E.W. Leuliette, D. Byrne, M.C. Naeije, and G.T. Mitchum. Rads: Consistent multi-mission products. In *Proc. of the Symposium on 20 Years of Progress in Radar Altimetry*, page 4, Venice, Italy, 2013.

J.B. Settelmaier, A. Gibbs, P. Santos, T. Freeman, and D. Gaer. Simulating waves nearshore (swan) modeling efforts at the national weather service (nws) southern region (sr) coastal weather forecast offices (wfos). In *91th AMS Annual Meeting*, Seattle, WA, 22-28 January 2011.

E.D.R. Shearmann and M.D. Moorhead. Pisces: A coastal ground-wave hf radar for current, wind and wave mapping to 200km ranges. In *Proceedings of the International Geoscience And Remote-Sensing Society*, pages 773–776, Edinburgh, Scotland, 1988.

R.P. Signell, S. Carniel, L. Cavaleri, J. Chiggiato, J.D. Doyle, J. Pullen, and M. Sclavo. Assessment of wind quality for oceanographic modelling in semi-enclosed basins. *Journal of Marine Systems*, 53:217–233, 2005. doi: 10.1016/j.jmarsys.2004.03.006.

R. L. Snyder, F.W. Dobson, J.A. Eliott, and R.B. Long. Array measurements of atmospheric pressure fluctuations above surface gravity waves. *Journal of Fluid Mechanics*, 102:1–59, 1981.

B. Strong, B. Brumley, E.A. Terray, and G.W. Stone. The performance of adcp derived directional wave spectra and comparison with other independent measurements. In *IEEE Oceans Conference*, pages 1195–1203, Providence, Rhode Island, USA, 2013.

C.C. Teague, J.F. Vesecky, and Z.R. Hallock. A comparison of multifrequency hf radar and adcp measurements of near-surface currents during cope-3. *IEEE Journal of Oceanic Engineering*, 26:399–405, 2001.

E.A. Terray, B.H. Brumley, and B. Strong. Measuring waves and currents with an upward-looking adcp. In *Proc. IEEE 6th Working Conference on Current Measurement*, pages 66–71, 1999.

The SWAN Team. *SWAN User Manual SWAN Cycle III version 40.51.* Delft University of Technology, 2006.

E.R. Thieler and E.S. Hammar-Klose. National assessment of coastal vulnerability to future sea level rise : Preliminary results for us atlantic coast. Online report, US Geological Survey, USA, 1999.

H.L. Tolman. Effects of numerics on the physics in a third-generation wind-wave model. *Journal of Physical Oceanography*, 22:1095–1111, 1992.

H.L. Tolman. User manual and system documentation of wavewatch-iii version 1.15. Technical note 151, National Oceanic and Atmospheric Administration, Washington, 1997.

H.L. Tolman. User manual and system documentation of wavewatch-iii version 1.18. Technical note 166, National Oceanic and Atmospheric Administration, Washington, 1999a.

H.L. Tolman. User manual and system documentation of wavewatch-iii version 3.14. Technical note 276, National Oceanic and Atmospheric Administration, Washington, 2009.

A.J. Van der Westhuysen, M. Zijlema, and J.A. Battjes. Nonlinear saturation-based whitecapping dissipation in swan for deep and shallow water. *Coastal Engineering*, 54:151–170, 2007.

S. Vignudelli, H.M. Snaith, F. Lyard, P. Cipollini, F. Venuti, F. Birol, J. Bouffard, and L. Roblou. Satellite radar altimetry from open ocean to coasts: challenges and perspectives. In *United States Society of Photo-Optical Instrumentation Engineers (SPIE)*, volume 6406, page 6, 2006.

Group WAMDI. A third-generation ocean wave prediction model. *Journal of Physical Oceanography*, 18:1775–1810, 1988.

J. Wang, Y. Shen, and Y. Guo. Seasonal circulation and influence factors of the boahi sea: a numerical study based on lagrangian particle tracking method. *Ocean dynamics*, 60: 1581–1596, 2010. doi: 10.1007/s10236-010-0346-7.

Z.F. Wang, K.J. Wu, L.M. Zhou, and L.Y. Wu. Wave characteristics and extreme parameters in the bohai sea. *China Ocean Engineering*, 61:341–350, 2012.

L.R Wyatt. The measurements of the ocean wave directional spectrum from h.f. radar doppler spectra. *Radio Science*, 21:473–485, 1986.

L.R Wyatt. A relaxation method for integral inversion applied to h.f. radar measurement of the ocean wave directional spectrum. *International Journal of Remote Sensing*, 11: 1481–1494, 1990.

L.R Wyatt. High-frequency radar measurements of the ocean wave directional spectrum. *IEEE Journal of Oceanic Engineering*, 16:163–169, 1991.

L.R. Wyatt. the ocean wave directional spectrum. *Oceanography*, 10:85–89, 1997.

L.R. Wyatt and J.J. Green. Measuring high and low waves with hf radar. In *IEEE Oceans Conference*, Bremen, Germany, 2009.

L.R. Wyatt, S.P. Thompson, and R.R. Burton. Evaluation of high frequency wave measurement. *Coastal Engineering*, 37:259–282, 1999.

L.R. Wyatt, G. Liakhoveetski, H. Graber, and B.K. Haus. Factors affecting the accuracy of showex hf radar wave measurements. *Journal of Atmospheric and Oceanic Technology*, 22:847–859, 2005.

L.R. Wyatt, J.J. Green, and A. Middleditch. Hf radar quality requirements for wave measurements. *Coastal Engineering*, 58:327–336, 2011.

L. Yan. An improved wind input source term for third generation ocean wave modelling. Technical Report WR-No 87-8, The Netherlands : scientific report, 1987.

S. Yang, Z. Wang, Y. Dou, and X. Shi. A review of sedimentation since the last glacial maximum on the continental shelf of eastern china. In F.L. Chiocci and A.R. Chivas, editors, *Continental shelves of the world, their evolution during the last glacio-eustatic cycle*, chapter 21, pages 293–303. The Geological Society, London, 2014.

Z. Yanling, Y. Yuzhen, Y. Xiaobao, and L. Tianjun. Wind-wave characteristics in the bohai sea, the yellow sea and the east china sea. In *Proc. 2nd International Conference on Remote Sensing, Environment and Transportation Engineering (RSETE)*, Nanjing, China, 2012.

K.J. Yu and F.G. Zhang. A three-dimensional numerical model of the tidal motions in the bohai sea. *Oceanologia et Limnologia Sinica*, 18(3):227–236, 1987.

Y. Zhang, Y. Ding, and Q. Li. A climatology of extratropical cyclones over east asia during 1958-2001. *Acta Meteorologica Sinica*, 3:261–277, 2012.

J. Zhao and M. Shi. Numerical modelling of three-dimension characteristics of wind-driven current in the bohai sea. *Chinese Journal of Oceanology and Limnology*, 11(1):70–79, 1993.

K. Zubier, V. Panchang, and Z. Demirbilek. Simulation of waves at duck (north carolina) using two numerical models. *Coastal Engineering Journal*, 45:439–469, 2003. doi: 10.1142/S0578563403000853.

K. M. Zubier, Y. O. Abulnaja, and A. M. Al-Subhi. Development of an operational wave prediction system for the red sea: Experimental phase. In *Offshore Arabia 2008 Conference*, Dubai, United Arab Emirates, 2008.

List of Figures

List of Tables

Acronyms

ADCIRC ADvanced CIRCulation. 31

ADCP Acoustic Doppler Current Profiler. 4, 47, 49, 51, 52, 55, 62, 66, 68, 74, 82

BSBT Backward Space Backward Time. 21

CAU Christian-Albrechts-University. 11, 95

CMS Coastal Monitoring System. 30, 31, 83

CODAR Coastal Ocean Dynamics Applications Radar. 6

DSS Decision Support System. iv, 8, 62, 63, 68, 69, 70, 73, 75, 83

DWD German Weather Service. 3, 9, 24, 31, 32, 39, 49, 65, 77, 81, 82

ECMWF European Centre for Medium range Weather Forecasts. 3, 46, 77

ETOPO1 Earth TOPOgraphy 1′. 9, 19, 78

FMCW Frequency Modulated Continuous Wave. 7, 48

GEBCO GEneral Bathymetric Charts of the Oceans. 9, 19, 34, 65, 78

GEOMAR Helmholtz-Centre for Ocean Research. 42

GFS Global Forecast System. 31, 69

GME Global Meteorological Model. 19, 95

HF High Frequency. 4, 6, 7, 48, 49, 51, 52, 54, 68, 79, 82

HYCOM HYbrid Coordinate MOdel. 65, 69

KAU King Abdullah University. 27, 42

KAUST King Abdulaziz University of Science and Technology. 19, 21, 27, 30, 31, 33, 95

NCEP FNL Centres for Environmental Prediction's Global Final Analysis. 31

NDBC National Data Buoy Centre. 19

NOAA National Oceanic and Atmospheric Administration. 2

NOGAPS US Navy's Operational Global Atmospheric Prediction System. 31

ODINWESTPAC Ocean Data and Information Network for the Western Pacific Region. 49

OSCR Ocean Surface Current Radar. 6

RADS Radar Altimeter Data Acquisition Service. 33

RMS Root Mean Square. 22, 99

SI Scatter Index. 22, 99

SWAN Simulating WAves Nearshore. 2, 3, 7, 11, 20, 21, 22, 26, 31, 34, 39, 40, 42, 46, 47, 49, 55, 63, 64, 68, 77, 78, 81, 95, 96, 99

TPXO Global Model of Ocean Tides. 65

WAM WAve Model. 2, 77

WERA WEllen RAdar. 6, 7, 48

WRF-ARW Weather Research and Forecasting Model with advance Research. 31

WW3 WAVEWATCH-III. 2, 11, 63

Appendix A

Specific contributions to the manuscripts

The contributions of the authors to the manuscripts are indicated as follow :

N. Fery, G. Bruss, A. Al-Subhi, and R. Mayerle. Numerical study of wind generated waves in the Red Sea. In University of Ghent, editor, Book of proceedings 4^{th} International Conference Coastlab12, Ghent, Belgium, 2012.

Specific contributions : N. Fery prepared the concept of the paper, proceeded to the data analysis/interpretation and the writing. G. Bruss gave his support in the data interpretation and analysis. R. Mayerle and A. Al-Subhi are the project holders.

Fery, N, A.M. Al-Subhi, K.M. Zubier, and G. Bruss. Evaluation of the sea state near Jeddah based on recent observations and model results. Journal of Operational Oceanography, 8(1): 1-10, 2015. doi: 10.1080/1755876X.2015.1014636.

Specific contributions : N. Fery prepared the concept of the paper, proceeded to the data analysis/interpretation and the writing. Contributions to the manuscript were done by K.M. Zubier and G. Bruss. A.M. Al-Subhi is the project holder.

Fery, N, C. Tang, and R. Mayerle. Validation experiment of wind and wave properties from High Frequency radar in the vicinity of Yantai, China. Manuscript submitted for publication in Regional Studies in Marine Science, 2017.

Specific contributions : N. Fery prepared the concept of the paper, proceeded to the data analysis/interpretation and the writing. C. Tang and R. Mayerle are the project holders.

G.L. Dalledonne, X. Zheng, **N. Fery**, C. Tang, and R. Mayerle. Decision support system for the management of the shandong peninsula, China. In 35^{th} International Conference of Coastal Engineering (ICCE), Antalya, Turkey, 2016.

Specific contributions : The authors G.L. Dalledonne and X. Zheng made contributions to the manuscript and to the writing. N. Fery contributed to the setting of the hydrodynamic models and provided the wave analysis. N. Fery contributed as well to the writing. C. Tang and R. Mayerle are the project holders.

Appendix B

Acknowledgements

First and foremost, I would like to express my gratitude to my advisor Professor Dr. R. Mayerle. He taught me to work on my own and as a team member. I thank him for letting me participating in numerous projects within the Coastal Research Laboratory, in conferences and meetings, and for funding my PhD studies.

I wish to thank the other members of my committee who took the time to read my thesis.

Particular thanks go to Dr. G. Bruss who gave a lot of his time to teach me, help me and guide me. I thank him for reading and giving suggestions to the manuscripts I wrote. I really appreciated the years working and the hours running with him.

I thank my colleagues at the Coastal Research Laboratory for the constructive discussions, the encouragements and the fun over the last years.

Acknowledgements to pets might appear to be unusual and strange, but special thanks go to my cat Kiwi for his way of supporting me whether scratching or purring, his loyalty and his constant presence.

Lastly, my biggest thanks go to my father and my stepmother for their permanent support and patience during all phases of my thesis. I thank them for their understanding, their moral and financial help. To them, I dedicate this thesis.

Appendix C

Eidesstattliche Erklärung

Natacha Fery
Hamburger Chausse 11
24114 Kiel

Eidesstattliche Erklärung zu meiner Dissertation mit dem Titel:
'Nearshore wind-wave modelling in semi-enclosed seas: cross calibration and application'

Sehr geehrte Damen und Herren,

ich versichere hiermit an Eides statt, dass ich die vorliegende Arbeit selbstständig angefertigt und ohne fremde Hilfe verfasst habe, keine außer den von mir angegebenen Hilfsmitteln und Quellen dazu verwendet habe und die den benutzten Werken inhaltlich und wörtlich entnommenen Stellen als solche kenntlich gemacht habe. Ich versichere, dass die Arbeit weder ganz noch zum Teil schon einer anderen Stelle im Rahmen eines Prüfungsverfahrens vorgelegen hat.

Ort, Datum Unterschrift